



# ELECTRICORE, INC.

The Consortium for Advanced Technologies

27943 Smyth Drive, Suite 105

Valencia, CA 91355

Phone: (661) 607-0260

Fax: (661) 607-0264

[www.electricore.org](http://www.electricore.org)

---

May 29, 2008

Mr. Blaine Keener  
Technical Manager  
U.S. Department of Transportation  
Pipeline and Hazardous Materials Safety Administration  
Washington, D.C. 20590

**RE: Pipeline Safety Research and Development Other Transaction Agreement DTPH56-05-T-0003 153 – Interim Final Report**

Dear Mr. Keener:

This letter serves as notification that Electricore, Inc. has submitted interim final reports detailing the activities, results, and conclusions for the original statement of work under the U.S. Department of Transportation Other Transaction Agreement (OTA) DTPH56-05-T-0003, "Consolidated Research and Development Program to Assess the Structural Significance of Pipeline Corrosion." Electricore has conducted this work through a collaborative effort with Advantica, Inc. and the Pipeline Research Council International, Inc. (PRCI), which are providing technical research, technical review, and program management support for the program through separate agreements.

The work being conducted under the agreement has been divided into following four individual projects:

1. Project #153H, "Corrosion Assessment Guidance for Higher Strength Pipelines"
2. Project #153K, "Behavior of Corroded Pipelines Under Cyclic Pressure"
3. Project #153L, "Assessment of Older Corroded Pipelines with Reduced Toughness and Ductility"
4. Project #153J, "Remaining Strength of Corroded Pipe Under Secondary (Biaxial) Loading"

The original scopes of work for these projects were completed in December 2006, and draft reports presenting the results were submitted to the DOT in 2007. Based on the results of the initial work completed, as presented in the draft final report submitted to the DOT, additional work was identified by the DOT, PRCI and Advantica to augment the work conducted under the original scope of work. This additional work includes:

**1. Project #153H Corrosion Assessment Guidance for Higher Strength Steels - Advantica Report R9017**

It was agreed that no further work was required and the report could be issued once review comments from PRCI had been addressed. However, since the issue of this report, additional work has been commissioned by DOT with Advantica. This work is described in Advantica Report 6781. It was agreed that the output of this additional work, which was presented in its own separate report (i.e., Report 6781), should also be included in the report presenting the results for Project #153H.

**2. Project #153J Remaining Strength of Corroded Pipe Under Secondary (Biaxial) Loading - Advantica Report R9068**

The aim of the work was to determine the limits of existing assessment methods such as B31G and RSTRENG when pipelines were subject to significant external loading. Failure loci have been

derived under combined pressure and bending or axial loading for three (D/t) ratios and two materials (X65 and B/X42). It was agreed that these failure loci should be normalized. An investigation of whether the normalized loci could be generalized for other materials and (D/t) ratios would also be undertaken. Once this investigation has been completed user friendly guidance will be formulated for incorporation into the PRCI Guidance Document.

**3. Project #153K Behavior of Corroded Pipelines Under Cyclic Pressure - Advantica Report R8928**

It was agreed that the following additional tasks were required:

- Re-analyze the finite element results to separate the effects of axial and hoop stresses and repeat curve fitting analysis carried out previously.
- Consider the effects of the transition radius at the edge of the corroded area. However, it is considered that it would not be realistic to carry out an extensive study on this aspect as current inspection tools will not provide any information on local radii.
- Analyze the strain gauge data from the DOT Phase 2 project on 153H relating to the BP X100 Operational Trial to determine stress concentration factors. These experimental values will be compared with the numerical predictions.
- Revise and expand the proposed assessment algorithm given in the draft report and include a flow chart of the algorithm.

**4. Project #153L The Remaining Strength of Corroded Low Toughness Pipe - Advantica Report R9247**

It was agreed that the implications of the EMCC work on transition temperature shifts needed to be considered as part of this project. The results of recent tests by Gaz de France on gouges in low toughness pipe will be considered as these may be relevant to the project.

Pending completion of the additional scopes of work for these four projects, Advantica has finalized the draft reports and submitted an interim final report for each project. The interim reports were posted to the DOT's web site on May 29, 2008. The reports are considered interim reports that are subject to modification based on the findings of the additional work being conducted by Advantica under the OTA. Any necessary modification will be incorporated into a revised final report that will be submitted to DOT following completion of the additional scope. We have prepared a disclaimer statement to that effect that is included in each of the interim final reports.

Because the results of the additional work being conducted may affect the prior report conclusions and results please keep the Interim Final Reports confidential and internal to the US Department of Transportation.

Electricore appreciates DOT's continued cooperation and support with this important project, and we look forward to the successful completion of the comprehensive program in 2008. If you have any questions regarding this draft report, or require additional information please contact me at 661-607-0261.

Thank you,

Ian C. Wood  
Program Manager  
Electricore, Inc.

cc: Robert Smith, DOT      Vinod Chauhan, Advantica  
Jim Merritt, DOT      Mark Piazza, PRCI



*R8928 Issue 1*

*October 2006*

---

## **INTERIM FINAL REPORT**

### **PROJECT #153K BEHAVIOR OF CORRODED PIPELINES UNDER CYCLIC PRESSURE**

---

*Confidential*

*Restricted to US DOT, PRCI, Electricore &  
Advantica*

**PREPARED FOR:**

B Keener, US DOT Office of  
Pipeline Safety

M Piazza, Pipeline Research  
Council International, Inc.

**PREPARED BY:**

R M Andrews, T Swankie, J Liu and J Crossley  
**Advantica**

Ashby Road  
Loughborough  
Leicestershire  
LE11 3GR

**United Kingdom**

Tel: +44 (0)1509 282749

Fax: +44 (0)1509 283119

E-mail: [bob.andrews@advanticagroup.com](mailto:bob.andrews@advanticagroup.com)

Website: [www.advanticagroup.com](http://www.advanticagroup.com)

DTPH56-05-T-0003

Customer Reference:



*This Report is protected by copyright and may not be reproduced in whole or in part by any means without the approval in writing of Advantica Ltd. No Person, other than the Customer for whom it has been prepared may place reliance on its contents and no duty of care is assumed by Advantica toward any Person other than the Customer.*

*This Report must be read in its entirety and is subject to any assumptions and qualifications expressed therein. Elements of this Report contain detailed technical data which is intended for analysis only by persons possessing requisite expertise in its subject matter.*

*Registered in England and Wales No. 3294136.*

**REGISTERED OFFICE: 1-3 STRAND, LONDON, WC2N 5EH**

## Report Issue Record

Report Title: Project #153K Behavior of Corroded Pipelines under Cyclic Pressure	
Report Number: R8928	Project SAP Code: 1/07620

Issue	Description of Amendment	Originator/Author	Checker	Approver	Date
1	Interim Report	R M Andrews, T Swankie, J Liu, J Crossley	V Chauhan	P Ingham	October 2006

Previous issues of this document shall be destroyed or marked **SUPERSEDED**

## Distribution

Name	Company
J Merritt	US DOT Office of Pipeline Safety
R Smith	US DOT Office of Pipeline Safety
B Keener	US DOT Office of Pipeline Safety
M Piazza	Pipeline Research Council International, Inc.
R Owen	National Grid plc
N Sanderson	BP Exploration
Ian Wood	Electricore, Inc.

---

Recipients of this page may obtain a copy of this report from:  
Advantica, Ashby Road, Loughborough,  
Leicestershire, LE11 3GR. Telephone 01509 282000 Facsimile 01509 283131

## Disclaimer

This interim report details the activities, results, and conclusions for the original Statement of Work under the U.S. Department of Transportation (DOT) Other Transaction Agreement DTPH56-05-T-0003, "Consolidated Research and Development Program to Assess the Structural Significance of Pipeline Corrosion." Under the agreement, the work was segregated into the following four individual projects:

1. Project #153H, "Corrosion Assessment Guidance for Higher Strength Pipelines"
2. Project #153K, "Behavior of Corroded Pipelines Under Cyclic Pressure"
3. Project #153L, "Assessment of Older Corroded Pipelines with Reduced Toughness and Ductility"
4. Project #153J, "Remaining Strength of Corroded Pipe Under Secondary (Biaxial) Loading"

This report presents the results for Project #153K, "Behavior of Corroded Pipelines Under Cyclic Pressure".

The initial scope of work for this project was completed by Advantica in December 2006, and a draft final report was prepared and submitted to DOT in 2007. Based on the results of the initial work completed, as presented in the draft final report submitted to DOT, additional work has been identified by the DOT and Advantica to augment the work conducted under the original scope of work. The findings and conclusions of the supplemental work will be incorporated into a revised final report, as appropriate, that will be submitted to DOT (submittal date estimated at the end of 2008). Because the results of the additional work to be conducted may affect the prior report conclusions and results, this report is being submitted as an interim final report and is subject to change, modification, and/or amendment, and may be supplemented through the preparation of a revised report or an addendum to this interim report.

This report is furnished to the U.S. Department of Transportation (DOT), Electricore, Inc. (Electricore) and Pipeline Research Council International, Inc. (PRCI) under the terms of DOT contract DTPH56-05-T-0003 between the DOT and Electricore, Electricore agreement DTPH56-05-T-0003 between Electricore and Advantica, and PRCI contract PR-273-0323 between PRCI and Advantica Inc. (Advantica). The contents of this report are published as received from Advantica. The opinions, findings, and conclusions expressed in the report are those of the authors and not necessarily those of the DOT, Electricore, or PRCI, including PRCI's member companies, or their representatives. Publication and dissemination of this report should not be considered an endorsement by Electricore, PRCI, or Advantica, or the accuracy or validity of any opinions, findings, or conclusions expressed herein.

In publishing this report, Electricore, PRCI and Advantica make no warranty or representation, expressed or implied, with respect to the accuracy, completeness,



usefulness, or fitness for purpose of the information contained herein, or that the use of any information, method, process, or apparatus disclosed in this report may not infringe on privately owned rights. Electricore, PRCI and Advantica assume no liability with respect to the use of, or for damages resulting from the use of any information, method, process, or apparatus disclosed in this report. The text of this publication, or any part thereof, may not be reproduced or transmitted in any form by any means, electronic or mechanical, including photocopying, recording, storage in an information retrieval system, or otherwise, without the prior, written approval of PRCI.

## Executive Summary

A range of methods exists for assessing the remaining strength of a corroded pipeline under static pressure loading and these have now matured to the extent that they are incorporated in regulations and standards. However, there is currently no guidance for assessing the performance of a corroded pipeline under cyclic pressure loading. This is of potential concern to operators where there are significant pressure variations, for example where there is a demand for linepack storage. It is possible that a corrosion defect could be assessed as acceptable for the maximum operating pressure of a pipeline, but fail by fatigue due to internal pressure fluctuations.

Advantica has been contracted by PRCI and DOT to develop an assessment method for pipelines containing corrosion defects which are subject to fluctuating pressure loadings. This forms the subject of the present report.

The method involves estimating the stress raising effect of the corrosion defect to determine the enhanced cyclic stress range associated with the feature. This stress range is then used with a stress – life (S-N) curve to derive the fatigue life of the corrosion defect. This life can then be used to determine if the defect is acceptable, or the time until a repair is required.

The following main conclusions can be drawn from this work:

1. There is no available published method for assessing the life of volumetric corrosion defects under cyclic loading. An assessment method based on determining the stress raising effect of the corrosion defect combined with a S-N curve for parent plate material in a corrosive environment is proposed.
2. A wide range of defect geometries have been analyzed to determine elastic stress concentration factors which can be used to determine the effect of cyclic loading.
3. The proposed approach has been verified by a small set of fatigue tests. The experimental results were generally consistent with the predictions.

It is recommended that the work completed in this project be extended to cover the following activity to enhance the method described in this report:

1. Further analysis should be carried out to determine closed form equations to predict the stress raising effects of volumetric corrosion defects.
2. Additional cyclic loading tests are required to confirm the predictive method developed in this project. This should cover both the fatigue life and the stress raising effect of the defects.
3. A screening method should be developed using the results produced in this project to identify cases where cyclic loading of volumetric corrosion defects requires special consideration.



# Contents

<b>1</b>	<b>INTRODUCTION.....</b>	<b>1</b>
<b>2</b>	<b>LITERATURE REVIEW .....</b>	<b>1</b>
2.1	Issues associated with fatigue of corrosion defects.....	1
2.2	Existing assessment methods .....	2
2.3	Methods of determining stress concentration factors.....	3
<b>3</b>	<b>FINITE ELEMENT ANALYSIS.....</b>	<b>3</b>
3.1	Geometry and Material Properties .....	4
3.2	Finite Element Models.....	4
3.3	Loading and Boundary Conditions.....	5
3.4	Finite Element Results and Assessment.....	5
3.4.1	914.4 mm x 12.7 mm Pipe .....	5
3.4.1.1	Effect of Corrosion Size – length, width and depth .....	6
3.4.1.2	Effect of ‘Capped End Force’ .....	6
3.4.1.3	Effect of radius at the transition region .....	7
3.4.2	508 mm x 12.7 mm Pipe .....	7
3.4.3	1270 mm x 12.7 mm Pipe .....	7
3.4.4	Effect of Pipe Size .....	7
3.5	Conclusions from finite element analysis.....	8
<b>4</b>	<b>CYCLIC PRESSURE TEST .....</b>	<b>8</b>
4.1	Material.....	8
4.2	Test vessel design and construction.....	9
4.2.1	Introduction of defects.....	9
4.2.2	Vessel fabrication .....	9
4.2.3	Defect instrumentation .....	10
4.3	Test Method .....	10
4.3.1	Test facility.....	10
4.3.2	Test method.....	11
4.4	Test results .....	12
4.5	Metallurgical examination.....	13
4.6	Experimental Stress Concentration Factors.....	13
4.7	Analytical Fatigue Life Assessment .....	14
4.8	Comparison of Actual and Predicted Fatigue Lives.....	14
<b>5</b>	<b>DISCUSSION.....</b>	<b>15</b>
5.1	Interpolation in Finite Element Results .....	15
5.2	Comparison of Strain Gauge and Finite Element Results .....	17
5.2.1	Comparisons.....	17
5.2.2	Effects of pipe dimensional tolerances.....	17
5.3	General Remarks.....	18
5.3.1	Validity of Results .....	18
5.3.2	Effects of High Stress Concentration Factors .....	19
5.3.3	Effect of defect circumferential size .....	19
5.3.4	Recommended Fatigue Assessment Code.....	20
<b>6</b>	<b>OUTLINE OF PROPOSED ASSESSMENT METHOD .....</b>	<b>21</b>



7 CONCLUSIONS..... 21

8 RECOMMENDATIONS..... 22

9 REFERENCES..... 23

APPENDIX A MATERIAL TEST CERTIFICATE ..... 31

APPENDIX B INSPECTION CERTIFICATE (DEFECTS) ..... 31

# 1 INTRODUCTION

A range of methods exists for assessing the remaining strength of a corroded pipeline under static pressure loading and these have now matured to the extent that they are incorporated in regulations and standards. However, there is currently no guidance for assessing the performance of a corroded pipeline under cyclic pressure loading. This is of potential concern to operators where there are significant pressure variations, for example where there is a demand for linepack storage. It is possible that a corrosion defect could be assessed as acceptable for the maximum operating pressure of a pipeline, but fail by fatigue due to internal pressure fluctuations.

Advantica has been contracted by PRCI and DOT to develop an assessment method for pipelines containing corrosion defects which are subject to fluctuating pressure loadings. This forms the subject of the present report.

The method developed is based on the approach to the fatigue design of welded structures in codes such as API RP 2A [1] and BS 7608 [2]. In these a set of stress – life, or S-N curves are presented in terms of the nominal stress range acting on a particular weld detail. If necessary the nominal stress range is magnified by a stress concentration factor to take account of the local structural geometry at the weld detail. The stress raising effect of the actual weld geometry is included in the S-N curve. For the present application the stress concentration is derived for the corrosion feature. This can then be used in conjunction with an appropriate S-N curve for the particular material and environment.

Section 2 of this report reviews the available literature relevant to the project. The finite element analyses carried out to derive stress concentration factors are presented in Section 3. A fatigue test under cyclic pressure loading was carried out on a vessel containing machined simulated corrosion defects; this also provided experimental measurements of the stress concentration factors for comparison with the numerical predictions. The details of the test are given in Section 4. The discussion in Section 5 considers the fitting of curves to the numerical results, comparison of the numerical predictions and experimental stress concentration factors and the results of the cyclic pressure test. Based on the work carried out, an outline of the proposed assessment method for corrosion defects subject to cyclic pressure loading is given in Section 6. Conclusions are given in Section 7 and recommendations in Section 8.

## 2 LITERATURE REVIEW

### ***2.1 Issues associated with fatigue of corrosion defects***

It was not possible to locate any public domain information on the behavior of volumetric corrosion (as opposed to stress corrosion cracking) defects in pipelines. However, it is intuitively obvious that the environment giving rise to the volumetric metal loss would

have an effect on the fatigue performance of the exposed pipe surface<sup>1</sup>. The voluminous literature on metal fatigue recognizes that a corrosive environment will reduce the fatigue life of a component below the life which would be obtained in air. There are many factors that contribute towards this reduction, and a review of these is outside the scope of the present project. However, the factors can generally be grouped into two main areas, the effects on crack initiation and effects on crack propagation.

A corrosive environment will reduce, or even eliminate entirely, the crack initiation period. It is generally accepted that the bulk of the fatigue life of smooth components at low to medium stresses is consumed by the initiation of a crack. The initiation period, and hence the fatigue life, is sensitive to factors such as surface roughness and residual stresses. In a corrosive environment pitting and other forms of surface attack provide initiation points for cracks and so the initiation period is largely removed. This gives rise to the fact that in many corrosive environments there is no fatigue limit.

Once a crack has initiated, there will be a period of crack growth until final failure occurs. During this period a corrosive environment will cause accelerated crack growth. For example, in Section 8.2.3.5 of BS 7910 [3] a freely corroding seawater environment increases the crack growth rate by a factor of 4.4 compared with an air environment when using the “screening” crack growth curves. Fatigue crack growth data for X65 linepipe exposed to sour crude oil showed similar levels of increase [4] [5] when compared to data obtained in air.

This brief analysis shows that predicting the effect of a corrosive environment on fatigue life is complex. For pipelines with significant metal loss, there is a further complication. This is that the stress raising effects of the corrosion defect would reduce life as this area is exposed to higher stresses (in addition to the environment). This stress raising effect is still present, even if the underlying corrosion problem is resolved by coating repairs or the introduction of corrosion inhibitor. Hence it is considered that an assessment method for pipeline corrosion defects should include both effects. The approach taken in this project is to separate the two. The stress raising effect of the metal loss defect is considered by an estimation based on the geometry and elastic stress analysis. This is then combined with a fatigue life estimation which includes the effect of a corrosive environment.

## ***2.2 Existing assessment methods***

A Code Case for the ASME Boiler and Pressure Vessel Code, N597-2 [6], was located. This is principally concerned with failure of nuclear power station piping which has suffered wall loss due to erosion or erosion – corrosion. The main loading is pressure or system loading, but there is a brief consideration of cyclic loading in paragraph –3625. If the loss in wall thickness is less than 25% of the nominal thickness and the loading is less than 150 full temperature cycles, the defect is considered acceptable. If this

---

<sup>1</sup> If remedial action is taken, for example coat and re-wrap or the introduction of an effective inhibitor system, then the corrosive environment would no longer be affecting the life.

criterion is not met, a code pipe stress analysis is required using stress intensification<sup>2</sup> factors revised to take account of the geometry of the thinned areas. No guidance is given on how these revised factors should be determined. Alternatively, a set of stress range reduction factors are given which assume that the stress intensification factors increase linearly over the fatigue life by a factor of 2. This degree of stress increase at the defect may not be large enough for some cases, and it is also not clear how this should be applied to plain pipe. Furthermore, this approach does not appear to take account of aggressive environments. However, it is consistent with the general approach taken in the present project of modifying the basic fatigue performance by a factor to take account of the stress raising effect of the feature.

A search of the published literature using the “Compendex” database revealed a number of papers published in Japan concerning the assessment of thinned pipework. However, these were found to consider the behavior of power station piping under external seismic loads, with stresses exceeding yield, and were not relevant to corrosion defects in typical transmission pipelines.

One paper was located which is relevant to the present work. This study by Kim and Son [7] used three-dimensional finite element analysis to calculate stress concentration factors for ellipsoidal defects located at the bore of pipes. The loading was either internal pressure or external bending moment. The results from this work are discussed in more detail in Section 5.3.1.

## ***2.3 Methods of determining stress concentration factors***

There are published collections of stress concentration factors and these were reviewed to determine if there were any available solutions which could be used. None were found to be suitable, as they mainly related to two-dimensional cases such as a hole in a plate or a notch in the edge of a strip. These are not directly relevant to the three-dimensional case of a groove or pit in a curved shell. Hence these could not be used for the determination of stress concentration factors (SCFs) for volumetric defects. A numerical approach using the finite element method was therefore adopted.

## **3 FINITE ELEMENT ANALYSIS**

SCFs have been derived using linear elastic finite element analysis for a range of idealized corrosion defects. The analysis and results are presented in this section. Note that, although the analyses have been presented for specific dimensions typical of service pipelines, as the analyses are linear elastic the results can be applied to other geometrically similar cases. The effects of varying parameters such as the diameter to thickness ( $D/t$ ) ratio are discussed in more detail in Section 5 below.

---

<sup>2</sup> These are the ASME code stress intensification factors for pipework, and should not be confused with the stress intensity factor used in fracture mechanics analysis.

### **3.1 Geometry and Material Properties**

Three pipes were chosen with outside diameters (D) and wall thicknesses (t) of 914.4 mm (36") x 12.7 mm (0.5"), 508 mm (20") x 12.7 mm and 1270 mm (50") x 12.7 mm, with D/t ratios of 72, 40 and 100, respectively. These were chosen to represent the typical range of geometries encountered in transmission pipelines. The majority of the analyses were carried out on the D/t = 72 geometry, with a smaller range of cases being analyzed for D/t = 40 and D/t = 100 to investigate the effect of the D/t ratio on the SCF.

Both the axial corrosion length (ACL) and the circumferential corrosion length (CCL) in Figure 1 vary from 13 mm to 500 mm. The corrosion depths (CD) modeled were 20%, 40%, 60% and 80% of the pipe wall thickness. These were chosen to cover a range slightly deeper than the typical manufacturing under tolerance of 10% through to a depth of 80%, where assessment codes such as ASME B31.G [9] require repair. It should be noted that only one quarter of the corrosion area is shown in Figure 1, therefore ACL and CCL represent half of the total axial corrosion length and half of the total circumferential corrosion length, respectively. The corrosion defects have been idealized as having a smooth transition radius and a flat bottom.

The radius at the transition region around the corrosion edge in Figure 1 is  $r = t$  ( $r/t = 1$ ) for most of analyses. The effect of varying the radius  $r$  was investigated for 914.4 mm x 12.7 mm pipes by reducing the transition radius to  $r/t = 0.5$ .

The assumed elastic properties were appropriate for a ferritic steel, a Young's modulus of  $210 \times 10^3 \text{ N/mm}^2$  and a Poisson's ratio of 0.3.

### **3.2 Finite Element Models**

The finite element models were constructed using the PATRAN 2001 r3 [8] mesh generating software and analyzed using the general-purpose FE code ABAQUS version 6.4 [10]. Typical meshes generated for the assessment are shown in Figure 2 - Figure 5 with  $r/t = 1$ , CD = 40% and the corrosion size ACL x CCL = 13 mm x 13 mm, 13 mm x 500 mm, 500 mm x 13 mm and 500 mm x 500 mm, respectively. The models used quadratic cubic elements (20 node bricks), with the mesh design based on previous studies of the behavior of corrosion defects carried out by Advantica. Figure 2 represents a small circular pit, whilst Figure 3 is a long circumferentially oriented groove, such as might occur with preferential girth weld corrosion. In Figure 4 the groove orientation is axial. A square patch is shown in Figure 5; this has radiused sides and corners. Figure 6 shows the mesh for a defect with a smaller transition radius,  $r/t = 0.5$  but with the other dimensions, (CD = 40% and ACL x CCL = 13 mm x 13 mm) identical to those in Figure 2. The smaller transition radius has resulted in short straight sections at the edges.

A mesh sensitivity study using a finer mesh with 10 elements through the remaining ligament at the base of the corrosion defect showed only a 1% increase in the stress concentration factor, and so it was concluded that the mesh design was sufficiently refined.

### 3.3 Loading and Boundary Conditions

The internal pressure was calculated to generate a hoop stress  $\sigma_h = 1 \text{ N/mm}^2$  based on the internal diameter,

$$p = \frac{\sigma_h t}{R - t} = \frac{t}{R - t} \quad (1)$$

where R and t are the pipe outside radius and wall thickness.

In order to represent the pipe sections being 'capped off' downstream, a distributed load was applied to the pipe surfaces, given by:

$$q = \frac{\pi p (R - t)^2}{\pi [R^2 - (R - t)^2]} = \frac{R - t}{2R - t} \quad (2)$$

It shows that if the internal pressure is given by equation (1), the circumferential stress in the pipe will be  $\sigma_h = 1 \text{ N/mm}^2$  and the axial stress from equation (2) will be about  $0.5 \text{ N/mm}^2$  when  $R \gg t$ . A limited number of analyses were carried out without this end load to investigate the effect of this load on the results, particularly for long circumferential grooves.

Nodal restraints were applied to the symmetry faces so that the quarter model represented a complete pipe with the defect. Additional restraints were also applied to the bottom of the pipe to prevent rigid body movements.

### 3.4 Finite Element Results and Assessment

#### 3.4.1 914.4 mm x 12.7 mm Pipe

A total of 253 analyses were carried out on the 914.4 mm x 12.7 mm pipe geometry. The maximum principal stresses from these analyses are listed in Table 1 - Table 7 as functions of the ACL, CCL and CD.

Figure 7 shows that maximum principal stresses at locations away from corrosion are apparently in the range  $0.54 \text{ N/mm}^2$  to  $1.12 \text{ N/mm}^2$ . This large apparent range is due to the automatic scaling of contour levels by the post-processing software. Further investigation shows that results were in the range  $0.93 \text{ N/mm}^2$  to  $1.1 \text{ N/mm}^2$ . The circumferential stress of the pipe with the internal pressure given by equation (1) is equal to unity, and hence provides confidence in the FE model. The highest maximum principal stress (HMPS) ( $8.7 \text{ N/mm}^2$  in Figure 7), which occurred in the corroded region, is defined as the stress concentration factor (SCF) for the corrosion defect. In most cases, the highest maximum principal stress occurred either around the centre of the corrosion shown in Figure 8 or around the corrosion transition region shown in Figure 9.



### **3.4.1.1 Effect of Corrosion Size – length, width and depth**

The SCFs in Table 1 - Table 4 are from FE analyses on corroded pipes with  $r/t = 1$  and with  $CD = 20\%$ ,  $40\%$ ,  $60\%$  and  $80\%$  wall thickness, respectively. These SCFs are also plotted in Figure 10 - Figure 13 as functions of the ACL and CCL. The figures show that, in general, the SCF increases with an increase of ACL but decreases with an increase of CCL until it reaches an approximately constant plateau value. However, for corroded pipes with a short ACL (13 mm or 20 mm), the SCF may decrease with an increase of ACL and increase with a decrease of CCL, as clearly shown in Figure 12 and Figure 13.

The SCFs are also plotted in Figure 14a – f with variation of the corrosion depth CD, showing that both the SCF and the gradient increase as corrosion depth becomes greater.

### **3.4.1.2 Effect of ‘Capped End Force’**

For corroded pipes with a short ACL but long CCL (i.e. circumferential grooves), the distributed load defined by equation (2) due to the ‘capped end force’, may play a major role on SCF values. Local axial, hoop and radial component stresses have been extracted from the results at the location of the highest maximum principal stress. Table 8 lists these stresses for pipes with  $CD = 80\%$ . It shows that

- For ACL larger than or equal to 50 mm, the maximum principal stress is approximately equal to the local circumferential stress.
- When ACL equals 13 mm and 20 mm, the axis of maximum principal stress changes from the circumferential direction to the pipe axial direction with an increase of CCL, i.e., for CCL less than about 50 mm, the maximum principal stress is approximately equal to the local circumferential stress. However, for CCL larger than or equal to 50 mm, the maximum principal stress is approximately equal to the local axial stress.

Local axial, local circumferential and local radial stresses for pipes with short ACL (13 mm and 20 mm) and with  $CD = 20\%$  and  $40\%$  are also given in Table 9 and Table 10 respectively. These tables show that

- For  $CD = 20\%$  with both  $ACL = 13$  mm and  $ACL = 20$  mm, the maximum principal stress in Table 9 is approximately equal to the local circumferential stress, hence the axis of maximum principal stress remains the circumferential direction with the increase of CCL.
- For  $CD = 40\%$  with  $ACL = 20$  mm, the maximum principal stress in Table 10 is approximately equal to the local circumferential stress. However, for  $ACL = 13$  mm, the maximum principal stress is approximately equal to the local circumferential stress only when the CCL is less than 50 mm, and for CCL greater than 100 mm, the maximum principal stress is approximately equal to the local axial stress.



Therefore, the 'capped end force', will play a major role when the corrosion size ACL is small and the corrosion depth CD is large. In this case, the SCF is approximately equal to the local axial stress. Otherwise the SCF is approximately equal to the local circumferential stress.

SCFs from FE analyses with  $CD = 80\%t$  and without the 'capped end force' acting on the end of pipes are given in Table 5 and plotted in Figure 15. It shows that the SCF increases with an increase of ACL and decreases with an increase of CCL even for short lengths of  $ACL = 13 \text{ mm}$  and  $20 \text{ mm}$ .

#### **3.4.1.3 Effect of radius at the transition region**

SCFs with transition radius  $r = 0.5t$  are given in Table 6 and Table 7 for  $CD = 20\%t$  and  $CD = 40\%t$ , respectively. Comparing these values with the data for  $r/t = 1$  in Table 1 and Table 2 shows that the SCF is higher for the smaller transition radius,  $r$ . The increased percentage of SCF, when the transition radius  $r/t = 1$  decreases to a more acute transition radius  $r/t = 0.5$ , is listed in Table 11. It shows that the maximum percentage increase is less than 10%.

SCFs are also plotted in Figure 16 and Figure 17 for  $CD = 20\%t$  and  $CD = 40\%t$  respectively. The trend of the graph is similar to that in Figure 10 and Figure 11, except for the case with  $ACL = 13 \text{ mm}$  and  $CD = 40\%$  which shows that the 'capped end force' influence on the SCF is less when  $r = 0.5t$ .

#### **3.4.2 508 mm x 12.7 mm Pipe**

A total of 72 finite element (FE) analyses have been carried out on 508 mm x 12.7 mm pipes. The maximum principal stresses from these FE analyses are listed in Table 12 with the variation of ACL, CCL and CD. Table 12 shows that, in general, the SCF increases with an increase of ACL and decreases with an increase of CCL until it reaches an approximately constant value.

#### **3.4.3 1270 mm x 12.7 mm Pipe**

There are a total of 48 finite element (FE) analyses carried out on 1270 mm x 12.7 mm pipes. The maximum principal stresses from these FE analyses are listed in Table 13 with the variation of ACL, CCL and CD. Table 13 shows that SCF increases with an increase of ACL.

#### **3.4.4 Effect of Pipe Size**

SCFs from the three pipes (508 mm x 12.7m, 914.4 mm x 12.7 mm and 1270 mm x 12.7 mm) with  $CCL = 13 \text{ mm}$  and  $20 \text{ mm}$  are plotted in Figure 18 to Figure 21 for  $CD = 20\%t - 80\%t$  respectively. Table 14 and Table 15 show the increment/decrement percentage in the SCF for 508 mm pipe and for 1270 mm as compared with 914.4 mm pipe, respectively. It should be noted that some care is required in comparing the results for defects in different diameter pipes, as the fixed width defects will subtend different angles in pipes of different diameter and so would be expected to have different SCFs.

### **3.5 Conclusions from finite element analysis**

The following conclusions can be drawn directly from the finite element analysis phase of the project:

- In general, the SCF increases as the axial crack length increases, but decreases as the circumferential crack length increases until it reaches a constant value.
- For corroded pipes with a short axial crack length the axis of the maximum principal stress may change, due to the 'capped end force' effect, from the circumferential direction to the axial direction as the circumferential length rises. Where this condition occurs, the SCF will increase with increasing circumferential crack length.
- The SCF increases with increasing corrosion depth.
- The effect of reducing the transition radius was small, producing typically less than 10% change in the SCF.
- There was no consistent trend in the SCF with varying pipe diameter, but the effects were generally less than 10% when compared with the base case of  $D/t = 72$ .

## **4 CYCLIC PRESSURE TEST**

A limited test programme was undertaken to provide validation of the FE analyses described in Section 3. This used a vessel containing four machined metal loss defects which was subjected to pressure cycling. Strain measurements were made at each defect and used to determine SCF values for comparison with the finite element results. Three of the four defects failed and the fourth defect survived beyond the predicted life. This section describes the test program and the results obtained; an analysis of the data is given in Sections 4.7 and 4.8.

### **4.1 Material**

The test section consisted of a 12m length of 12" nominal bore (323.9 mm outside diameter) seamless linepipe. The material grade was X52 to API 5L [11] which has a specified minimum yield strength of 52 ksi (359 N/mm<sup>2</sup>) and a specified minimum tensile strength of 66 ksi (455 N/mm<sup>2</sup>). The pipe nominal wall thickness was 8.4 mm, giving a pipe diameter to wall thickness (D/t) ratio of 38.5. This is marginally below the lowest D/t ratio analyzed in the FEA. The pipe manufacturer was Dalmine. The mill certificate is provided in Appendix A.

## 4.2 Test vessel design and construction

### 4.2.1 Introduction of defects

For handling and machining purposes, the pipe was cut in half (i.e., 2 lengths of pipe, both approximately 6m in length). Each half comprised 2 machined defects that were equally spaced along the length of the pipe, and offset to one another around the pipe circumference by approximately  $\frac{1}{4}$  of the pipe circumference. The purpose of this offset was to mitigate against the possibility of a rupture from a failed defect propagating into an adjacent defect.

The defect types and target dimensions are summarized below.

Defect 1 : axial groove,  $d/t=20\%$ ,  $L=400$  mm,  $r=8.5$  mm ( $W=10.1$  mm)

Defect 2 : axial groove,  $d/t=40\%$ ,  $L=400$  mm,  $r=8.5$  mm ( $W=13.5$  mm)

Defect 3 : axial groove,  $d/t=60\%$ ,  $L=400$  mm,  $r=8.5$  mm ( $W=15.5$  mm)

Defect 4 : patch,  $d/t=60\%$ ,  $L=400$  mm,  $W=140$  mm,  $r=8.5$  mm

Where  $t$  is the pipe wall thickness,  $d$  is the defect depth (from the outer pipe surface),  $L$  and  $W$  are the defect length and width in the pipe axial and circumferential directions measured along the outer surface of the pipe, and  $r$  is the blend radius (which is approximately equal to the pipe wall thickness).

The actual dimensions of the machined defects are compared with the target dimensions in Table 16 (see also Appendix B for the defect inspection certificate). Due to the large tolerances on wall thickness for seamless pipe a 50 mm x 50 mm grid was marked onto the surface of the machined-out patch defect. At each grid intersection, ultrasonic wall thickness measurements were undertaken to determine the variation in remaining ligament thickness. The remaining ligament thickness for each groove defect was determined using an ultrasonic thickness meter applied to the base of the groove.

After the defects had been machined, the surface of each defect was shot blasted. The pipe was then left outside for a period to permit the surface of the defects to corrode (this was to ensure that the number of fatigue cycles to crack initiation was truly representative of a corrosion defect and not unduly influenced by surface profile). The purpose of grit blasting the machined defects was to create a 'highly active' surface to promote accelerated corrosion.

### 4.2.2 Vessel fabrication

The two pipe sections were first butt welded together. To enable a full-scale fatigue test to be undertaken, two dome-ended pup pieces were constructed, which were welded to either end of the test pipe to form a pressure vessel.

The material used to construct the pup piece test ends was API 5L grade X52. The pup wall thickness measured 12.7 mm (0.5"). The domed ends were forged from P460 NL1 plate[12] with the same wall thickness as the test end pipe pup material. Each test end

had a 1" BSPT 6,000 psi rated thread-o-let welded to the outside diameter to allow for filling (and discharging) and venting of the completed vessel.

The vessel was constructed from two test ends circumferentially welded to the test section, with the thread-o-lets positioned 180° opposed to ensure removal of air during filling and venting of the vessel.

An illustration of the test vessel is shown in Figure 22.

### 4.2.3 Defect instrumentation

Each defect was strain gauged prior to testing. The groove defects each had 3 strain gauges; one located central to the length/width of the groove, and one at either end approximately 2-3 mm from the blend radius. The patch defect had 4 strain gauges; one located central to the length/width of the patch, one located around the patch circumference approximately 2-3 mm from the blend radius (central to the patch length), one located along the pipe length approximately 2-3 mm from the blend radius (central to the patch width), and the final gauge was located at a corner of the patch approximately 2-3 mm from the blend radius. The four strain gauges in the patch defect enveloped a quadrant of the patch, in the region where the thinnest remaining ligament was measured.

At the location where each strain gauge was positioned, the surface rust was locally removed to reveal bright metal to aid adhesion of the strain gauge.

Strain gauge rosettes were used at each location. Two types were used,

- Type 1. CEA-06-062WT-350: two elements 90° to each other, one stacked on top of the other (see Figure 23).
- Type 2. CEA-06-062UT-350: two elements 90° to each other, located side by side (see Figure 23).

Strain gauge type (1) was used where space was limited, at the blend radii. Type (2) was used at the centre (length/width) of the groove and patch defects. The locations of the strain gauges are shown in Figure 24.

## 4.3 Test Method

### 4.3.1 Test facility

The test was carried out with the test vessel mounted on freestanding vee support frames with the thread-o-lets positioned at 12 and 6 o'clock around the pipe circumference. The vessel was connected to the hydraulic system and filled with water. Once the vessel was full and all air had been removed, a 160bar<sup>3</sup> pressure transducer was connected to the upper thread-o-let of the vessel.

---

<sup>3</sup> 1 bar = 14.50377 PSI.

The test was undertaken according to a generic burst test risk assessment, which included the use of an exclusion zone and of the placement of 1 ton sand bags at either end of the vessel to help contain debris should catastrophic failure occur.

A data logger was used to log the output from the pressure transducer, and a 'K' type stainless steel sheathed thermocouple was used to measure ambient air temperature. The data was logged periodically at high frequency for a short time interval in an attempt to capture the minimum and maximum pressures associated with each pressure cycle. In addition, a strip chart recorder was used to continually monitor the pressure history during the test. The hydraulic power pack enabled a cyclic pressure rate of up to 6 cycles per minute.

### 4.3.2 Test method

The vessel was pressurized to 16 barg, after an initial shakedown (i.e., 3 pressure cycles from 0 – 16 – 0 barg). This pressure was considered sufficient to ensure that the strain gauges were working correctly and to enable calculation of the maximum permissible pressure that each defect could sustain without yielding the remaining ligament ahead of the defect. The strain gauge data were analyzed to determine the magnitude of hoop stress  $\sigma_h$  in the reduced ligament of each defect, using the following equation,

$$\sigma_h = \frac{E}{1-\nu^2} (\varepsilon_h + \nu \varepsilon_a) \quad (3)$$

where  $E$  = Elastic modulus (assumed 210 kN/mm<sup>2</sup>)

$\nu$  = Poisson's ratio (assumed 0.3)

$\varepsilon_h$  = hoop strain

$\varepsilon_a$  = axial strain

The maximum measured hoop stress from each defect was then compared with the material's specified minimum yield strength (SMYS) of 358 N/mm<sup>2</sup>. For each defect the maximum pressure to give a hoop stress in the remaining ligament equal to SMYS was predicted by multiplying the initial 'calibration' pressure (16 barg) by the ratio SMYS/ $\sigma_h$ . These maximum pressures corresponded to the planned maximum pressure in the pressure cycle for each defect. The intention was to cycle the vessel using the lowest of these maxima, so that the other defects would not be overstressed. After failure of the first defect, the maximum pressure could be increased if necessary to that calculated for the next lowest defect.

The minimum pressure in the pressure cycle was initially set at 10 barg, and the test started. The maximum pressure was set at 33.3 barg, based on the strain gauge readings for the most onerous defect, D3. The strain gauge readings from the first full pressure cycle were re-analyzed to confirm elastic behavior in the remaining ligament of defect D3 (i.e., linear pressure v strain load and unload history) and to confirm earlier calculations of maximum pressure for the other defects.

After almost 100,000 pressure cycles of 23.3 bar range, the minimum pressure was decreased to 8.5 barg, the lowest possible pressure whilst avoiding un-necessary lag in the pressure reversal and ensuring optimum cyclic test frequency. This increased the pressure range. In addition, the maximum pressure for each defect was increased; the maximum pressure being of sufficient magnitude to give a hoop stress equal to the material's measured yield strength of 390 N/mm<sup>2</sup> (see Appendix A, Test N.R7133 Heat N.990178, transverse oriented tensile test). Testing resumed based on the updated minimum and maximum pressures.

The minimum and maximum pressures in the pressure cycle for each defect are given in Table 17.

## **4.4 Test results**

When a fatigue crack had grown through the pipe wall due to pressure cycling, the test was temporarily stopped, the vessel drained, and the defect area repaired. The fatigue life associated with that defect was then logged and testing was resumed once the vessel was re-filled. To enable the fatigue life of each defect to be determined, repairs were undertaken on each occurrence of a crack growing through the pipe wall.

The repair method used was to flame cut out a pup piece containing the defect, of length just greater than the defect length and butt weld the two remaining pipe sections together. The procedure is shown schematically in Figure 25.

The test started with minimum and maximum pressures of 10.0 and 33.3 barg (pressure range of 23.3 bar), where 33.3 barg was predicted to give a hoop stress in defect 3 equal to the material's specified minimum yield strength. After 98,951 cycles, the minimum pressure was decreased to 8.5 barg and the maximum pressure was increased to 39.9 barg (pressure range of 31.4 bar). The increase in maximum pressure increased the hoop stress in defect 3 to equal the material's measured yield strength. Defect 3 endured a further 229,071 cycles before failure occurred.

Defect 2 was predicted to fail next. The minimum pressure remained at 8.5 barg, but the maximum pressure was increased to 52.2 barg, giving a pressure range of 43.7 bar. The maximum pressure corresponded to a hoop stress in defect 2 equal to the material's measured yield strength. In addition to the previous pressure regimes and corresponding number of cycles, defect 2 endured a further 447,344 cycles of 43.7bar pressure range before failure occurred.

Defect 4 was predicted to fail next. The minimum pressure remained at 8.5 barg, but the maximum pressure in the cycle was increased to 62.9 barg, giving a pressure range of 54.4 bar. The maximum pressure corresponded to a hoop stress in defect 4 equal to the material's measured yield strength. In addition to the previous pressure regimes and corresponding number of cycles, defect 4 endured a further 100,575 cycles of 54.4bar pressure range before failure occurred.

With only defect 1 remaining, the maximum pressure in the pressure cycle was increased to 94.3 barg, giving a pressure range of 85.8 bar with the minimum pressure



remaining at 8.5 barg. Again, the maximum pressure corresponded to a hoop stress in defect 1 equal to the material's measured yield strength. In addition to the previous pressure regimes and corresponding number of cycles, defect 1 endured a further 370,419 cycles of 85.8 bar pressure range before the test was terminated due to a failure in the pipework of the pressurization system.

The test results are summarized in Table 18.

## **4.5 Metallurgical examination**

The pipe sections were examined, and sectioned to remove the through thickness length of the crack (generally shorter in the inner surface). After sectioning the crack sections were opened. Where necessary, the sections were cooled in liquid nitrogen and a sharp hammer blow was applied to fracture any remaining ligament to expose the crack surfaces.

The crack faces were examined by eye and using a stereo optical microscope. Images were taken as opened, and after cleaning of deposits by immersion in an inhibited acid solution (Clark's solution). For defect D3, see Figure 26, for D2 see Figure 27 and for D4 see Figure 28. The crack surfaces were characteristic of low stress, high cycle fatigue crack propagation. Step markings on D3 (Figure 26) along the outer surface suggested multiple crack initiation. Beach markings on cracks D2 and D3 were consistent with crack initiation at the outer surface and crack propagation across the remaining pipe wall ligament at the defect. In contrast, for D4 multiple crack initiation sites were observed on the inner pipe surface and the crack propagated across the remaining pipe wall ligament to the outer pipe surface. This is likely to be due to the increased surface roughness on the inner surface of the pipe compared with the smooth machined finish of the patch on the outer pipe surface.

The cleaned crack surfaces were examined using a CAMSCAN S4 scanning electron microscope to confirm the mode of failure. For defect D3 see Figure 29, for D2 see Figure 30 and for D4 see Figure 31. The appearance of all crack faces was very similar, consistent with transgranular separation with crack propagation on multiple fine scale paths. Fine striations were also visible at high magnification. These observations are characteristic of low stress, high cycle fatigue crack propagation. On cracks D2 and D3, numerous secondary cracks were also visible towards the inner surface, orientated perpendicular to the direction of crack propagation. These secondary cracks are also characteristic of low stress, high cycle fatigue crack propagation, and are generally more apparent when crack propagation velocity is high.

## **4.6 Experimental Stress Concentration Factors**

Experimental stress concentration factors have been obtained from the strain gauge readings for comparison with the finite element predictions. Equation (3) was used to obtain the hoop stress range corresponding to the strain change during a pressure cycle. This stress range was then normalized by the corresponding nominal stress range due to the pressure swing calculated using the external diameter and the *nominal*

wall thickness of 8.4 mm. The experimental SCF values are given in Table 19. This table also shows the actual measured wall thicknesses local to the defect. A comparison of the measured SCF values and the finite element predictions is given in Section 5.2, which also considers the significance of variations in wall thickness from the nominal when evaluating the SCFs.

## 4.7 Analytical Fatigue Life Assessment

The procedures described in BS 7608 [2] have been used to calculate the fatigue life of the defects. The procedures are based on the quantitative relationship between fatigue strength (S) and the number of cycles (N) corresponding to a specific probability of failure.

The analysis is based on the maximum local hoop stress range in the defect, which for these tests was determined from strain gauges located in the defect area. The fatigue life using this approach is given by,

$$\text{Log}N = \text{Log}C_o - d\sigma - m\text{Log}S_r \quad (4)^4$$

- where, N = Number of cycles to failure
- C<sub>o</sub> = A constant relating to the mean S<sub>r</sub>-N curve
- d = Number of standard deviations below the mean
- σ = Standard deviation of Log N about the mean line
- S<sub>r</sub> = Maximum local hoop stress range (units: N/mm<sup>2</sup>)
- m = The inverse slope of the Log S<sub>r</sub> versus Log N curve

Despite the mild corrosion on the surface of the defects, for these assessments the Class B fatigue design curve was considered appropriate as it is considered representative of a plate with mill scale or an equivalent rough surface finish. The constants C<sub>o</sub>, σ and m are 15.3697, 0.1821 and 4.0 respectively. Logarithms are to base 10.

For each defect, fatigue life has been calculated based on the mean S-N curve (representative of a 50% probability of survival), 1 standard deviation below the mean (representative of an 84% probability of survival) and 1 standard deviation above the mean (representative of a 16% probability of survival). The predicted fatigue lives for each defect are given in Table 20.

## 4.8 Comparison of Actual and Predicted Fatigue Lives

As discussed in Section 4.4, each defect was subjected to two or more pressure ranges during the fatigue test. To enable a direct comparison with the predicted fatigue lives in

<sup>4</sup> The equation taken from BS 7608:1993 contains a typographical error in the British Standard document. The original equation, expressed as  $\log(N) = \log(C_o) - (d/\sigma) - m \log(S_r)$  is shown in its corrected form above.



Table 20, the equivalent number of pressure cycles ( $N_{eq}$ ) corresponding to the final test pressure range ( $\Delta P$ ) for each defect is determined from,

$$N_{eq} = N_1 \left( \frac{\Delta P_1}{\Delta P} \right)^m + N_2 \left( \frac{\Delta P_2}{\Delta P} \right)^m + N_3 \left( \frac{\Delta P_3}{\Delta P} \right)^m + \dots N_n \left( \frac{\Delta P_n}{\Delta P} \right)^m \quad (5)$$

where,  $N_{eq}$  = Number of cycles to failure of  $\Delta P$   
 $\Delta P$  = Pressure range for which N is to be calculated  
 $\Delta P_{1,2,3,\dots,n}$  = Pressure range for stage 1, 2, 3.....n  
 $N_{1,2,3,\dots,n}$  = Number of cycles for stages 1, 2, 3.....n  
 $M$  = The inverse slope of the Log  $S_r$  versus Log N curve (see [2])

The actual and predicted fatigue lives for each defect are compared in Table 21.

As can be seen from Table 21, with the exception of defect D3 (groove,  $d/t_{max}=0.57$ ), the actual fatigue life of each defect is equivalent to, or greater than the predicted fatigue life based on the mean +1 standard deviation Class B S-N curve. The actual fatigue life of defect D3 was equivalent to the predicted fatigue life based on the mean Class B S-N curve.

## 5 DISCUSSION

### 5.1 Interpolation in Finite Element Results

The finite element analysis has generated “point” values of the SCF associated with corrosion defects for the specific dimensions modeled. For practical application a method of obtaining SCF values for intermediate dimensions is needed. It was noted in Section 3.5 above that the effects of the transition radius and pipe D/t ratio were small. Therefore attempts to fit an equation to the SCF data were concentrated on the main set of results for  $D/t = 72$  and  $r/t = 1$ , as presented in Table 1 to Table 4.

Unfortunately it has not been possible to fit a closed form equation to the numerical results to an acceptable degree of accuracy. The best fit only achieved an error of about 45% when the range of circumferential defect half-lengths was restricted to 50 mm or less. Essentially this restricted the fitting to pits and axial grooves.

An insight into the reason why the fitting is difficult can be obtained from Figure 32 to Figure 35. These show the results plotted as a surface on axes of defect axial half-length and circumferential half-length. For shallow defects, Figure 32 and Figure 33 show a similar pattern, with high SCF values for low circumferential lengths, and a lower plateau for patches. There is a dip down to low values for low axial lengths, as these are circumferential grooves. As the defect depth increases, the shape of the surface becomes more complex, as shown in Figure 34 and Figure 35. A “valley” appears for circumferential groove defects, where the axially shortest grooves have higher SCFs

than slightly longer grooves. This is because for grooves which are long circumferentially but short axially, the SCF due to the axial end force is higher than the SCF due to the hoop stress. The changing relationship between the different factors controlling the SCF produces a complex surface which cannot readily be represented by a combination of simple functions.

An alternative approach for consideration in future work would be to fit surfaces to the hoop and axial stress results separately and then use the greater value to assess the defect. This approach would also have the advantage that the effect of axial cyclic stressing could be considered separately from that due to pressure cycling. The present work has assumed that the axial pressure cycle would be half the hoop stress cycle, as occurs in a pressure vessel. In a buried pipeline which is fully axially restrained, the axial stress range due to a pressure variation would only be 0.3 \* hoop stress range, producing less fatigue damage.

Hence the approach currently recommended is to interpolate linearly in the results tables to obtain intermediate values.

When interpolating in the results tables, the defect circumferential and axial lengths must be normalized to take account of the differences in pipe diameter and thickness. For the circumferential direction, the most appropriate normalization is considered to be the angle subtended by the defect. This approach is used in models for the net section stress of a circumferential crack, for example the solution due to Kastner [13] which is used in BS 7910 [3]. As the angle subtended by an arc of a circle is equal to the arc length divided by the radius, it can easily be shown that the circumferential length to be used for the interpolation,  $C_{int}$ , is given by:

$$C_{int} = CCL_{test} \frac{D_{scf}}{D_{test}} \quad (6)$$

where  $CCL_{test}$  is the circumferential extent of the defect in the test pipe,  $D_{scf}$  is the diameter used in the finite element model, 914 mm, and  $D_{test}$  is the test pipe diameter, 324 mm.

For the axial length direction, the possible normalizations are using the wall thickness, the diameter or the parameter  $\sqrt{(Dt)}$ , which is used in the theory of cylindrical shells [14] and in the Folias bulging factor [15] used for assessing corrosion defects. Hence the axial length for the interpolation  $A_{int}$  is given by:

$$A_{int} = ACL_{test} \frac{\sqrt{D_{scf} * t_{scf}}}{\sqrt{D_{test} * t_{test}}} \quad (7)$$

where  $t_{scf}$  is the wall thickness used in the finite element model and  $t_{test}$  the test pipe wall thickness.

## **5.2 Comparison of Strain Gauge and Finite Element Results**

This section presents a comparison of the experimental and numerical SCFs and also presents the results of limited further work carried out to investigate the effects of wall thickness tolerances in seamless pipe.

### **5.2.1 Comparisons**

The experimentally determined SCFs have been compared against the finite element model predictions. This has been done by a three way linear interpolation in the main set of results for the  $D/t = 72$  case, with the transition radius equal to the wall thickness. These results are presented in Table 1 to Table 4. These results have been used as they cover the widest range of geometry and the investigation of other cases described in Section 3.4.4 showed that varying the pipe geometry had a small effect on the SCF. The experiments described in Section 4 used a radius equal to the nominal wall thickness, i.e.  $r/t = 1$ , and so this is an appropriate comparison.

The interpolated and experimental SCFs are shown in Table 22. It is apparent that the experimental values are consistently below the numerical predictions when the nominal wall thickness is used, with the discrepancy increasing as the defect becomes deeper. When the actual wall thickness local to the defect is used, the discrepancies are reduced. This is because the actual thicknesses are greater than nominal; see Table 19. Hence the defects are shallower relative to the wall thickness, and so the SCF reduces. The effects of wall thickness variation and pipe geometric tolerances are considered in more detail in the next section.

It was speculated that one cause of the discrepancies between the experimental and numerical results was errors in the positioning of the gauge. The effects of averaging the strain over the active area of a strain gauge rather than taking point value were considered, as the grooves in the test vessel were relatively small. This study also considered the effect of the gauge being slightly offset circumferentially. The maximum difference, from the value at the centre point, was about 5.2% decrease in SCF and 6.6% decrease in strain, when averaged over the area of the strain gauge and offset by 1mm. Thus it was concluded that these errors are unlikely to account for all of the discrepancies.

### **5.2.2 Effects of pipe dimensional tolerances**

Two-dimensional plane strain models were developed to investigate the effect of tolerances on wall thickness on the predicted SCF values. The models were based on Defect 3 of the test vessel, with a groove 5.21 mm deep and a groove radius of 8.5 mm. The pipe outside diameter was fixed at 323.9 mm.

Figure 36 shows stress contours from models of an offset bore. The bore diameter is 305.7 mm, giving a basic wall thickness of 9.1 mm. The pressure is calculated to give a hoop stress of  $1.0 \text{ N/mm}^2$  based on these dimensions, and is the same in all three cases. In the top part of the figure, the bore is centrally located and the peak stress (equivalent to the SCF as the hoop stress is unity) at the bottom of the groove is

9.83 N/mm<sup>2</sup>. When the bore is located eccentrically giving the maximum thickness at the groove position, the SCF falls to 7.80. Note that the change in wall thickness is only about 8%, but the SCF has reduced by 21%. In the bottom part of Figure 36 the bore is offset in the opposite direction, so that the corrosion groove is now located at the minimum thickness. The SCF now increases to 12.8, an increase of 31% compared with the value for a concentric bore.

This analysis shows that eccentricity of the bore may have a significant effect on the stresses at the corrosion feature, beyond that due solely to changes in the wall thickness or the remaining ligament under the defect. In the case analyzed above the basic wall thickness changed by about 8% and the ligament under the defect by 18%, but the SCF increased by 30%. To investigate this effect further, this pipe geometry was analyzed without the corrosion groove, simulating a plain pipe with an eccentric bore. The results are shown in Figure 37. It is apparent that, even in the absence of a corrosion defect, it would be possible to obtain large local increases in stress if the pipe bore is offset by amounts allowable for seamless pipe in the basic API 5L specification [11].

The effect of varying the wall thickness of the pipe is investigated further in the results shown in Figure 38. In this case the bore is concentric with the outer diameter, but is varied to modify the wall thickness. The internal pressure loading was adjusted to maintain the nominal hoop stress at 1 N/mm<sup>2</sup> based on the outside diameter. The SCFs are shown in the figure. In this case the relative changes in the SCF are approximately the same as the changes in the remaining ligament under the groove, provided the analysis is based on the actual pipe wall thickness rather than a nominal value.

Overall, it is considered that the analyses in this section have shown that typical manufacturing tolerances on wall thickness can have a significant effect on the estimated SCF, and hence on any calculated fatigue life. This effect is likely to be greatest for seamless pipe, where the bore may be eccentric relative to the outside diameter producing a varying wall thickness. Where the pipe is formed from rolled plate or strip there is likely to be less variation in wall thickness.

It is recommended that the application of the method proposed in this report should be based on the actual wall thickness of the pipe joint in which the corrosion defect is located. If this is not possible, the minimum wall thickness should be used.

## **5.3 General Remarks**

### **5.3.1 Validity of Results**

The elastic SCF results have been compared with the similar predictions by Kim and Son [7]. The Advantica results were interpolated as described in Section 5.1 for comparison with the tabulated values in [7]. The Advantica results were above those in [7]. There did not appear to be a consistent trend to the differences. However, there are differences in the geometries analyzed, as the present work has considered essentially rectangular defects with radiused corners and a constant reduced ligament over the main area of the defect. In contrast, the defects modeled in [7] were essentially

ellipsoidal defects, so that the ligament was continuously varying. These would have been expected to have less of a stress raising effect than the constant reduced thickness defects analyzed in the present work. A further factor is that in [7] the SCF was evaluated at the root of the notch, rather than at the highest stress point. As the defects were in [7] were *internal*, rather than external, any bulging due to the internal pressure load would generate a bending stress which would reduce the stress at the notch root. In contrast, the SCF in the Advantica defects was taken on the *outer* surface, where bending due to bulging will act to increase the stress. This effect is clearly shown in Figure 9, where on the outer surface the SCF is 8.7, but on the inside it is only about 2. Thus, it is considered that the results in [7] are not at variance with those generated in the current work.

The test results suggest that the use of the Class B *design* curve from BS 7608 is conservative. The results in Section 4.8 show that the deepest groove, Defect 3, with the highest SCF, gave the lowest life relative to the predictions. In this case the experimental life was equal to the mean prediction, whilst the lower SCF grooves gave above mean predictions.

### 5.3.2 Effects of High Stress Concentration Factors

A concern is that when the elastic SCF is applied to a large hoop stress range, or the elastic SCF is itself large, the resultant local stress range may exceed SMYS. As the high stress area is contained, rather than the plasticity extending through the cross section, shakedown to elastic cycling should occur as long as the stress range does not exceed twice SMYS. If the stress range does exceed twice SMYS, cyclic plasticity will occur which may lead to a low cycle fatigue failure.

This effect is considered in Annex C of PD 5500 [16], where a plasticity correction factor is applied to stress ranges which exceed twice SMYS. The factor depends on the tensile and yield strengths of the material in addition to the stress range. As this correction is relatively complex, it is recommended that it is not used, and a simple criterion is adopted that the local stress range in the corrosion defect calculated using the elastic SCF is limited to twice SMYS.

### 5.3.3 Effect of defect circumferential size

The acceptance methods for static strength of corrosion defects such as RSTRENG [17][18] and the LPC-1 method [19] do not take account of the circumferential extent of the defect, as they require only the axial length and the defect depth. This work has shown that under cyclic loading the circumferential extent of the defect should be considered. The stress raising effect appears to be worst for deep, narrow axial defects, where there is effectively a long notch. As the circumferential size increases, the SCF drops to a plateau level.

Thus, if there is linepacking the restrictions on circumferential size may be more onerous than if there is only static pressure. It is recommended that the results obtained in this work be further analyzed to determine screening criteria to highlight the areas where acceptable defect sizes are obtained.

### 5.3.4 Recommended Fatigue Assessment Code

The approach developed in this project is to combine the stress raising effect of the corrosion defect with a S–N curve for the material and the environment. As discussed in Section 2.1, the determination of fatigue lives in corrosive conditions is complex. If an appropriate S–N curve is available for the material and the environment, this should be used.

In most cases, it is unlikely that detailed guidance will be available. For ferritic steels, general guidance is available in BS 7608 [2]. This places different welded details into one of a set of stress – life, or S–N curves. These are presented in terms of the nominal stress range acting on a feature. For parent plate, the most appropriate class is B, described as “as rolled” plate or sections. This implies some surface roughness, which would be appropriate for a corroded surface. The mean minus two standard deviations (i.e. approximately 1 in 40 failure probability) S–N relationship for Class B is:

$$S^4 N = 1.01 * 10^{15} \quad (8)$$

where  $S$  is the stress range in  $\text{N/mm}^2$  and  $N$  is the number of cycles to failure under constant amplitude cycling at stress range  $S$ .

Equation (8) applies to a non-corrosive environment. In freely corroding seawater, Section 4.3.3 of BS 7608 recommends that the calculated life is reduced by a factor of 2 and there is no fatigue limit, so that all stress cycles are assumed to contribute to failure. The standard cautions that this correction may not apply to high strength materials with a yield strength above  $400 \text{ N/mm}^2$ ; this would affect pipeline steels of Grade X65 or above. However, the S–N curve approach of BS 7608 has been used for quenched and tempered materials up to  $700 \text{ N/mm}^2$  yield (e.g. RQT 701), and Section 1.1 of the standard states that the scope includes steels with a specified minimum yield strength up to this level. A review carried out for the UK Health and Safety Executive [20] suggests there is no significant difference in the corrosion fatigue behavior of steel structures and weldments up to  $900 \text{ N/mm}^2$  yield strength when compared with that of lower strength structural steels. Thus it is considered that the BS 7608 approach and S–N curves are currently the best available for assessing the base fatigue life.

BS 7608 also includes a “thickness correction”. This accounts for the fact that it has been shown by experiment and by theoretical fracture mechanics analyses that the fatigue life of a *welded* joint falls as the thickness increases. Hence a penalty is applied to the predicted life where the material thickness is greater than a reference thickness. For BS 7608 the reference thickness is 16 mm, so that the thickness correction would be required for some heavier walled pipelines. A similar thickness correction is included in Annex C of the UK pressure vessel curve PD 5500 [16] but with a higher reference thickness of 22 mm. Advantica’s opinion is that the correction is over-conservative for volumetric corrosion defects, which are relatively smooth compared with the sharp notch at the toe of a fusion weld. Hence the use of this correction is not recommended.

This approach to setting the fatigue life could be considered conservative compared with the situation in a real pipeline, as the defect is introduced at full depth, with the highest SCF, at the start of life and the pressure cycling is applied to this full size. In a



real pipeline the corrosion defects would be small during the earlier parts of the lifetime, and so the SCF and the resulting fatigue damage would be less during the earlier part of the life. However, it is appropriate for the situation where a defect is discovered by inspection and is being assessed at its current size for future operation.

## 6 OUTLINE OF PROPOSED ASSESSMENT METHOD

The proposed assessment method for volumetric corrosion defects subject to cyclic pressure loading is as follows. (It is assumed that a pressure-loading spectrum of pressure ranges and the number of occurrences of each range is available either from historical SCADA data or from predictions of the future operational regime of the pipeline.)

1. Determine the diameter, actual wall thickness and grade of the joint containing the defect.
2. Determine the maximum depth, the axial length and the circumferential extent of the defect.
3. Using the interpolation method presented in Section 5.1 of this report, determine the elastic stress concentration factor.
4. Calculate the hoop stress range for the largest pressure range in the loading spectrum. Multiply this range by the SCF determined in step (3) to determine the maximum elastic stress range for the defect.
5. If the maximum elastic stress range for the defect calculated for step (4) exceeds twice the specification minimum yield strength for the pipe, shakedown to elastic cycling cannot be guaranteed and the defect is not acceptable. Remedial action is required, or the cyclic loading must be reduced by changing the operational parameters of the pipeline.
6. Carry out a conventional fatigue analysis using the hoop stress ranges calculated from the pressure spectrum multiplied by the elastic SCF from step (3). The recommended method is that given in BS 7608, using the Class B fatigue design curve corrected for a freely corroding environment.
7. Compare the calculated fatigue life with the required life of the pipeline to determine when repair is required.

## 7 CONCLUSIONS

The following main conclusions can be drawn from this work:

1. There is no available published method for assessing the life of volumetric corrosion defects under cyclic loading. An assessment method based on determining the stress raising effect of the corrosion defect combined with a S-N curve for parent plate material in a corrosive environment is proposed.

2. A wide range of defect geometries have been analyzed to determine elastic stress concentration factors which can be used to determine the effect of cyclic loading.
3. The proposed approach has been verified by a small set of fatigue tests. The experimental results were generally consistent with the predictions.

## **8 RECOMMENDATIONS**

1. Further analysis should be carried out to determine closed form equations to predict the stress raising effects of volumetric corrosion defects.
2. Additional cyclic loading tests are required to confirm the predictive method developed in this project. This should cover both the fatigue life and the stress raising effect of the defects.
3. To avoid difficulties of interpretation due to manufacturing tolerances on wall thickness, further experiments should not be carried out using seamless pipe.
4. A screening method should be developed using the results produced in this project to identify cases where cyclic loading of volumetric corrosion defects requires special consideration.



## 9 REFERENCES

- [1] API. Recommended practice for planning, designing and constructing fixed offshore platforms - working stress design API RP 2A-WSD 21st Edition. Washington: American Petroleum Institute; 2000.
- [2] BSI. Code of practice for fatigue design and assessment of steel structures BS 7608 Incorporating amendment No. 1. London: British Standards Institution; 1993.
- [3] BSI. Guide to methods for assessing the acceptability of flaws in metallic structures BS 7910:2005. London: British Standards Institution; 2005.
- [4] Vosikovsky O. Fatigue crack growth in an X65 line-pipe steel in sour crude oil. Corrosion NACE 1976;32:472-5.
- [5] Vosikovsky O, Rivard A. Effect of hydrogen sulfide in crude oil on fatigue crack growth in a pipe line steel. Corrosion NACE 1982;38(1):19-22.
- [6] ASME. Case N-597-2 Requirements for analytical evaluation of pipe wall thinning, Section XI, Division 1. New York: American Society of Mechanical Engineers; 2003.
- [7] Kim Y-J, Son B-G. Finite element based stress concentration factors for pipes with local wall thinning. International Journal of Pressure Vessels and Piping 2004;81:897-906.
- [8] MSC/PATRAN 2001 r3, MacNeal-Schwendler Corporation.
- [9] ASME B31G. Manual for Determining the Remaining Strength of Corroded Pipelines A Supplement to ASME B31 Code for Pressure Piping, American Society of Mechanical Engineers, 1991.
- [10] ABAQUS/Standard Version 6.4, Hibbitt, Karlsson & Sorensen Inc., 2003.
- [11] API Specification 5L, 'Specification for line pipe', 43<sup>rd</sup> Edition, March 2004, American Petroleum Institute, USA.
- [12] 'Specification for flat products made of steels for pressure purposes. Part 3: Weldable fine grain steels, normalized', British Standards Institution, BS EN 10028-3, 2003.
- [13] Kastner W, Roehrich E, Schmitt W, Steinbuch R. Critical crack sizes in ductile piping. International Journal of Pressure Vessels and Piping 1981;9:197-219.
- [14] Timoshenko SP, Woinowsky-Krieger S. Theory of plates and shells, 2nd edition. New York: McGraw-Hill; 1959.
- [15] Folias ES. Failure correlation between cylindrical pressurized vessels and flat plates. International Journal of Pressure Vessels and Piping 1999;76:803-11.
- [16] BSI. Unfired fusion welded pressure vessels PD 5500. London: British Standards Institution; 2006
- [17] Kiefner JF and Veith PH: 'A Modified Criterion for Evaluating the Remaining Strength of Corroded Pipe', Final Report on PR-3-805 to the Pipeline Research Committee of the American Gas Association, Battelle, Ohio, 1989

- [18] Vieth PH and Kiefner JF: 'RSTRENG2 User's Manual, Final report on PR-218-9205 to Corrosion Supervisory Committee, Pipeline Research Committee, American Gas Association, Kiefner & Associates, Inc., Ohio, 1993
- [19] Fu, B. and Batte, A.D. 'Advanced Methods for the Assessment of Corrosion in Linepipe'. Summary Report OTO 97065, UK Health and Safety Executive
- [20] Healy J and Billingham J: A review of the corrosion fatigue behaviour of structural steels in the strength range 350-900 MPa and associated high strength weldments. HSE Offshore Technology Report OTH 97 532. London: HSE Books; 1997

<b>CCL (mm)</b>	<b>ACL (mm)</b>					
	<b>13</b>	<b>20</b>	<b>50</b>	<b>100</b>	<b>200</b>	<b>500</b>
<b>13</b>	1.77	1.89	2.19	2.32	2.35	2.37
<b>20</b>	1.66	1.76	2.03	2.19	2.25	2.30
<b>50</b>	1.63	1.70	1.86	1.97	2.02	2.11
<b>100</b>	1.60	1.67	1.79	1.84	1.85	1.90
<b>200</b>	1.60	1.66	1.77	1.81	1.79	1.80
<b>500</b>	1.66	1.70	1.82	1.86	1.82	1.80

Table 1. SCF for 914.4 mm x 12.7 mm pipe with CD = 20%t (r/t=1)

<b>CCL (mm)</b>	<b>ACL (mm)</b>					
	<b>13</b>	<b>20</b>	<b>50</b>	<b>100</b>	<b>200</b>	<b>500</b>
<b>13</b>	2.16	2.59	3.68	4.39	4.70	4.90
<b>20</b>	2.04	2.32	3.22	3.95	4.32	4.58
<b>50</b>	2.04	2.22	2.69	3.13	3.35	3.64
<b>100</b>	2.17	2.24	2.59	2.85	2.86	2.99
<b>200</b>	2.21	2.21	2.58	2.84	2.83	2.80
<b>500</b>	2.11	2.21	2.57	2.83	2.84	2.83

Table 2. SCF for 914.4 mm x 12.7 mm pipe with CD = 40%t (r/t=1)

<b>CCL (mm)</b>	<b>ACL (mm)</b>					
	<b>13</b>	<b>20</b>	<b>50</b>	<b>100</b>	<b>200</b>	<b>500</b>
<b>13</b>	2.44	3.26	5.66	8.14	9.74	10.70
<b>20</b>	2.18	2.58	4.22	6.24	7.67	8.70
<b>50</b>	2.68	2.59	3.39	4.41	5.09	5.52
<b>100</b>	3.64	2.78	3.39	4.29	4.59	4.61
<b>200</b>	4.05	3.16	3.37	4.34	4.64	4.62
<b>500</b>	3.95	2.99	3.33	4.30	4.62	4.59

Table 3. SCF for 914.4 mm x 12.7 mm pipe with CD = 60%t (r/t=1)

<b>CCL (mm)</b>	<b>ACL (mm)</b>							
	<b>13</b>	<b>20</b>	<b>50</b>	<b>100</b>	<b>200</b>	<b>350</b>	<b>500</b>	<b>800</b>
<b>13</b>	2.74	4.08	7.94	13.90	19.80	21.90	23.30	25.4
<b>20</b>	2.31	2.79	5.11	8.87	12.70	13.70	14.60	
<b>50</b>	3.40	3.00	5.40	6.84	8.95	8.71	8.94	
<b>100</b>	5.43	3.62	5.34	6.34	8.69	9.10	8.77	
<b>200</b>	7.35	4.91	5.46	6.50	8.35	8.70	8.98	
<b>500</b>	8.43	5.13	5.42	6.69	8.55	8.77	8.70	

Table 4. SCF for 914.4 mm x 12.7 mm pipe with CD = 80%t (r/t=1)

<b>CCL (mm)</b>	<b>ACL (mm)</b>					
	<b>13</b>	<b>20</b>	<b>50</b>	<b>100</b>	<b>200</b>	<b>500</b>
<b>13</b>	2.70	4.17	7.98	13.90	19.80	23.30
<b>20</b>	2.23	2.94	5.15	8.90	12.70	14.60
<b>50</b>	2.13	2.68	5.40	6.76	9.10	8.98
<b>100</b>	2.17	2.72	4.96	6.51	9.23	9.12
<b>200</b>	2.22	2.80	4.95	6.56	8.97	9.75
<b>500</b>	2.29	2.87	4.95	6.66	9.01	8.96

Table 5. SCF for 914.4 mm x 12.7 mm pipe with CD = 80%t (r/t=1) and without 'capped end force'

<b>CCL (mm)</b>	<b>ACL (mm)</b>					
	<b>13</b>	<b>20</b>	<b>50</b>	<b>100</b>	<b>200</b>	<b>500</b>
<b>13</b>	1.83	1.96	2.25	2.39	2.44	2.49
<b>20</b>	1.82	1.91	2.18	2.34	2.40	2.45
<b>50</b>	1.78	1.84	2.00	2.11	2.16	2.25
<b>100</b>	1.74	1.80	1.91	1.95	1.96	2.02
<b>200</b>	1.73	1.79	1.90	1.93	1.91	1.91
<b>500</b>	1.73	1.79	1.90	1.93	1.91	1.91

Table 6. SCF for 914.4 mm x 12.7 mm pipe with CD = 20%t (r/t=0.5)

<b>CCL (mm)</b>	<b>ACL (mm)</b>					
	<b>13</b>	<b>20</b>	<b>50</b>	<b>100</b>	<b>200</b>	<b>500</b>
<b>13</b>	2.34	2.69	3.72	4.50	4.86	5.11
<b>20</b>	2.22	2.47	3.30	4.04	4.43	4.75
<b>50</b>	2.24	2.43	2.84	3.28	3.48	3.81
<b>100</b>	2.27	2.45	2.81	3.09	3.08	3.20
<b>200</b>	2.24	2.41	2.75	3.02	3.02	2.99
<b>500</b>	2.24	2.40	2.76	3.04	3.04	3.02

Table 7. SCF for 914.4 mm x 12.7 mm pipe with CD = 40%t (r/t=0.5)

Corrosion Defect Size ACL x CCL (mm)	Max. Principal Stress (N/mm <sup>2</sup> )	Stresses (N/mm <sup>2</sup> )		
		Axial	Circumferential	Radial
13x13	2.74	1.33	2.71	0.03
13x20	2.31	1.56	2.29	0.01
13x50	3.4	3.39	2.00	0.01
13x100	5.43	5.43	2.86	0.02
13x200	7.35	7.34	3.91	0.02
13x500	8.43	8.43	4.37	0.10
20x13	4.08	1.26	4.08	0.00
20x20	2.79	1.21	2.79	0.02
20x50	3	HMPS occurs at the middle of corrosion corner		
20x100	3.62	3.62	2.58	0.00
20x200	4.91	4.91	3.50	0.00
20x500	5.13	5.13	3.75	0.00
50x13	7.94	1.87	7.94	0.00
50x20	5.11	1.16	5.11	0.00
50x50	5.4	3.36	5.40	0.00
50x100	5.34	0.93	5.34	-0.02
50x200	5.46	1.18	5.46	-0.02
50x500	5.42	1.13	5.42	-0.02
100x13	13.9	3.53	13.87	0.00
100x20	8.87	2.07	8.86	0.08
100x50	6.84	1.95	6.84	0.00
100x100	6.34	1.85	6.34	0.03
100x200	6.5	2.06	6.49	0.06
100x500	6.69	1.95	6.68	0.09
200x13	19.8	5.88	19.82	-0.01
200x20	12.7	3.78	12.69	0.11
200x50	8.95	2.85	8.94	0.07
200x100	8.69	2.96	8.67	0.07
200x200	8.35	2.94	8.34	0.08
200x500	8.55	2.81	8.54	0.11
500x13	23.3	7.42	23.34	-0.01
500x20	14.6	4.89	14.63	0.12
500x50	8.94	3.08	8.92	0.07
500x100	8.77	3.21	8.76	0.08
500x200	8.98	3.30	8.97	0.09
500x500	8.7	2.92	8.68	0.10

Table 8. Axial, circumferential and radial stress at locations of HMPS for 914.4 mm x 12.7 mm pipe with 80% of w/t corrosion depth (r/t = 1)

Corrosion Defect Size ACL x CCL (mm)	Max. Principal Stress (N/mm <sup>2</sup> )	Stresses (N/mm <sup>2</sup> )		
		Axial	Circumferential	Radial
13x13	1.77	0.87	1.76	0.04
13x20	1.66	0.89	1.65	0.04
13x50	1.63	0.93	1.62	0.04
13x100	1.60	1.01	1.58	0.05
13x200	1.60	1.01	1.57	0.06
13x500	1.66	0.92	1.65	0.03
20x13	1.89	0.88	1.88	0.04
20x20	1.76	0.89	1.75	0.04
20x50	1.70	0.92	1.69	0.04
20x100	1.67	0.92	1.66	0.04
20x200	1.66	0.91	1.65	0.03
20x500	1.70	0.91	1.69	0.03

Table 9. Axial, circumferential and radial stress at locations of HMPS for 914.4 mm x 12.7 mm pipe with 20% of w/t corrosion depth (r/t = 1)

Corrosion Defect Size ACL x CCL (mm)	Max. Principal Stress (N/mm <sup>2</sup> )	Stresses (N/mm <sup>2</sup> )		
		Axial	Circumferential	Radial
13x13	2.16	1.14	2.15	0.04
13x20	2.04	1.22	2.02	0.05
13x50	2.04	1.51	1.98	0.04
13x100	2.17	2.16	1.70	0.01
13x200	2.21	2.20	1.73	0.01
13x500	2.11	2.10	1.70	0.01
20x13	2.59	1.17	2.58	0.03
20x20	2.32	1.19	2.30	0.04
20x50	2.22	1.40	2.10	0.07
20x100	2.24	1.43	2.11	0.07
20x200	2.21	1.39	2.09	0.07
20x500	2.21	1.38	2.09	0.07

Table 10. Axial, circumferential and radial stress at locations of HMPS for 914.4 mm x 12.7 mm pipe with 40% of w/t corrosion depth (r/t = 1)

CD (%t)	CCL (mm)	ACL (mm)					
		13	20	50	100	200	500
20	13	3.39	3.70	2.74	3.02	3.83	5.06
	20	9.64	8.52	7.39	6.85	6.67	6.52
	50	9.20	8.24	7.53	7.11	6.93	6.64
	100	8.75	7.78	6.70	5.98	5.95	6.32
	200	8.12	7.83	7.34	6.63	6.70	6.11
	500	4.22	5.29	4.40	3.76	4.95	6.11
40	13	8.33	3.86	1.09	2.51	3.40	4.29
	20	8.82	6.47	2.48	2.28	2.55	3.71
	50	9.80	9.46	5.58	4.79	3.88	4.67
	100	4.61	9.38	8.49	8.42	7.69	7.02
	200	1.36	9.05	6.59	6.34	6.71	6.79
	500	6.16	8.60	7.39	7.42	7.04	6.71

Table 11. Percentage increase in SCF as transition radius decreases from  $r/t = 1.0$  to  $r/t = 0.5$

CD (%t)	CCL (mm)	ACL (mm)					
		13	20	50	100	200	500
20	13	1.70	1.84	2.12	2.22	2.26	2.30
	20	1.65	1.76	2.01	2.13	2.18	2.24
	50	1.64	1.71	1.85	1.90	1.94	2.02
	100	1.62	1.69	1.79	1.79	1.79	1.82
	200	1.60	1.67	1.78	1.78	1.78	1.77
	500	1.63	1.69	1.81	1.82	1.81	1.84
40	13	2.2	2.66	3.76	4.33	4.55	4.74
	20	2.07	2.38	3.27	3.83	4.07	4.34
60	13	2.52	3.4	6.01	8.16	9.1	9.97
	20	2.27	2.74	4.59	6.3	7.06	7.9
80	13	2.93	4.37	8.91	14.9	18.2	20.5
	20	2.75	3.03	6.12	9.88	11.7	12.8

Table 12. SCF for 508 mm x 12.7 mm pipe with  $r/t = 1$



CD (%t)	CCL (mm)	ACL (mm)					
		13	20	50	100	200	500
20	13	1.71	1.85	2.14	2.29	2.33	2.36
	20	1.68	1.78	2.05	2.23	2.29	2.33
40	13	2.16	2.58	3.67	4.42	4.80	4.99
	20	2.03	2.30	3.18	3.97	4.43	4.68
60	13	2.41	3.20	5.50	8.02	9.99	11.00
	20	2.15	2.52	4.05	6.11	7.92	9.07
80	13	2.76	3.98	7.51	13.10	20.20	24.70
	20	2.59	2.79	4.70	8.35	12.90	15.40

Table 13. SCF for 1270 mm x 12.7 mm pipe with  $r/t = 1$

CD (%t)	CCL (mm)	ACL (mm)					
		13	20	50	100	200	500
20	13	-3.95	-2.65	-3.20	-4.31	-3.83	-2.95
	20	-0.60	0.00	-0.99	-2.74	-3.11	-2.61
40	13	1.85	2.70	2.17	-1.37	-3.19	-3.27
	20	1.47	2.59	1.55	-3.04	-5.79	-5.24
60	13	3.28	4.29	6.18	0.25	-6.57	-6.82
	20	4.13	6.20	8.77	0.96	-7.95	-9.20
80	13	6.93	7.11	12.22	7.19	-8.08	-12.02
	20	19.05	8.60	19.77	11.39	-7.87	-12.33

Table 14. SCF percentage increase for 508 mm x 12.7 mm pipe over 914.4 mm x 12.7 mm pipe with the same defect depth, expressed as a percentage

CD (%t)	CCL (mm)	ACL (mm)					
		13	20	50	100	200	500
20	13	-3.39	-2.12	-2.28	-1.29	-0.85	-0.42
	20	1.20	1.14	0.99	1.83	1.78	1.30
40	13	0.00	-0.39	-0.27	0.68	2.13	1.84
	20	-0.49	-0.86	-1.24	0.51	2.55	2.18
60	13	-1.23	-1.84	-2.83	-1.47	2.57	2.80
	20	-1.38	-2.33	-4.03	-2.08	3.26	4.25
80	13	0.73	-2.45	-5.42	-5.76	2.02	6.01
	20	12.12	0.00	-8.02	-5.86	1.57	5.48

Table 15. SCF percentage increase for 1270 mm x 12.7 mm pipe over 914.4 mm x 12.7 mm pipe with the same defect depth, expressed as a percentage

Defect	Type	Defect dimensions			
		d/t*	L (mm)	r (mm)	W (mm)
D1	Groove	0.22 (0.2)	399.0 (400)	8.5 (8.5)	11.2 (10.1)
D2	Groove	0.40 (0.4)	404.5 (400)	8.5 (8.5)	13.9 (13.5)
D3	Groove	0.57 (0.6)	405.8 (400)	8.5 (8.5)	16.2 (15.5)
D4	Patch	0.68 (0.6)	398.5 (400)	8.5 (8.5)	137.8 (140)

**Notes:** \* denotes maximum defect depth measured (see Appendix B), dimensions in ( ) are target dimensions, **t** is pipe wall thickness, **d** is defect depth, **L** and **W** are defect length and width in the pipe axial and circumferential directions respectively (measured along the outer surface of the pipe) and **r** is the blend radius.

Table 16. Comparison of target and actual defect dimensions

Defect	Pressure limits		Pressure range	Stress range
	P <sub>min</sub> bar	P <sub>max</sub> bar	ΔP bar	Δσ N/mm <sup>2</sup>
D1 – Groove (d/t <sub>max</sub> =0.22)	8.5	94.3	85.8	354.8
D2 – Groove (d/t <sub>max</sub> =0.40)	8.5	52.2	43.7	326.5
D3 – Groove (d/t <sub>max</sub> =0.57)	8.5	39.9	31.4	306.8
D4 – Patch (d/t <sub>max</sub> =0.68)	8.5	62.9	54.4	337.3

**Note:** The vessel was initially pressure cycled between P<sub>min</sub> and P<sub>max</sub> limits of 10.0 and 33.3 barg for 98,951 cycles before the limits were adjusted to those shown above. The stress range is calculated from the strain gauge data.

Table 17. Minimum and maximum pressures in the pressure cycle for each defect

Defect	Number of cycles for a given pressure range ( $\Delta P$ )				
	23.3bar	31.4bar	43.7bar	54.4bar	85.8bar
D3 – Groove ( $d/t_{\max}=0.57$ )	98,951	229,071			
D2 – Groove ( $d/t_{\max}=0.40$ )	98,951	229,071	447,344		
D4 – Patch ( $d/t_{\max}=0.68$ )	98,951	229,071	447,344	100,575	
D1 – Groove ( $d/t_{\max}=0.22$ )	98,951	229,071	447,344	100,575	370,419

Table 18. Results: Number of cycles of each pressure range for each defect

Defect	Experimental SCF	Minimum local wall, mm	Maximum local wall, mm	Location of maximum stress
D1 – Groove	2.15	8.9	9.1	Centre
D2 – Groove	3.87	8.6	8.7	End
D3 – Groove	5.07	9.1	9.8	Centre
D4 – Patch	3.22	8.9	9.2	Centre of short (circumferential) side

Table 19. Experimental SCF results based on nominal wall thickness

Defect	$\Delta\sigma_{h(local)}$ N/mm <sup>2</sup>	Fatigue life		
		Mean +1SD	Mean	Mean -1SD
D1 – Groove (d/t <sub>max</sub> =0.22)	354.8	224,732	147,763	97,155
D2 – Groove (d/t <sub>max</sub> =0.40)	326.5	313,392	206,057	135,484
D3 – Groove (d/t <sub>max</sub> =0.57)	306.8	401,929	264,271	173,760
D4 – Patch (d/t <sub>max</sub> =0.68)	337.3	275,328	181,030	119,028

**Notes:**  $\Delta\sigma_{h(local)}$  is the hoop stress range in the defect. Values of fatigue life, **N** are given based on the mean S-N curve, and +/- 1 standard deviation about the mean curve, to represent different probabilities of survival.

Table 20. Predicted fatigue lives using the BS 7608 assessment method (Class B fatigue design curve).

Defect	$\Delta P$ bar	<b>N<sub>eq</sub></b>	<b>N<sub>BS7608</sub> (Class B)</b>	Comment
D1 – Groove (d/t <sub>max</sub> =0.22)	85.8	<b>421,423</b>	+1SD: 224,732 Mean: 147,763 -1SD: 97,155	No failure of defect
D2 – Groove (d/t <sub>max</sub> =0.40)	43.7	516,402	<b>+1SD: 313,392</b> Mean: 206,057 -1SD: 135,484	N <sub>eq</sub> >> Mean +1SD
D3 – Groove (d/t <sub>max</sub> =0.57)	31.4	259,071	+1SD: 401,929 <b>Mean: 264,271</b> -1SD: 173,760	N <sub>eq</sub> $\equiv$ Mean
D4 – Patch (d/t <sub>max</sub> =0.68)	54.4	315,614	<b>+1SD: 275,328</b> Mean: 181,030 -1SD: 119,028	N <sub>eq</sub> $\equiv$ Mean +1SD

**Notes:**  $\Delta P$  is the pressure range for the final stage of the fatigue test for the individual defect, **N<sub>eq</sub>** is the number of equivalent pressure cycles of the reference pressure range, and values of **N<sub>BS7608</sub>** are taken from Table 19.

Table 21. Comparison of actual and predicted fatigue lives.

Defect	Experimental SCF	Interpolated SCF from FEA results		
		Nominal wall	Minimum local wall	Maximum local wall
D1 – Groove	2.15	2.29	2.16	2.11
D2 – Groove	3.87	4.35	4.25	4.20
D3 – Groove	5.07	8.76	7.64	6.84
D4 – Patch	3.22	4.26	3.98	3.82

Table 22. Experimental and interpolated numerical SCF values for varying wall thicknesses

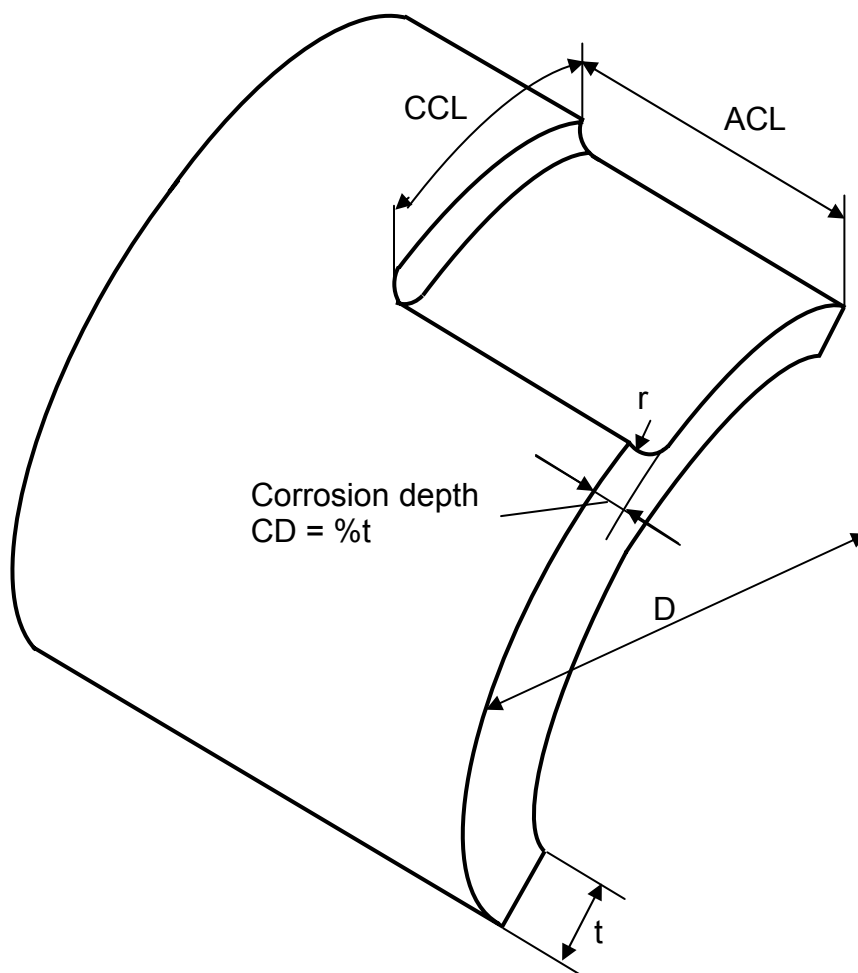


Figure 1. Geometrical Definition of Corroded Pipe

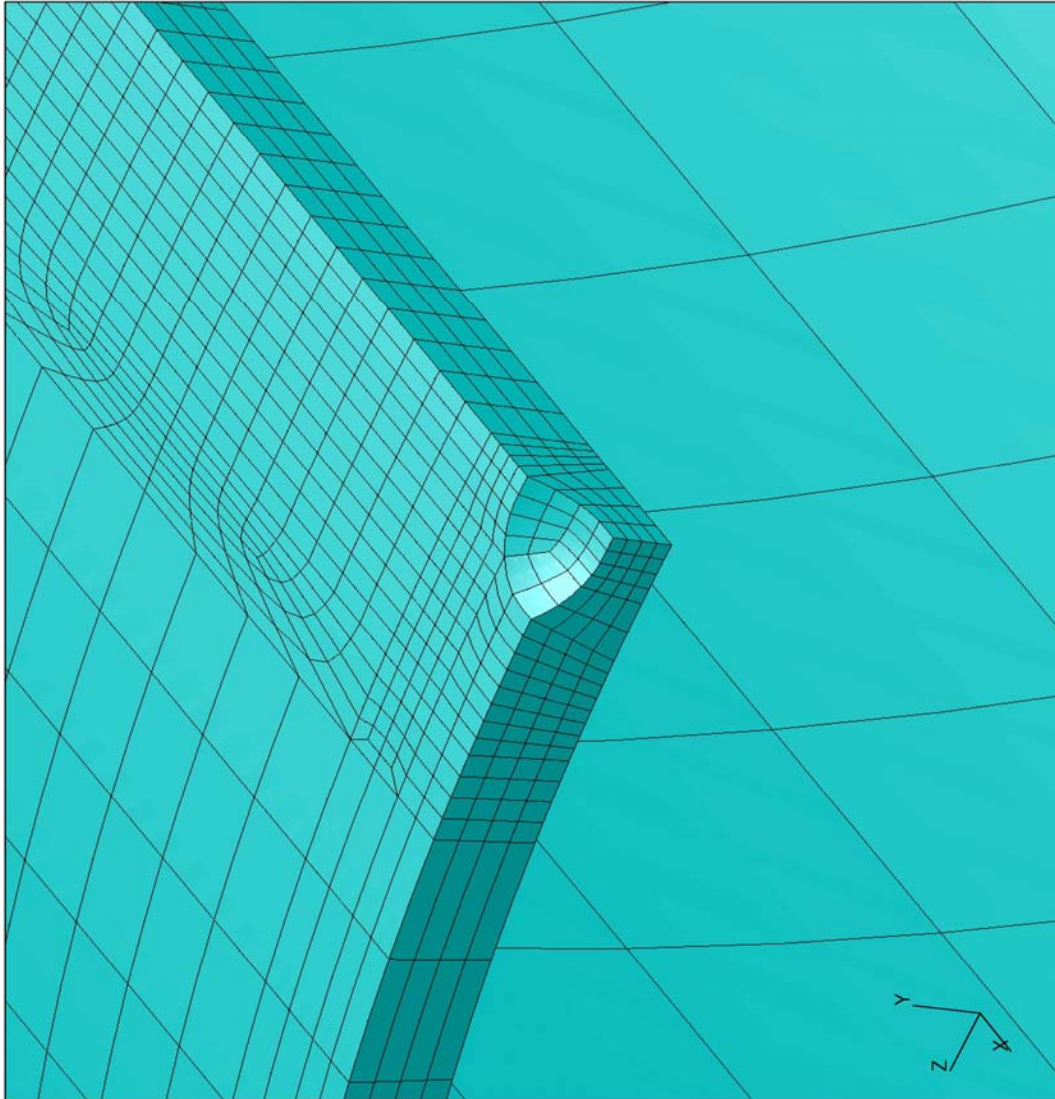


Figure 2 – Finite Element Mesh of 914.4 mm x 12.7 mm Pipe with a Corrosion Size of 13 mm x 13 mm and a Depth of 40% Wall thickness ( $r/t = 1$ )



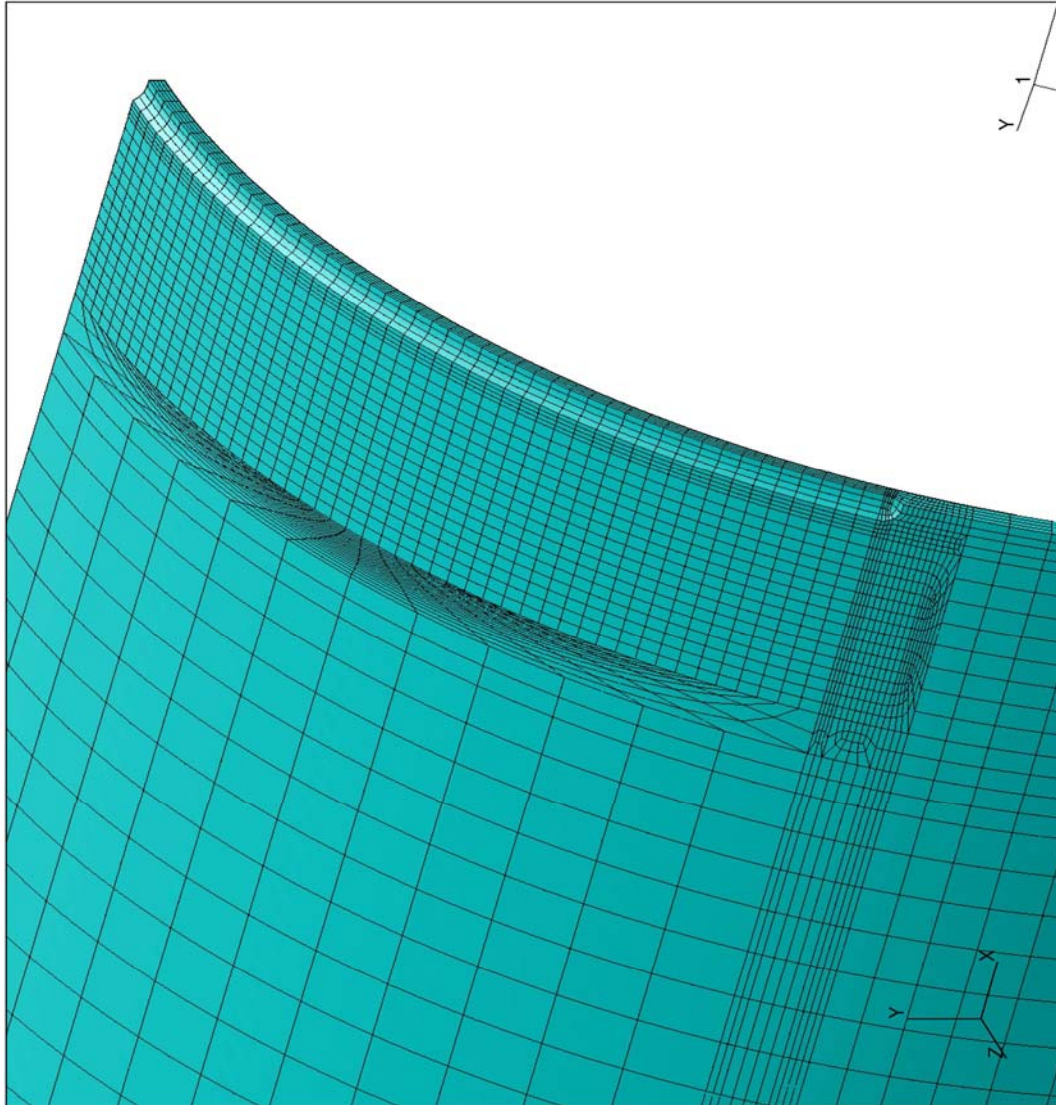


Figure 3 – Finite Element Mesh of 914.4 mm x 12.7 mm Pipe with a Corrosion Size of 13 mm x 500 mm and a Depth of 40% Wall thickness ( $r/t = 1$ )

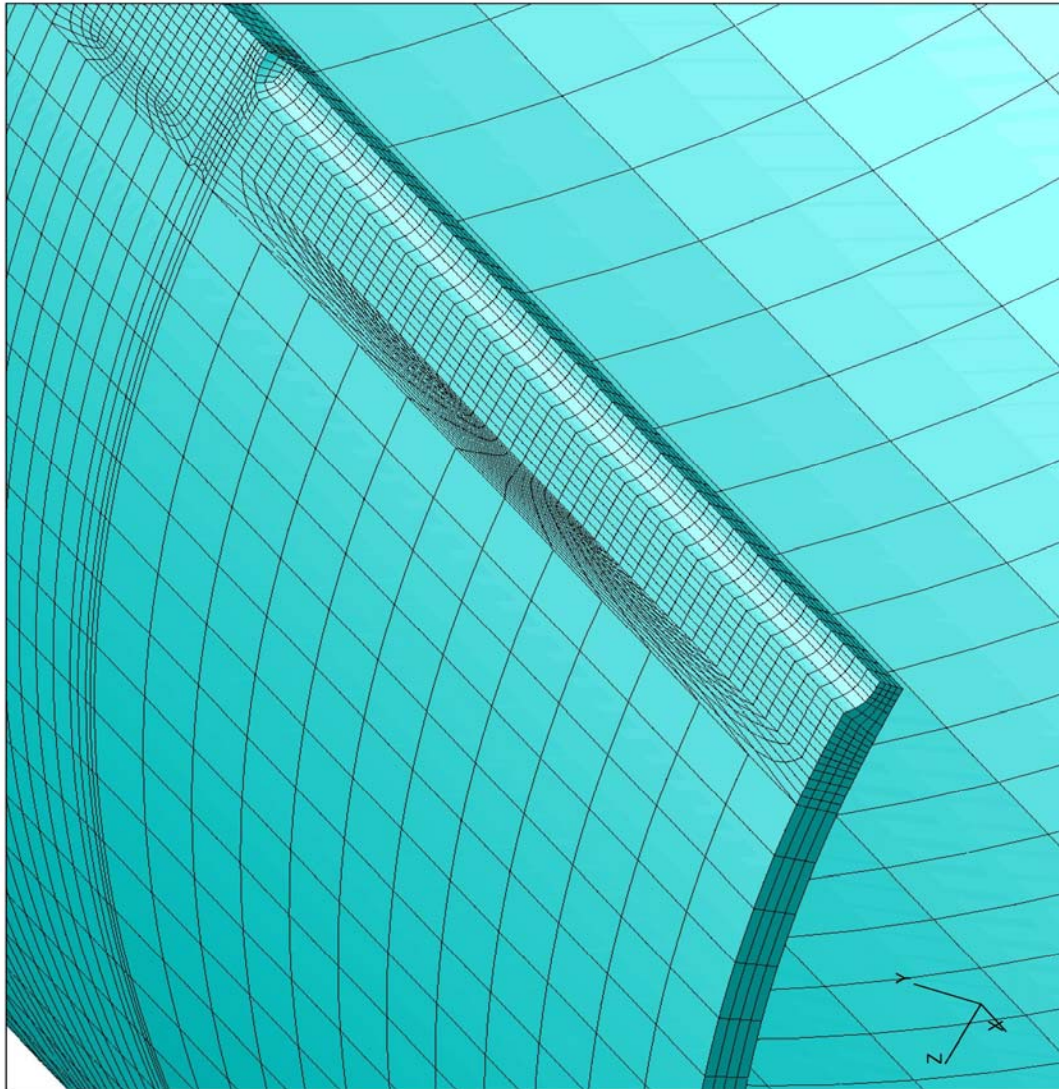


Figure 4 – Finite Element Mesh of 914.4 mm x 12.7 mm Pipe with a Corrosion Size of 500 mm x 13 mm and a Depth of 40% Wall thickness ( $r/t = 1$ )



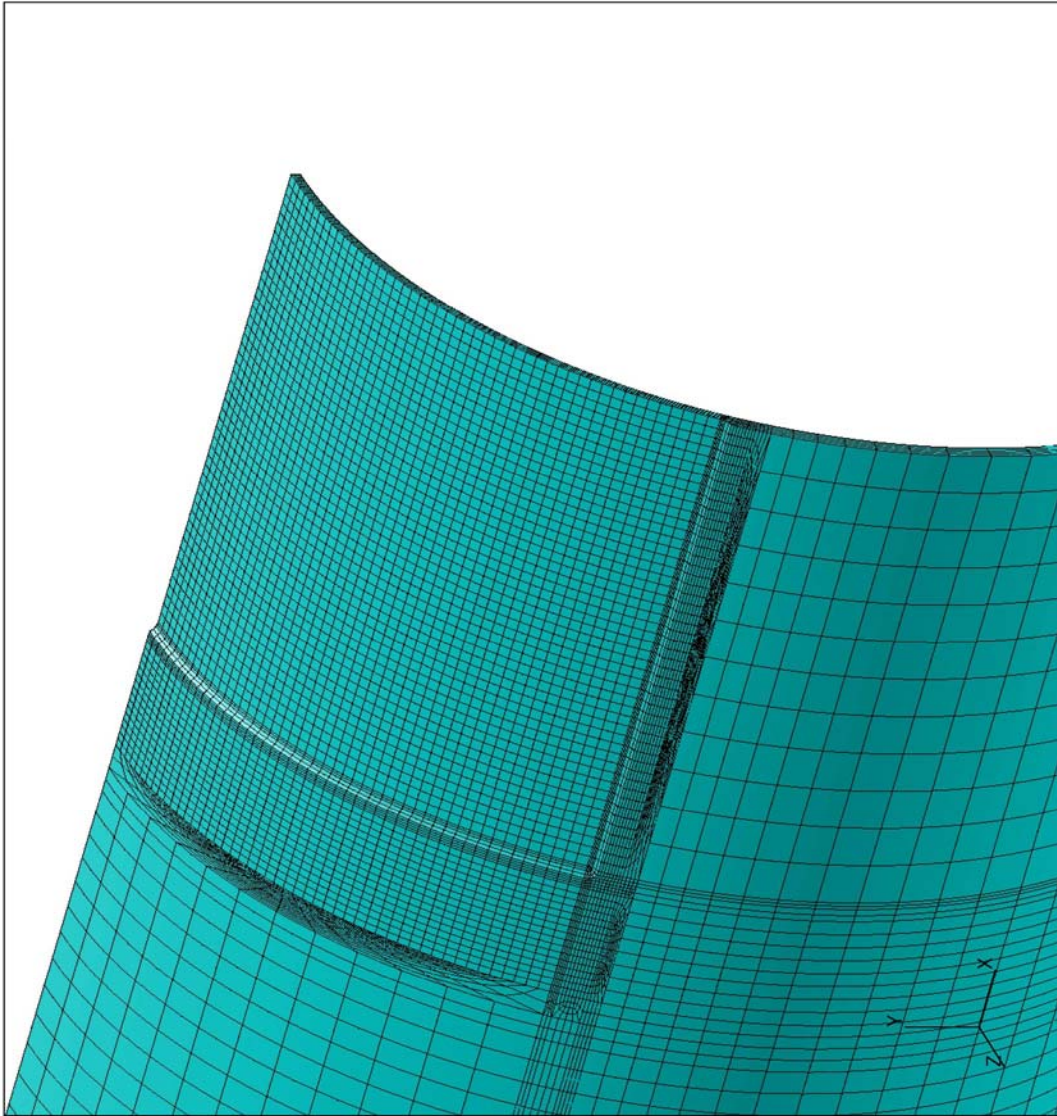


Figure 5 – Finite Element Mesh of 914.4 mm x 12.7 mm Pipe with a Corrosion Size of 500 mm x 500 mm and a Depth of 40% Wall thickness ( $r/t = 1$ )

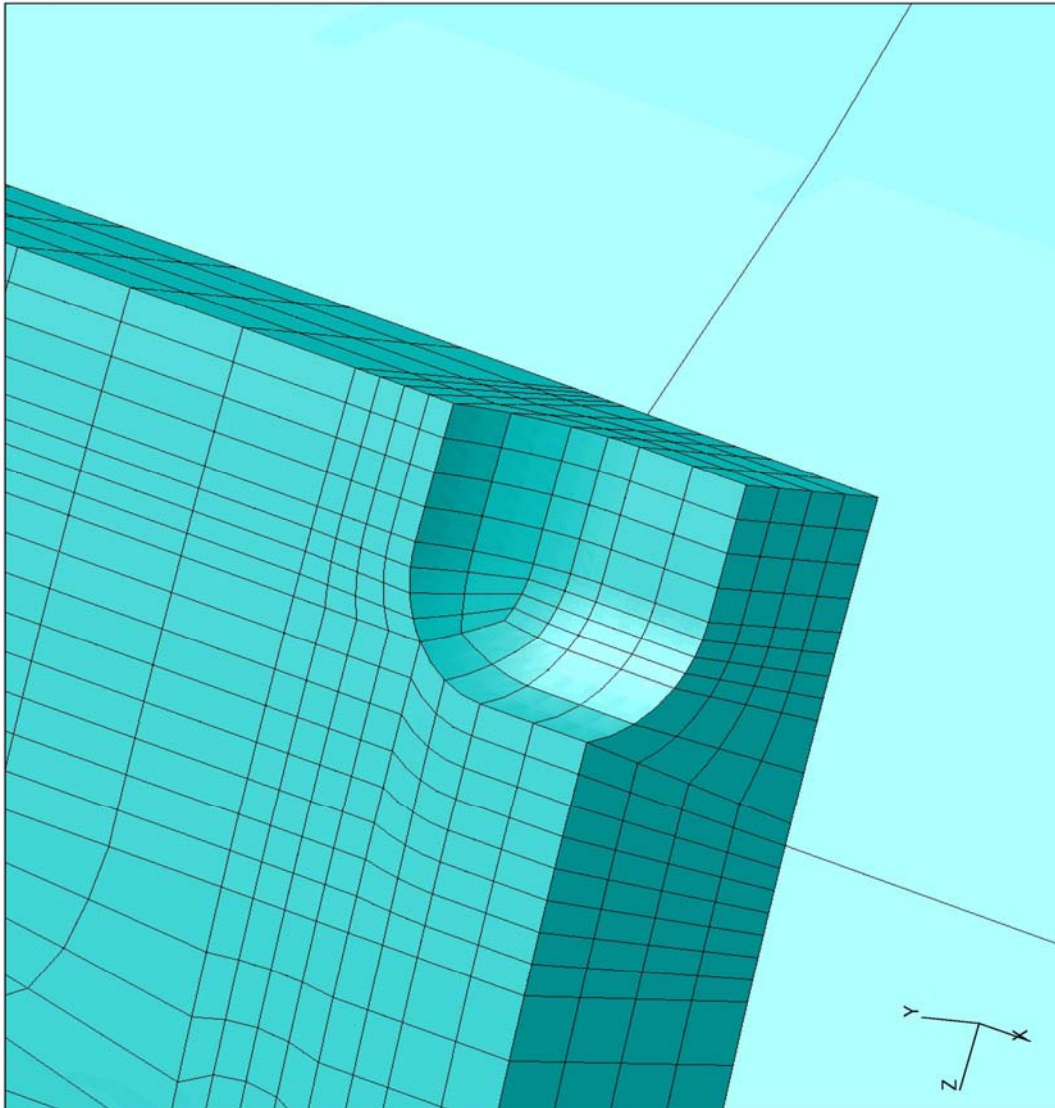


Figure 6 – Finite Element Mesh of 914.4 mm x 12.7 mm Pipe with a Corrosion Size of 13 mm x 13 mm and a Depth of 40% Wall thickness ( $r/t = 0.5$ )

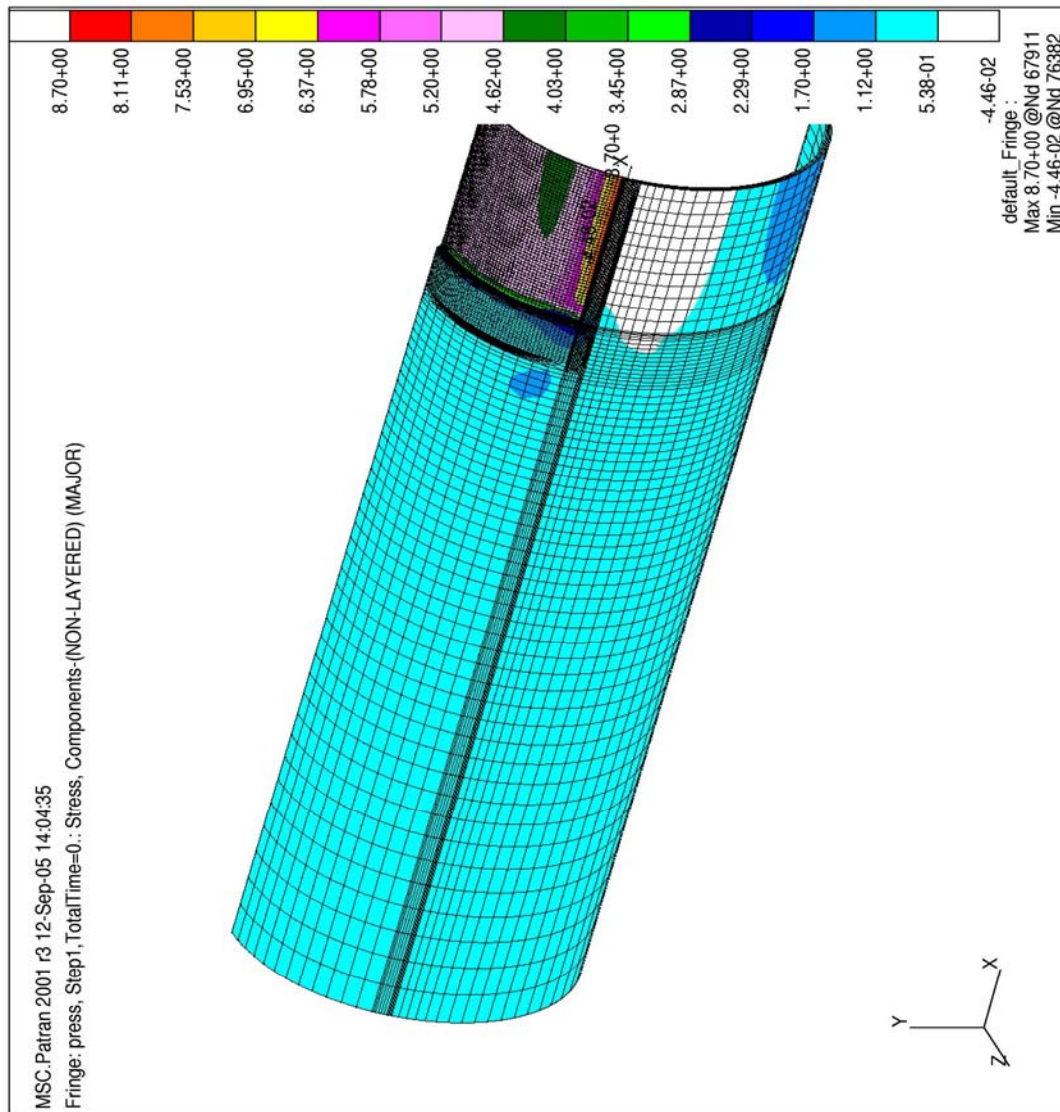


Figure 7 – Maximum Principal Stress of 914.4 mm x 12.7 mm Pipe with a Corrosion Size of 500 mm x 500 mm and a Depth of 80% Wall thickness



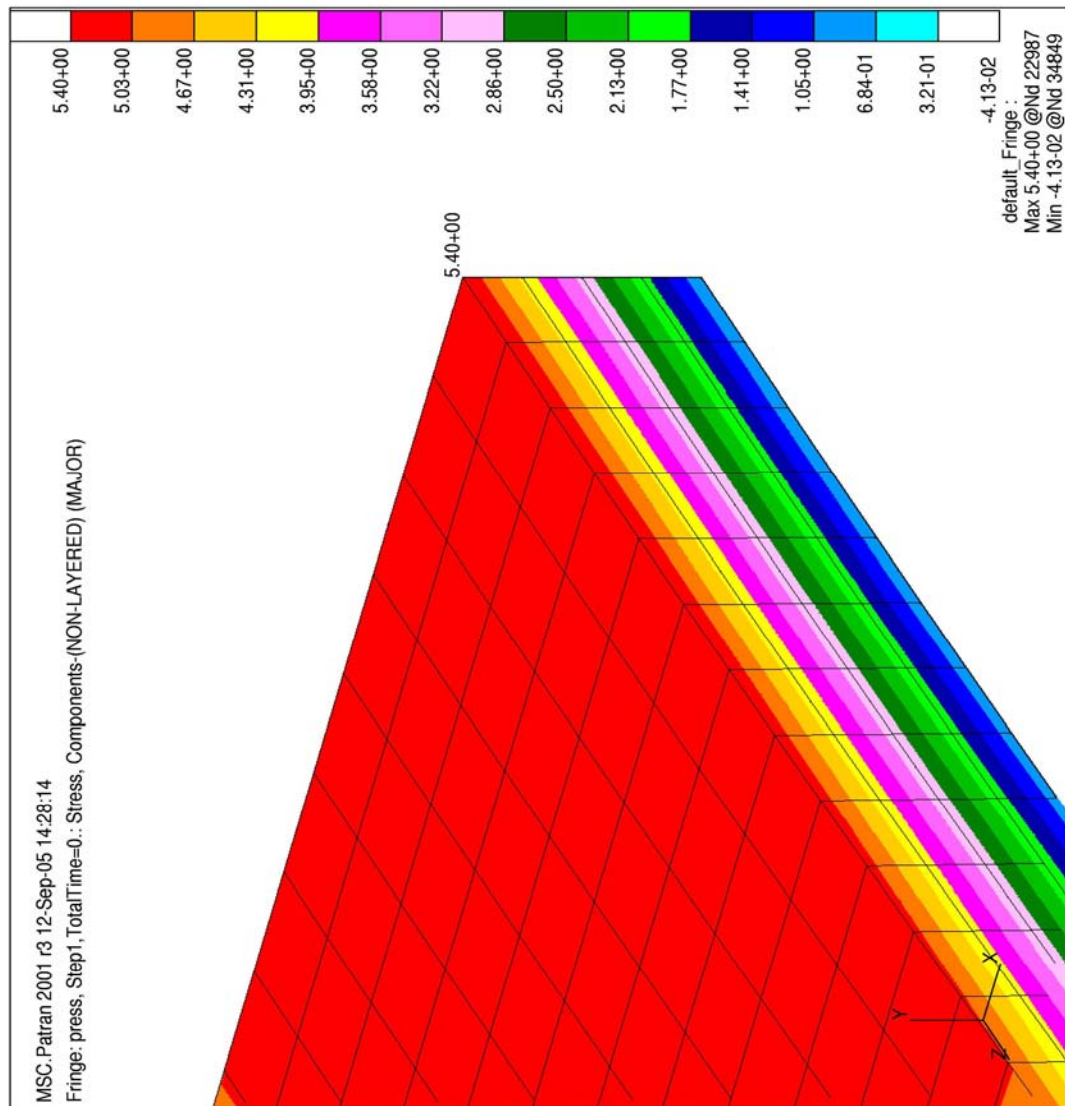


Figure 8 – Local View of Maximum Principal Stress of 914.4 mm x 12.7 mm Pipe with a Corrosion Size of 50 mm x 50 mm and a Depth of 80% Wall thickness

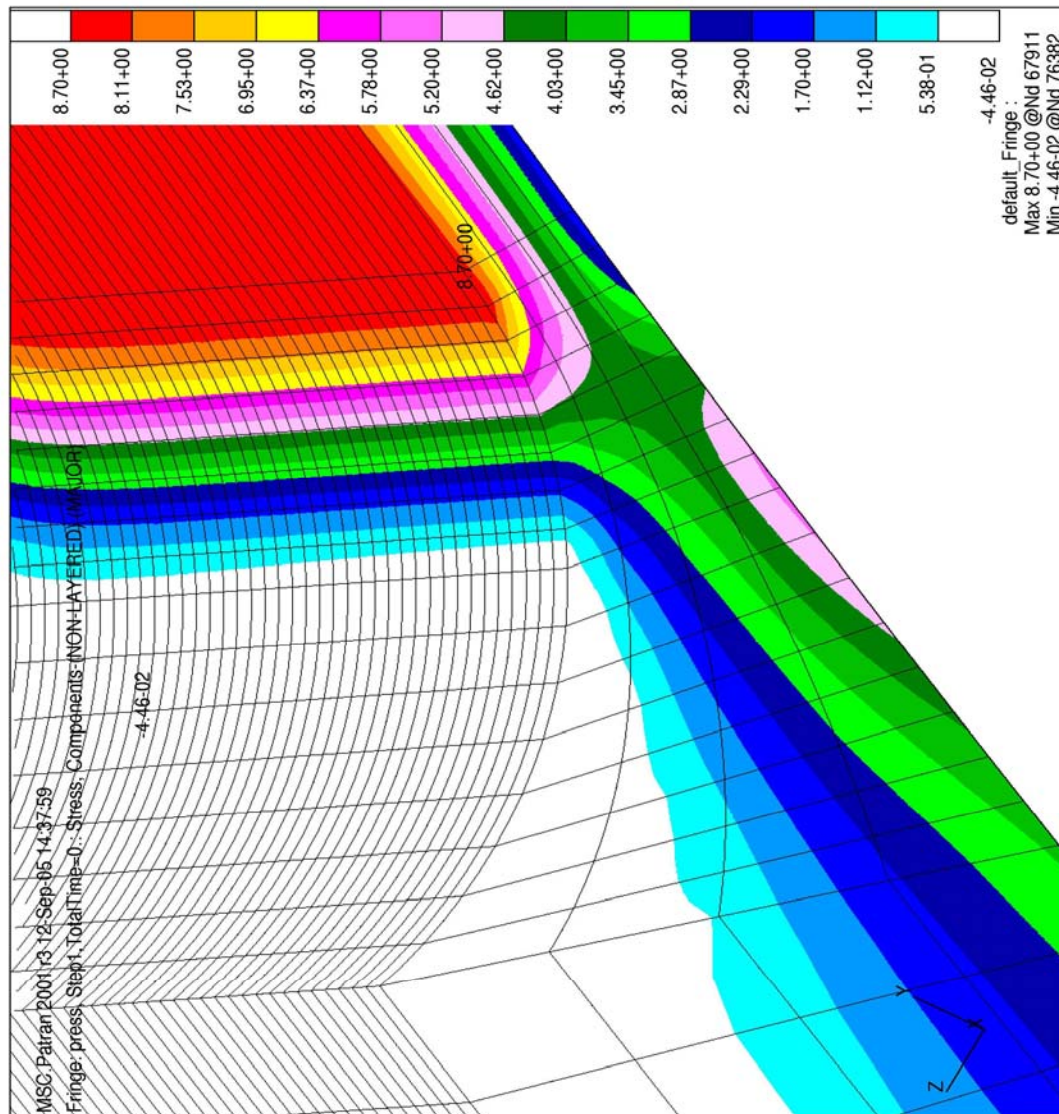
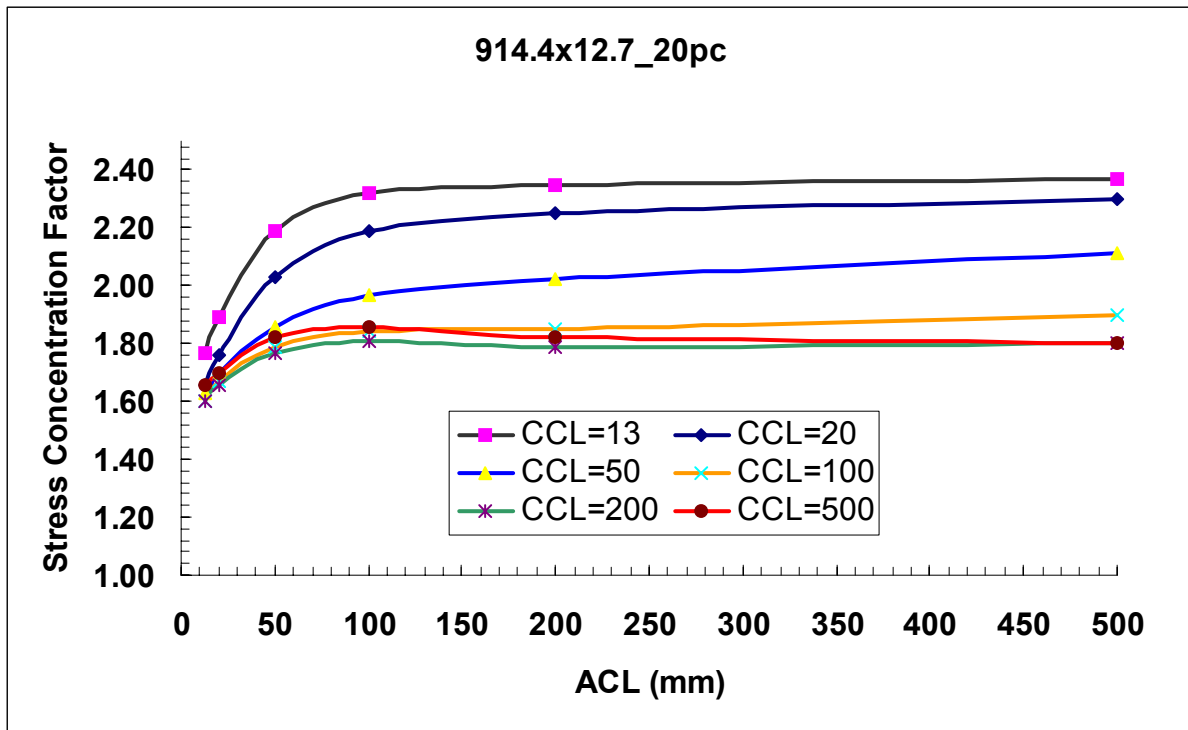
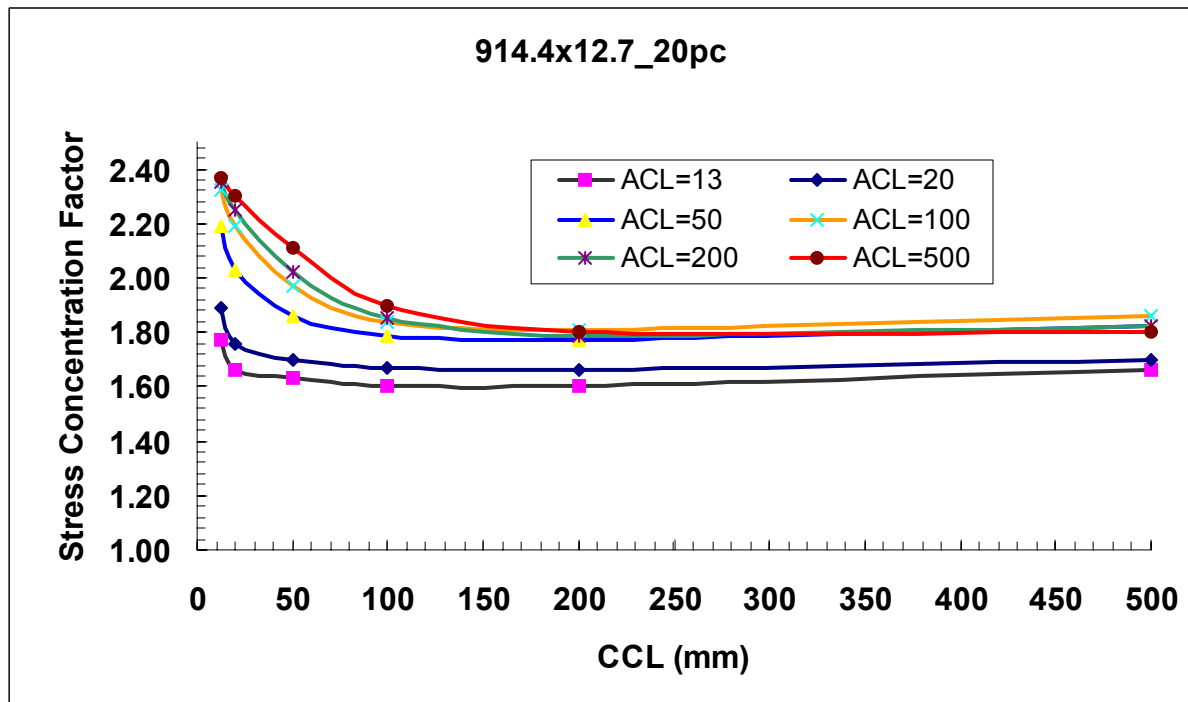


Figure 9 – Local View of Maximum Principal Stress of 914.4 mm x 12.7 mm Pipe with a Corrosion Size of 500 mm x 500 mm and a Depth of 80% Wall thickness



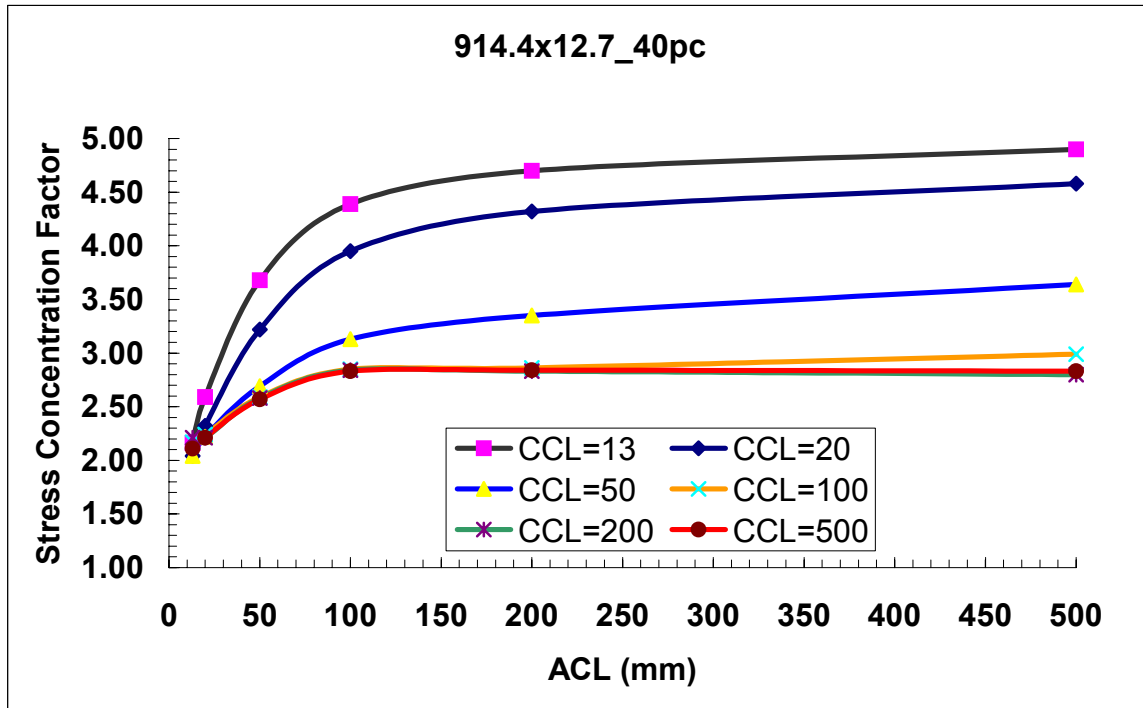


a): SCF with variation of axial corrosion length

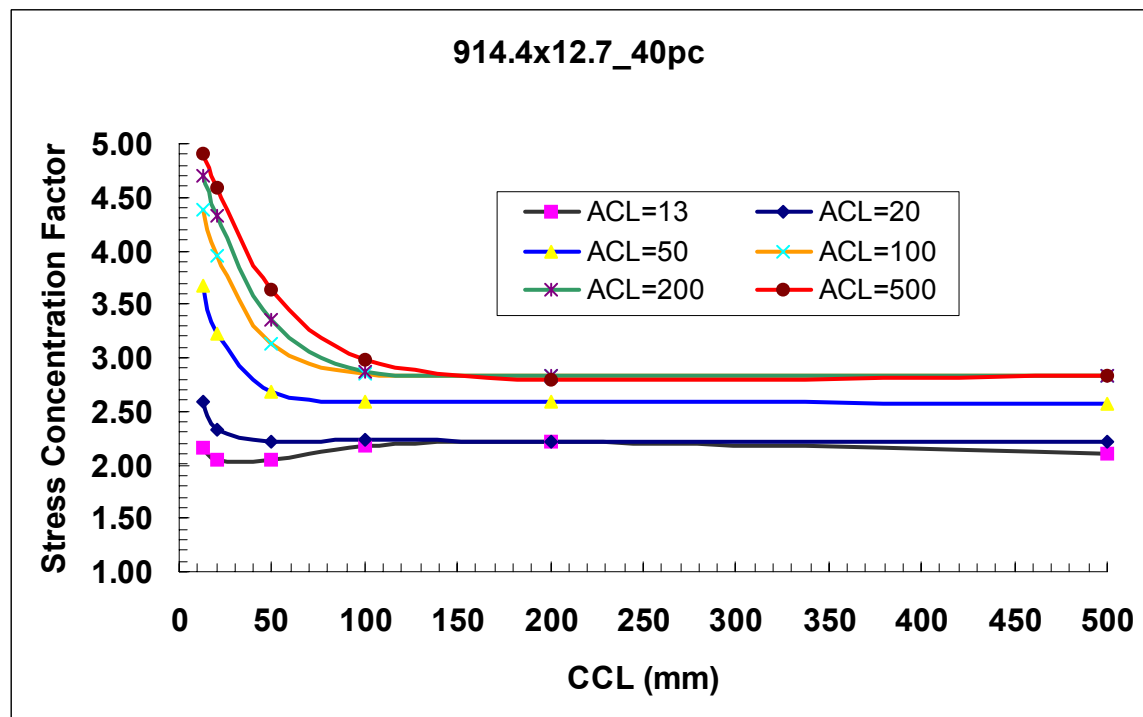


b): SCF with variation of circumferential corrosion length

Figure 10 – SCFs of 914.4 mm x 12.7 mm Pipe with CD = 20%t and r/t = 1

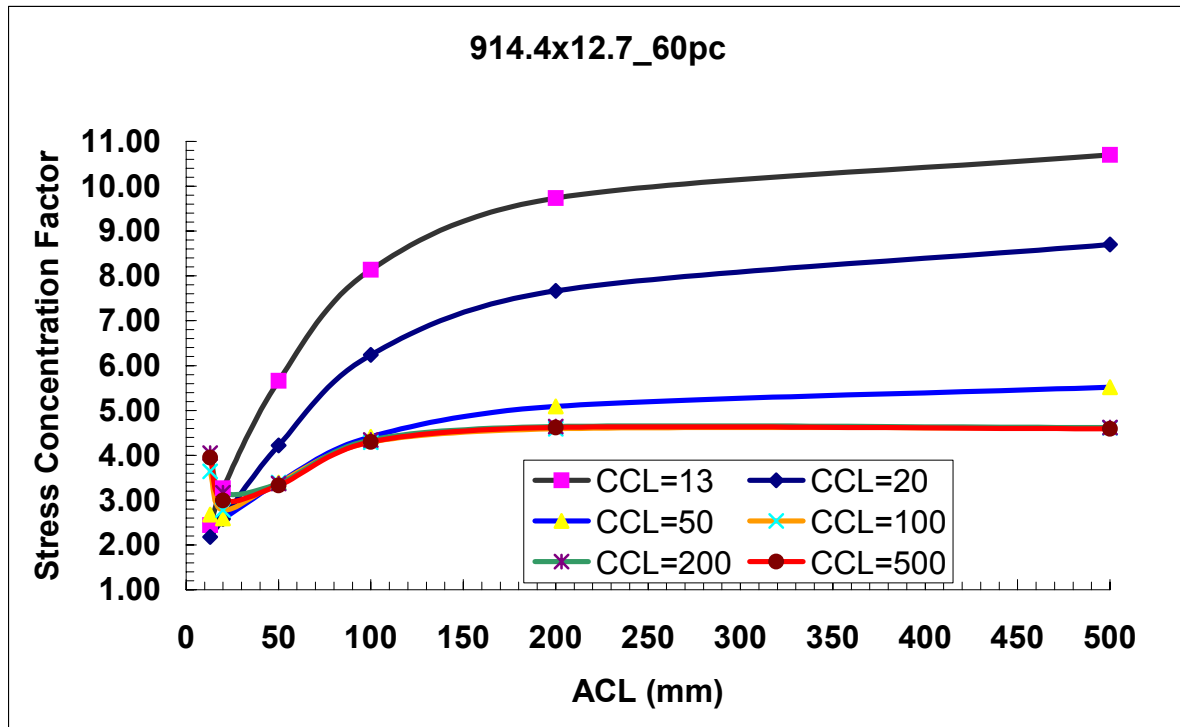


a): SCF with variation of axial corrosion length

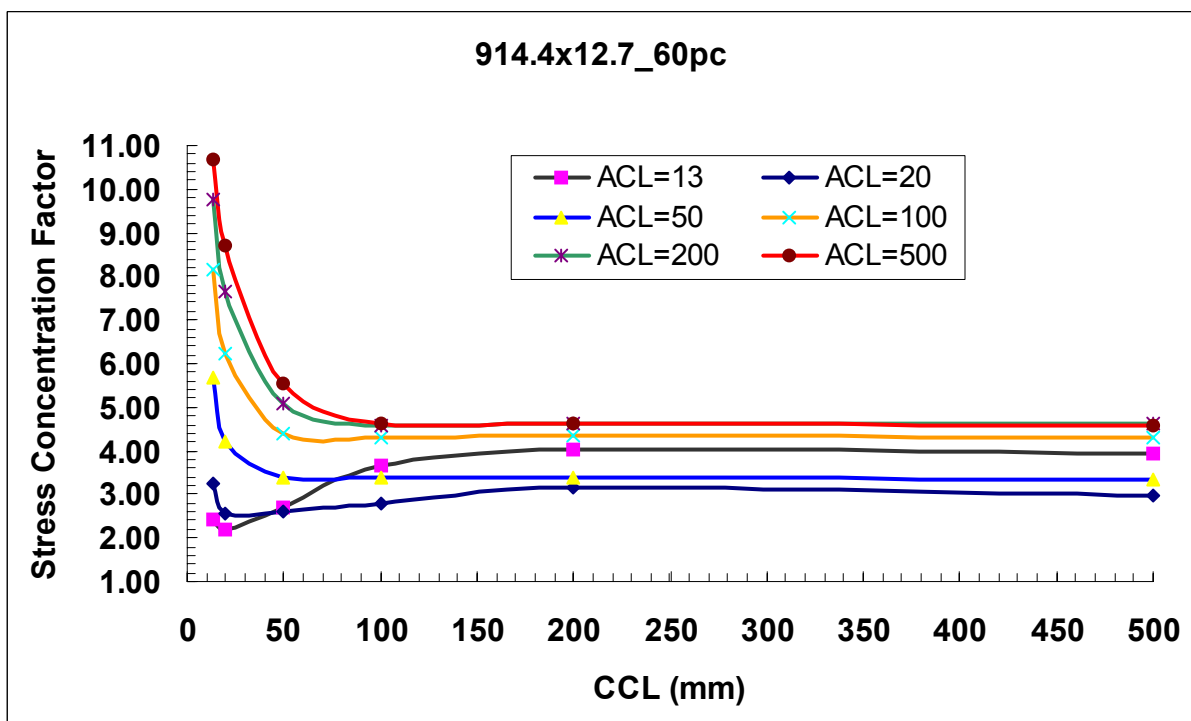


b): SCF with variation of circumferential corrosion length

Figure 11 – SCFs of 914.4 mm x 12.7 mm Pipe with CD = 40%t and r/t = 1

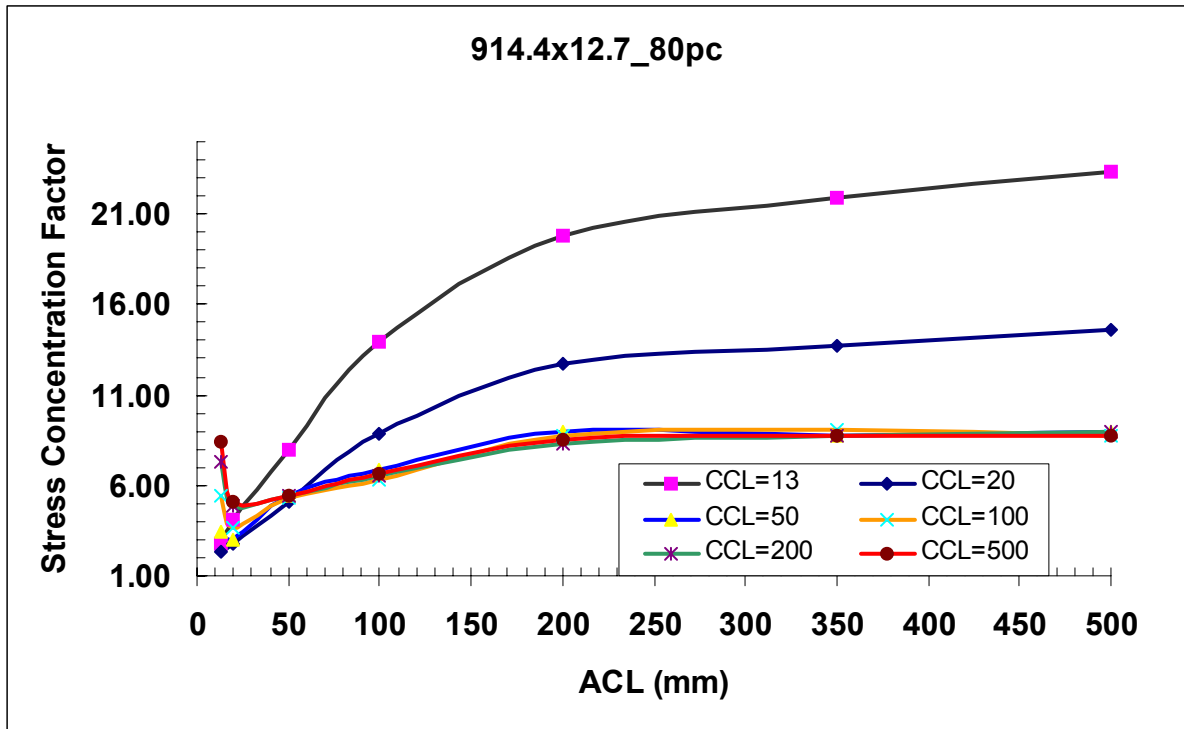


a): SCF with variation of axial corrosion length

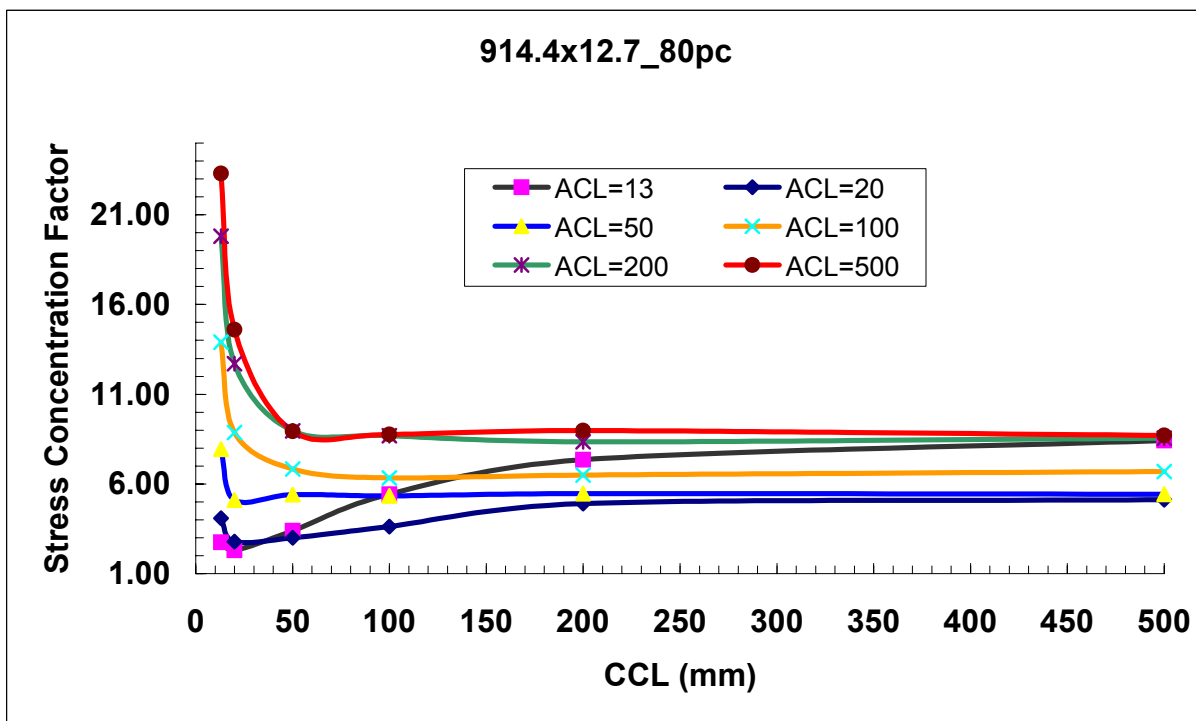


b): SCF with variation of circumferential corrosion length

Figure 12 – SCFs of 914.4 mm x 12.7 mm Pipe with CD = 60%t and r/t = 1



a): SCF with variation of axial corrosion length



b): SCF with variation of circumferential corrosion length

Figure 13 – SCFs of 914.4 mm x 12.7 mm Pipe with CD = 80%t and r/t = 1

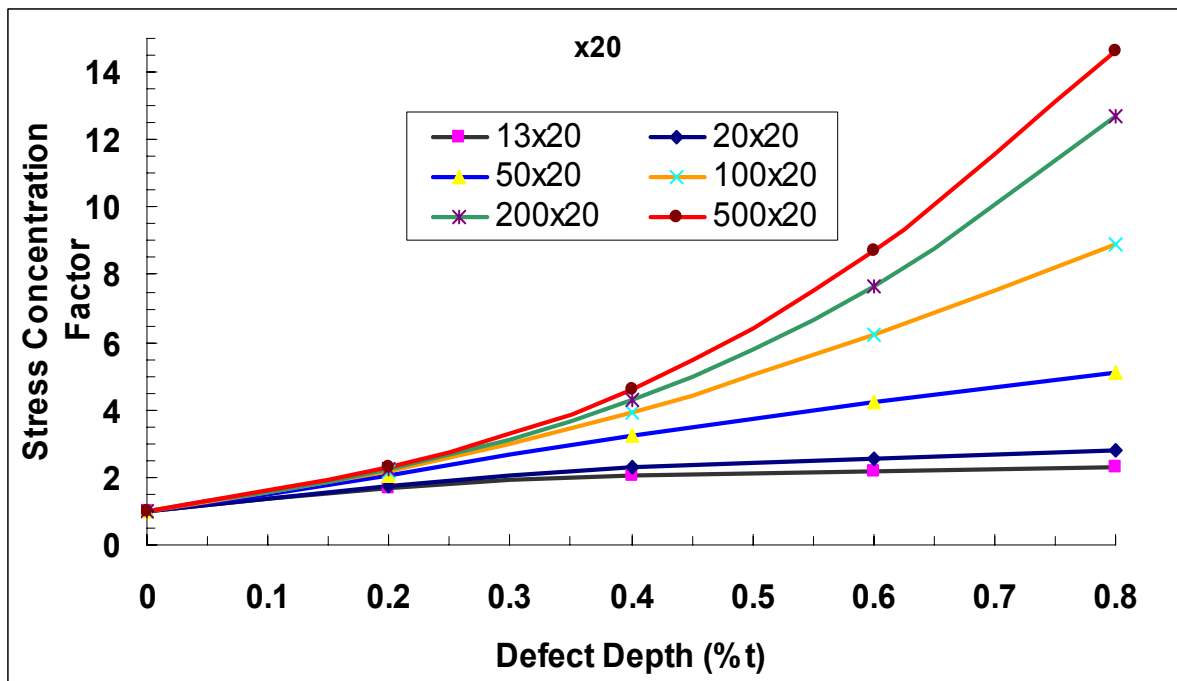
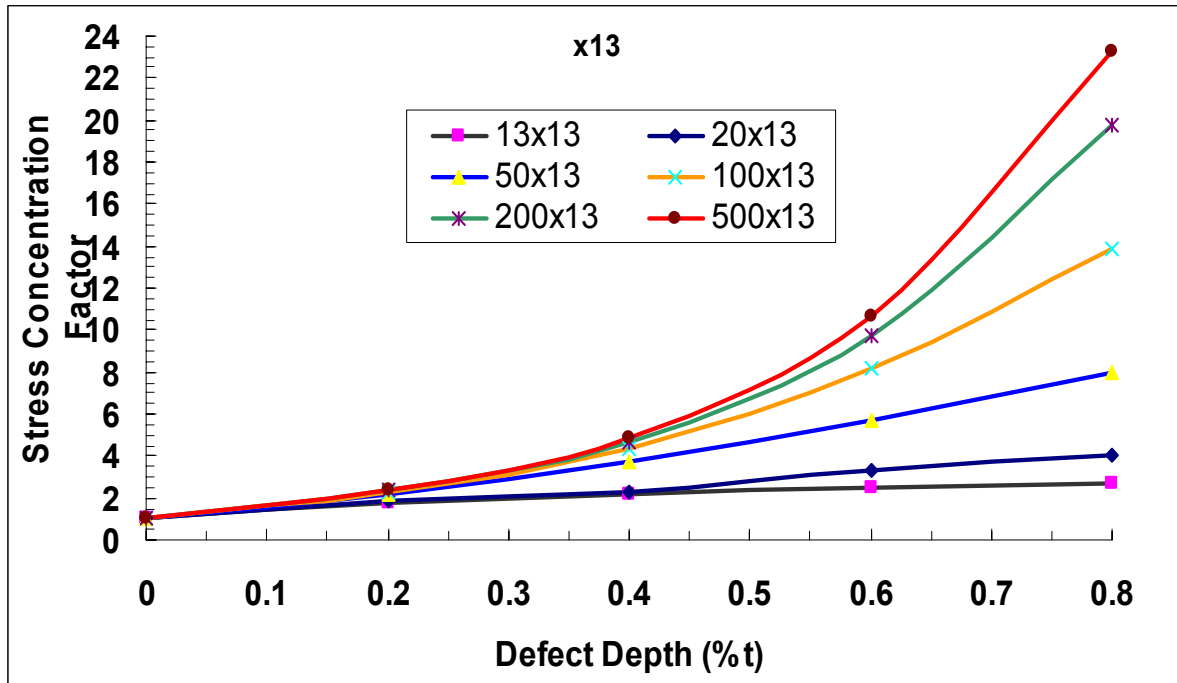
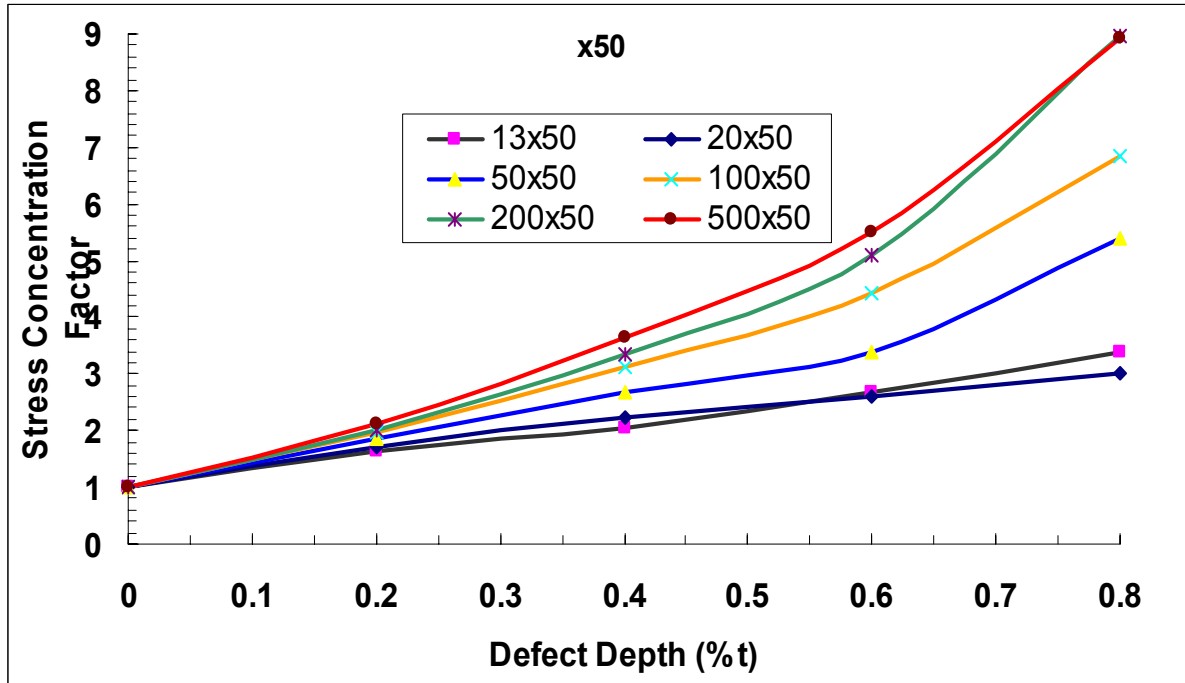
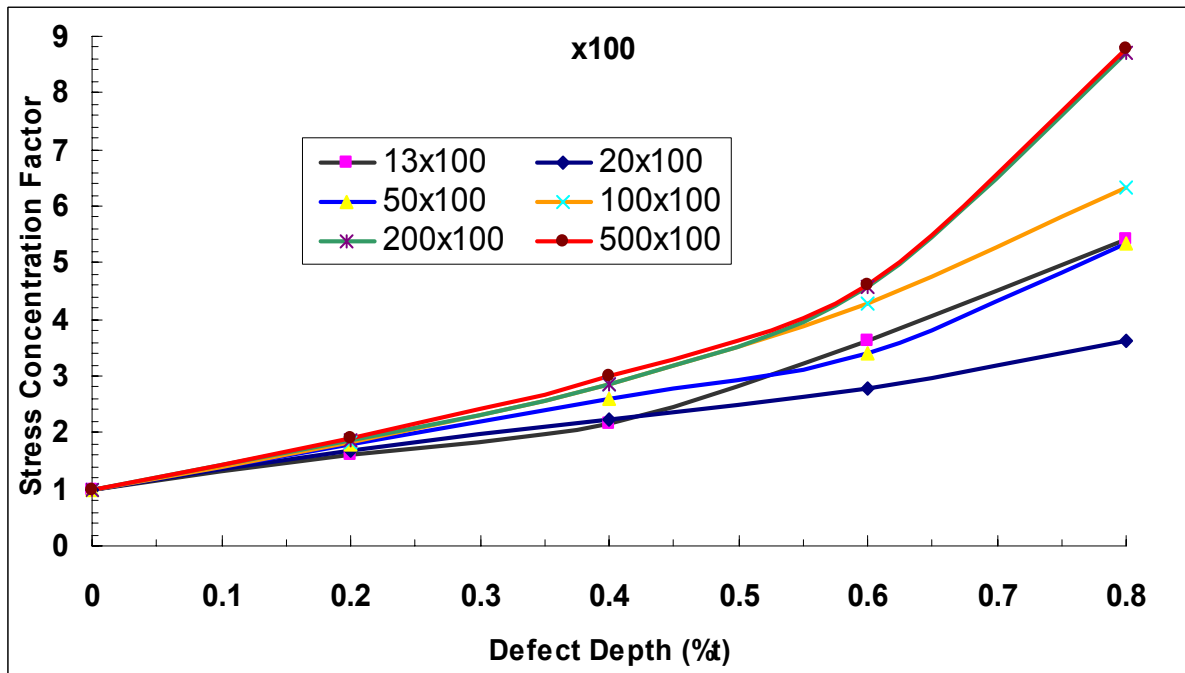


Figure 14 – SCFs of 914.4 mm x 12.7 mm Pipe with Variation of Corrosion Depth

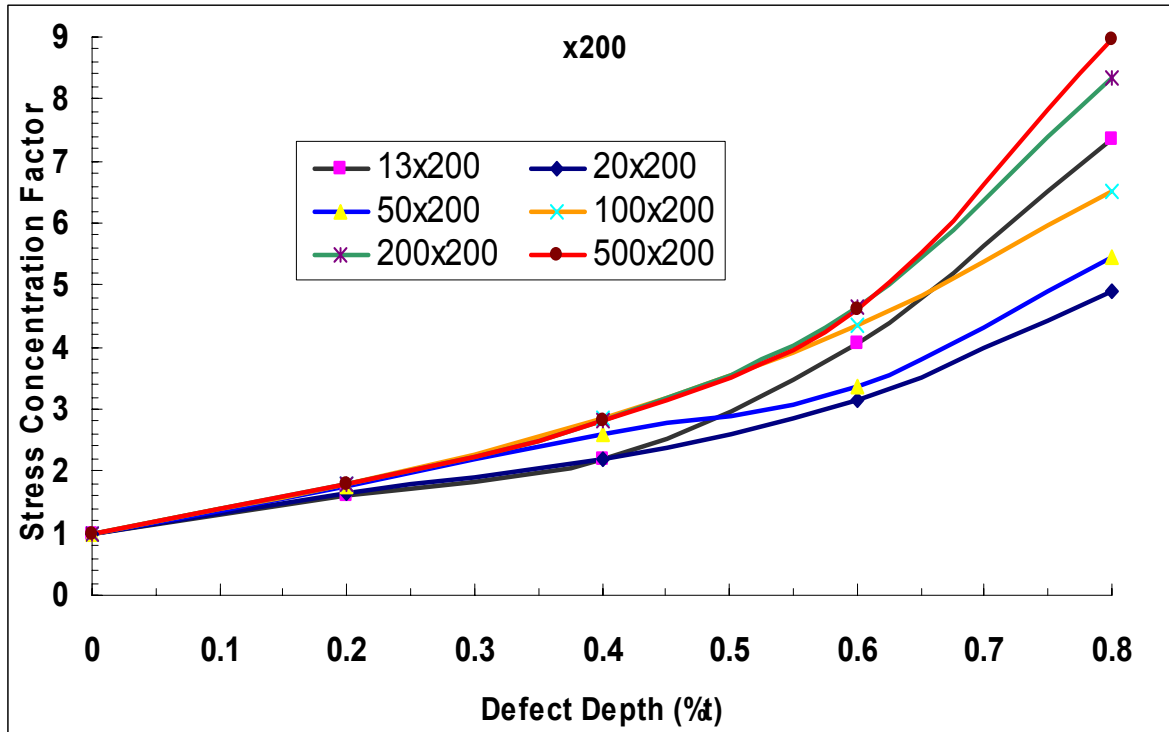


c): with CCL = 50 mm and ACL = 13 mm, 20 mm, 50 mm, 100 mm, 200 mm and 500 mm

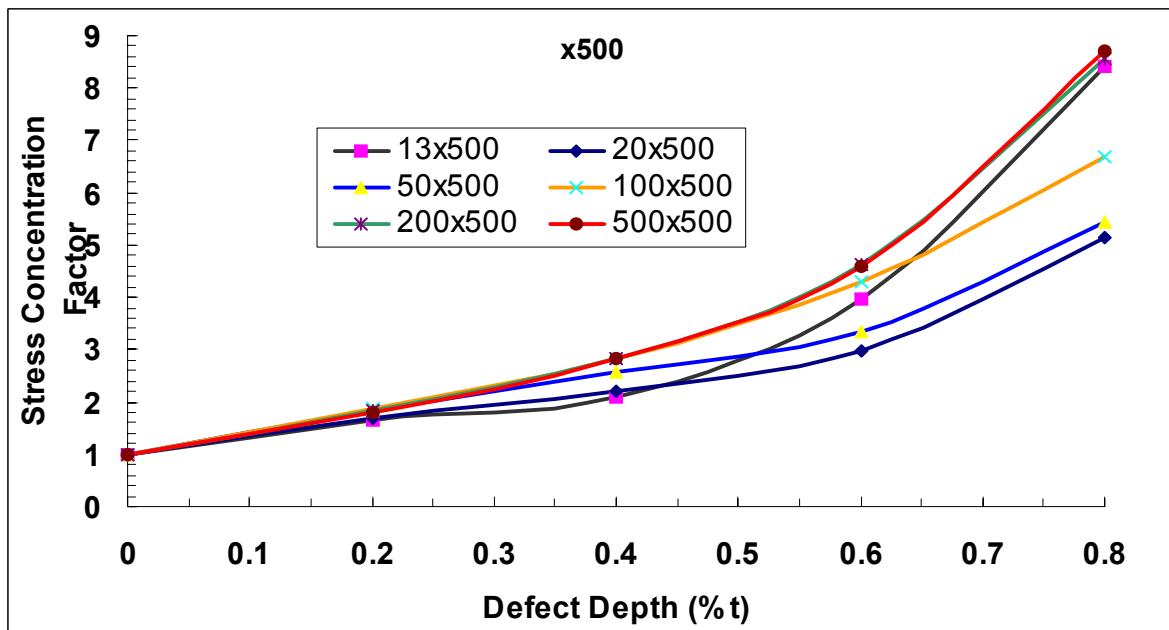


d): with CCL = 100 mm and ACL = 13 mm, 20 mm, 50 mm, 100 mm, 200 mm and 500 mm

Figure 14 – SCFs of 914.4 mm x 12.7 mm Pipe with Variation of Corrosion Depth



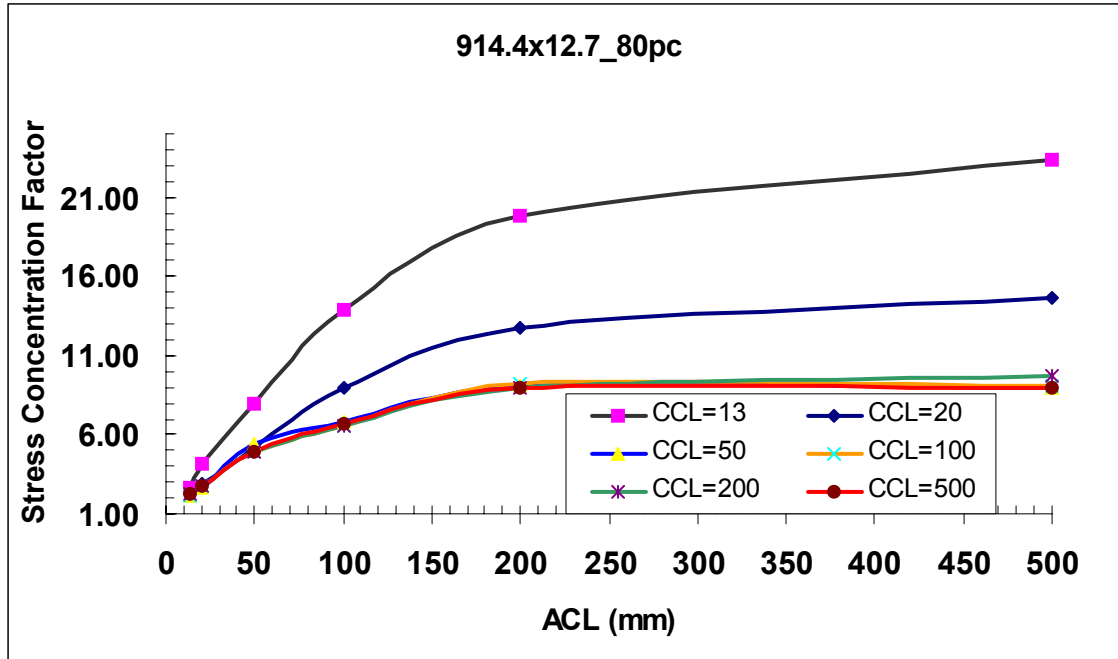
e): with CCL = 200 mm and ACL = 13 mm, 20 mm, 50 mm, 100 mm, 200 mm and 500 mm



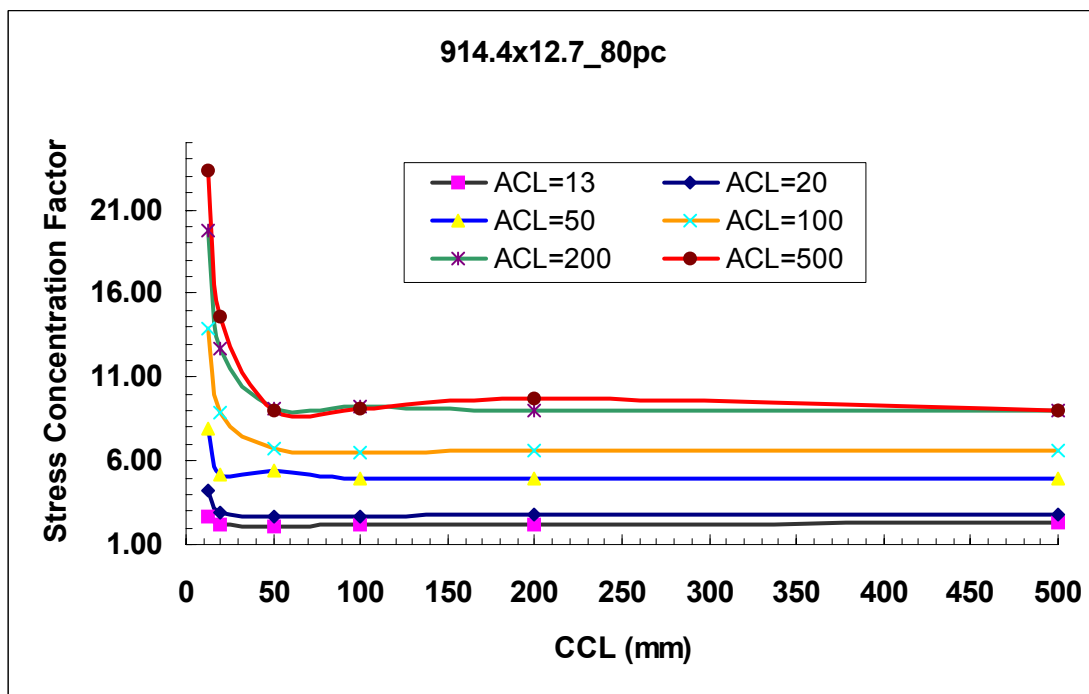
f): with CCL = 500 mm and ACL = 13 mm, 20 mm, 50 mm, 100 mm, 200 mm and 500 mm

Figure 14 – SCFs of 914.4 mm x 12.7 mm Pipe with Variation of Corrosion Depth



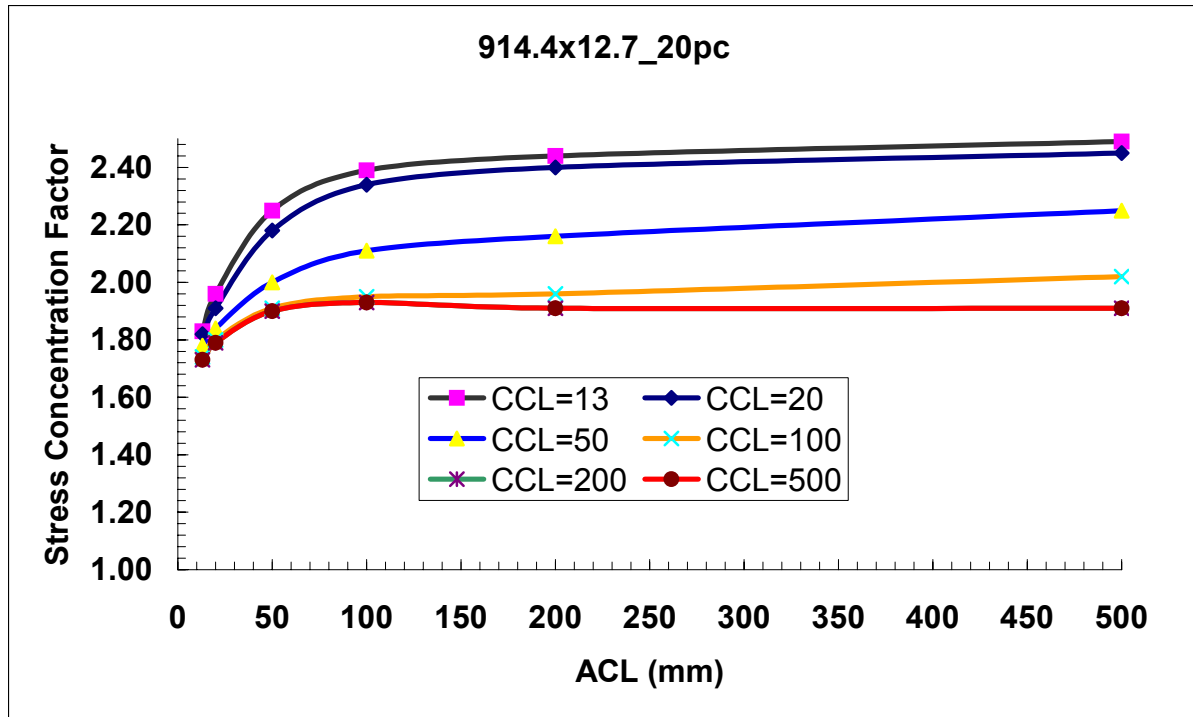


a): SCF with variation of axial corrosion length

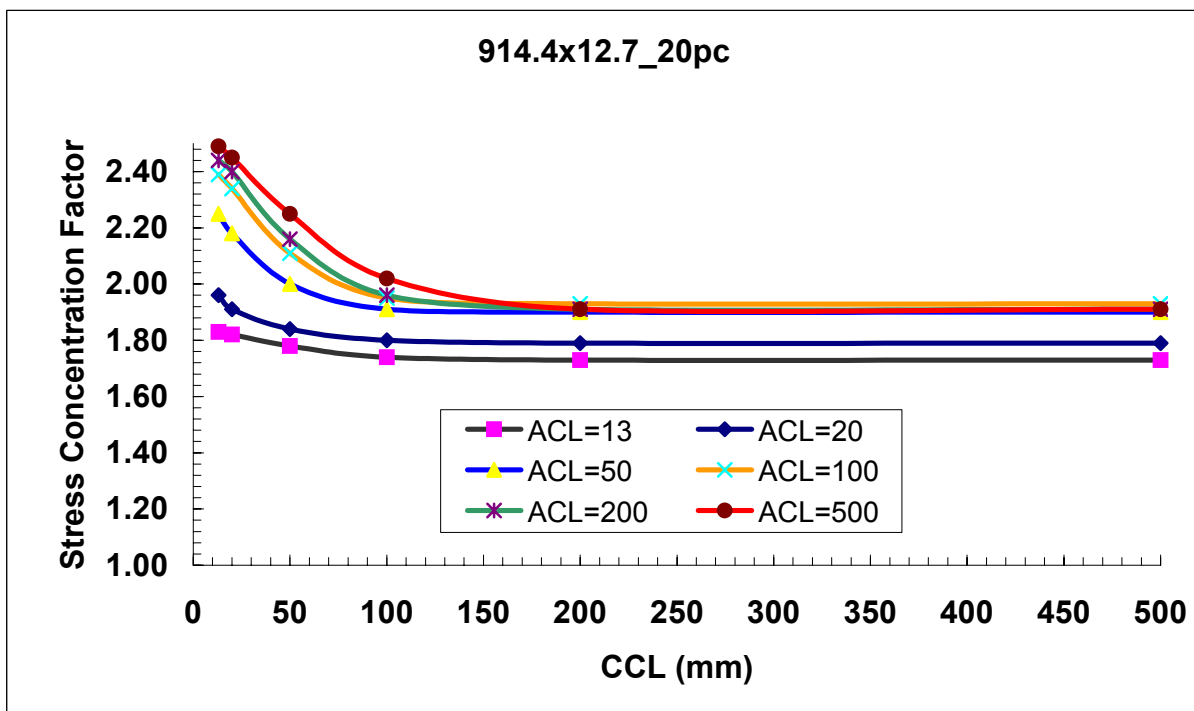


b): SCF with variation of circumferential corrosion length

Figure 15 – SCFs of 914.4 mm x 12.7 mm Pipe with CD = 80%t and r/t = 1 and without 'capped end force'

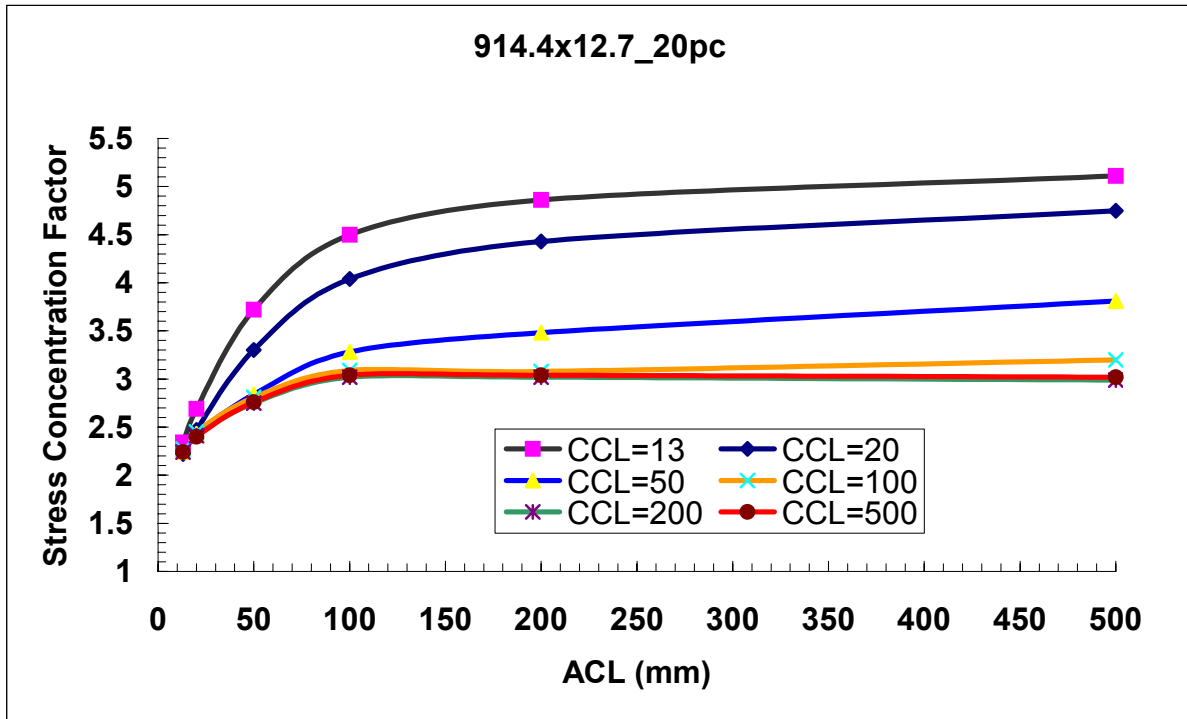


a): SCF with variation of axial corrosion length

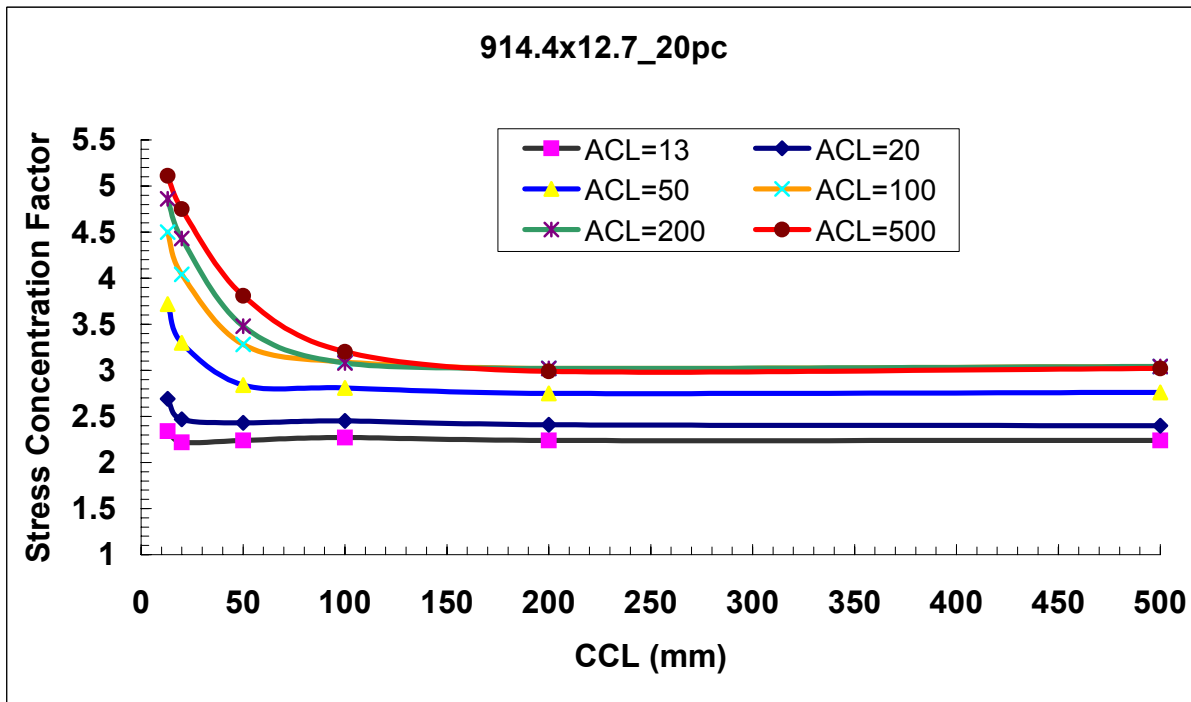


b): SCF with variation of circumferential corrosion length

Figure 16 – SCFs of 914.4 mm x 12.7 mm Pipe with CD = 20%t and r/t = 0.5



a): SCF with variation of axial corrosion length



b): SCF with variation of circumferential corrosion length

Figure 17 – SCFs of 914.4 mm x 12.7 mm Pipe with CD = 40%t and r/t = 0.5

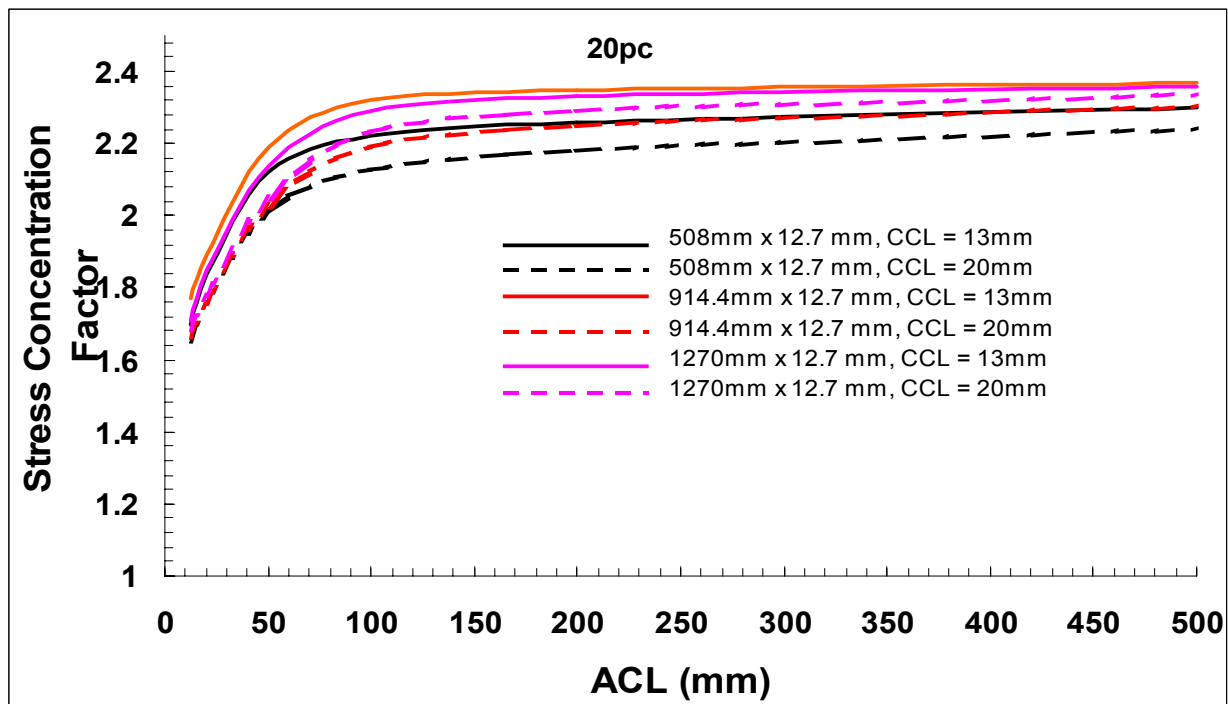


Figure 18 – SCF for 508 mm x12.7, 914.4 mm x 12.7 mm and 1270 mm x 12.7 mm Pipe with CD = 20%t ( $r/t = 1$ )

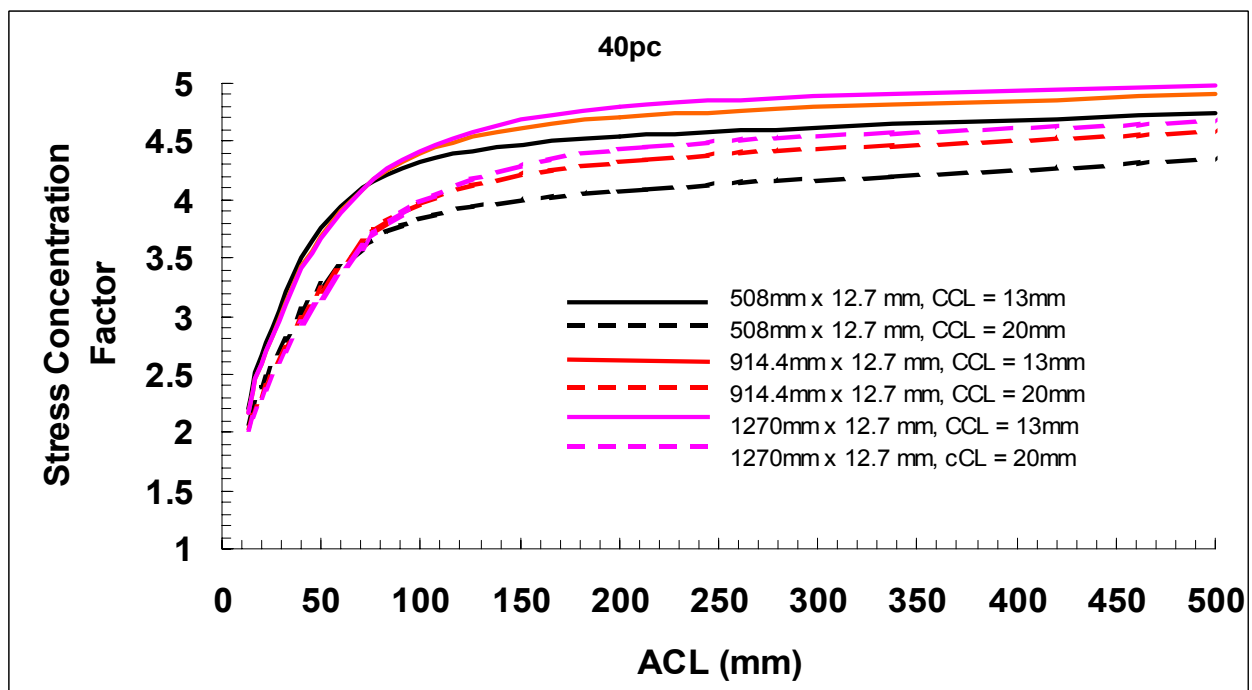


Figure 19 – SCF for 508 mm x12.7, 914.4 mm x 12.7 mm and 1270 mm x 12.7 mm Pipe with CD = 40%t ( $r/t = 1$ )

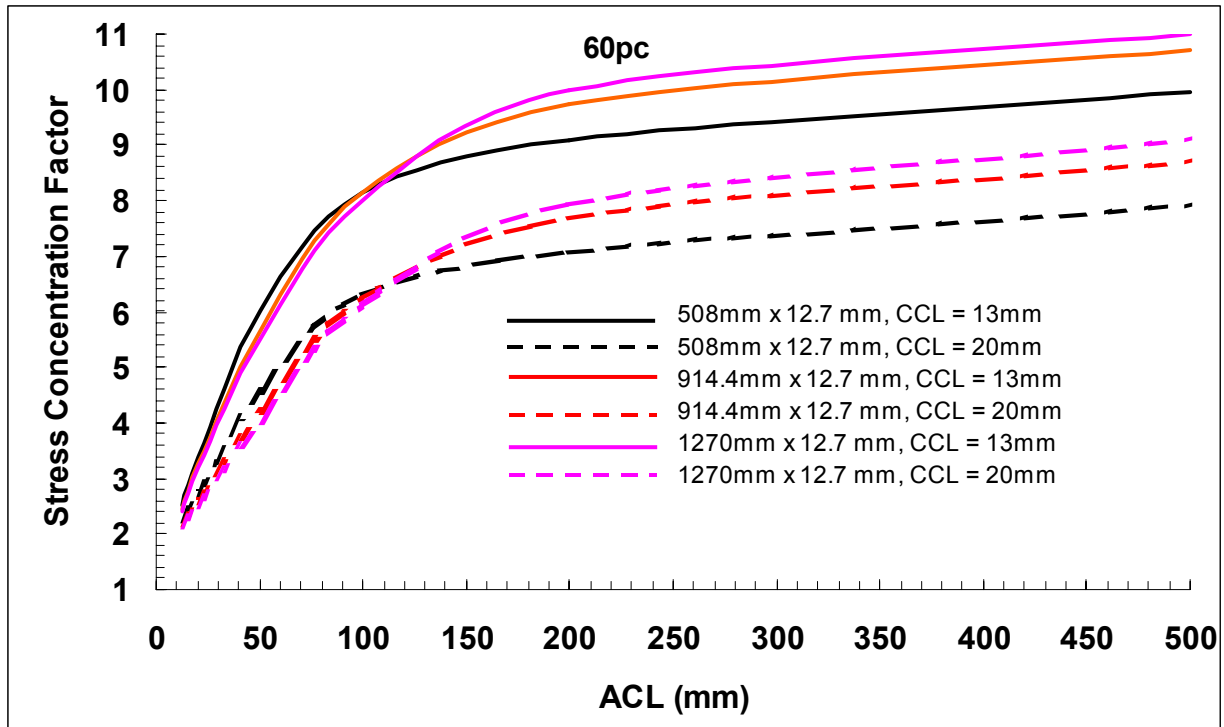


Figure 20 – SCF for 508 mm x12.7, 914.4 mm x 12.7 mm and 1270 mm x 12.7 mm Pipe with CD = 60%t ( $r/t = 1$ )

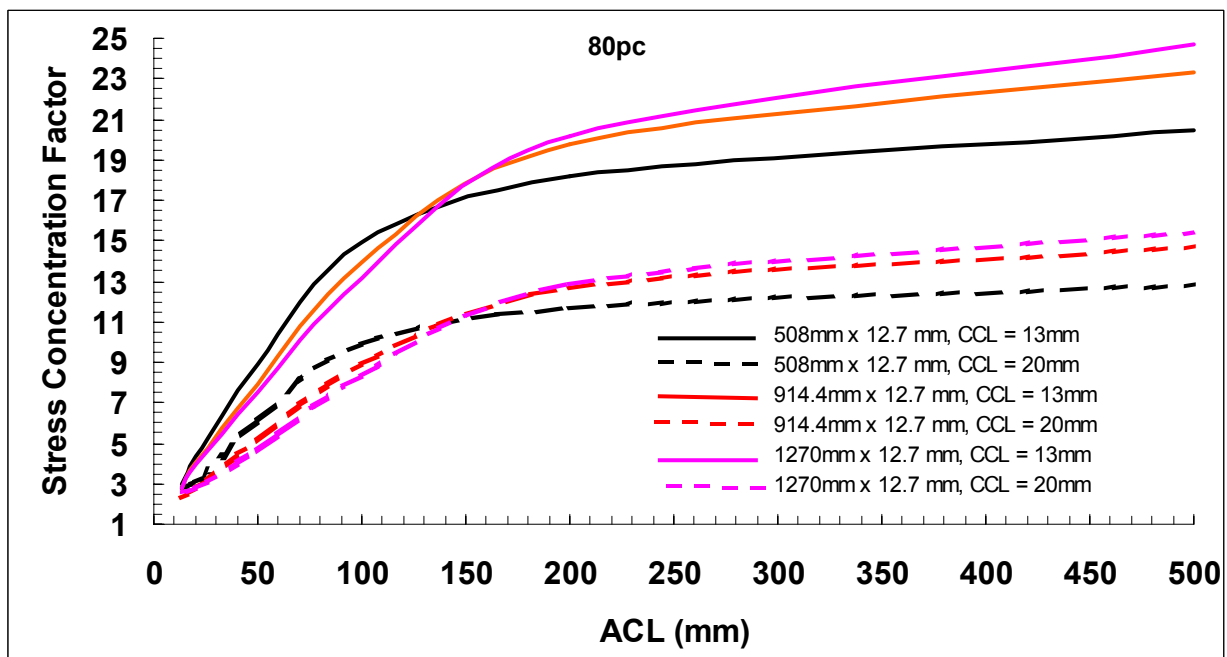
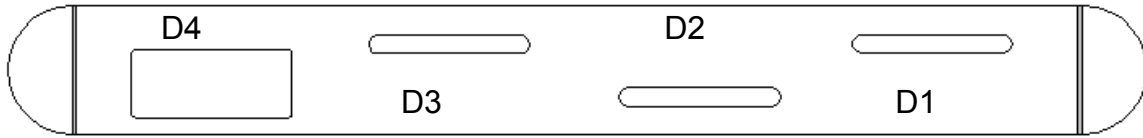
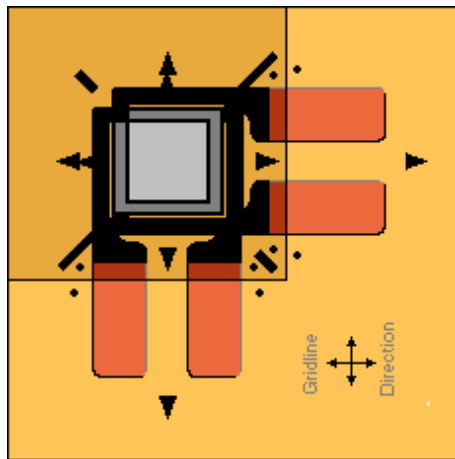


Figure 21 – SCF for 508 mm x12.7, 914.4 mm x 12.7 mm and 1270 mm x 12.7 mm Pipe with CD = 80%t ( $r/t = 1$ )

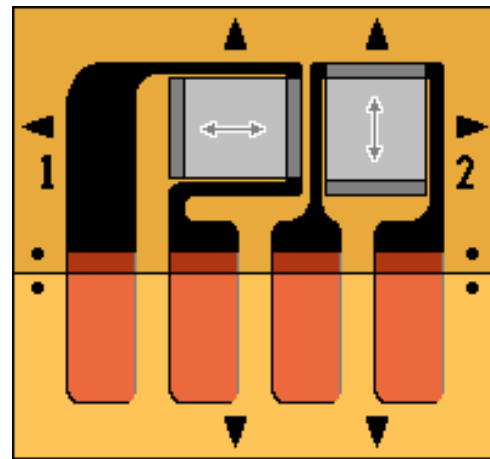


**Notes:** D1, D2, D3 and D4 refer to defects 1, 2, 3 and 4 respectively. For defect dimensions refer to Table 16.

Figure 22 – Illustration of test vessel and defect locations (not to scale)

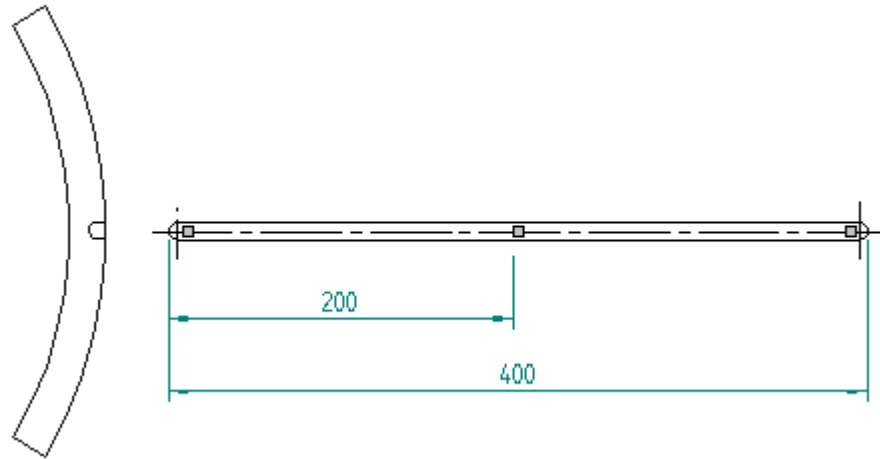


Type 1: CEA-06-062WT-350

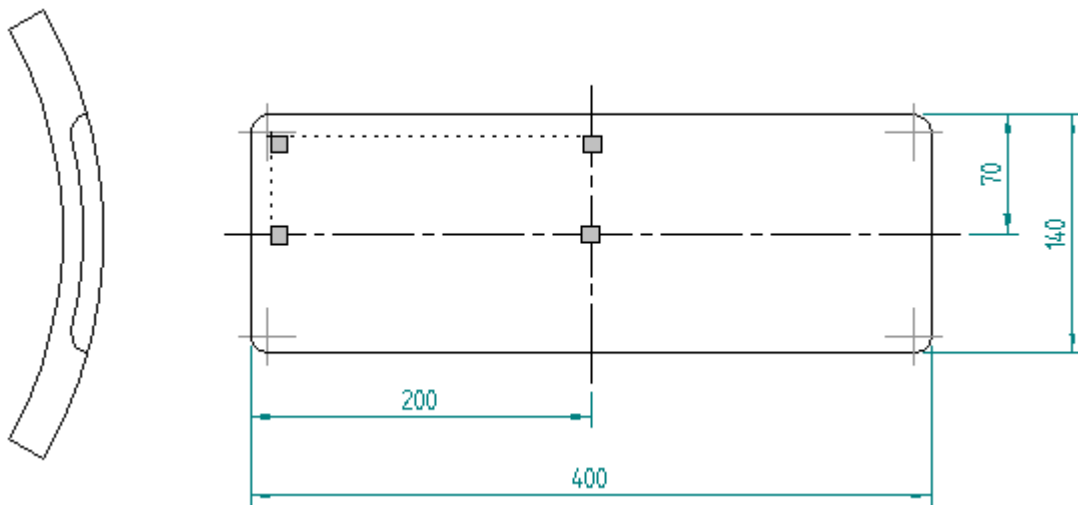


Type 2: CEA-06-062UT-350

Figure 23. Strain gauge rosettes used to measure the pipe axial and circumferential strains in the defect area.

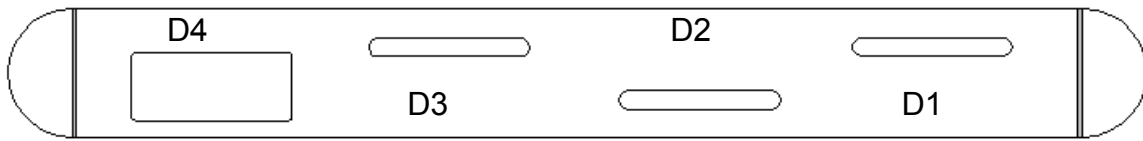


(a) Groove defect

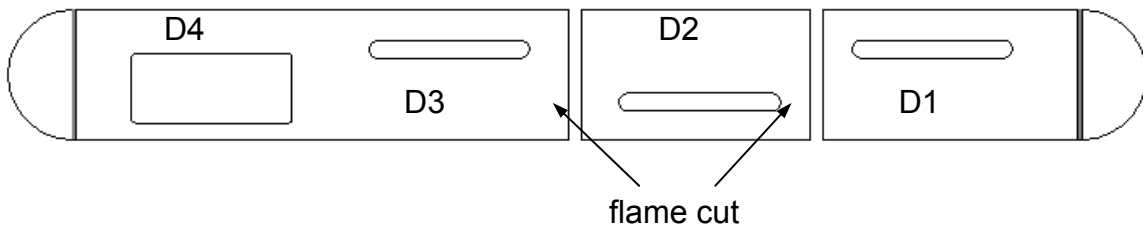


(b) Patch defect

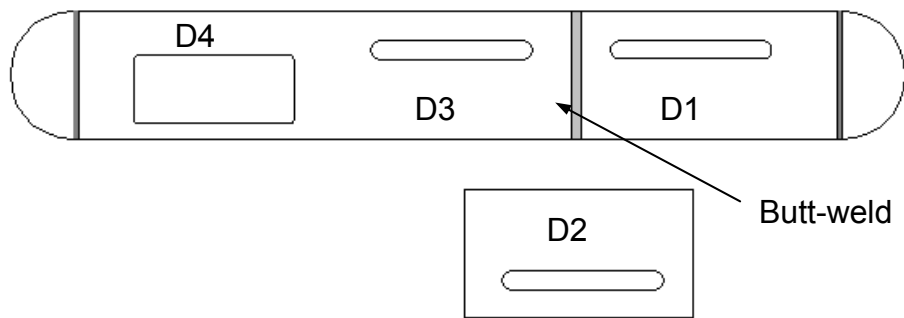
Figure 24. Strain gauge locations within the groove and patch defects.



(a) through wall cracking observed in defect D2



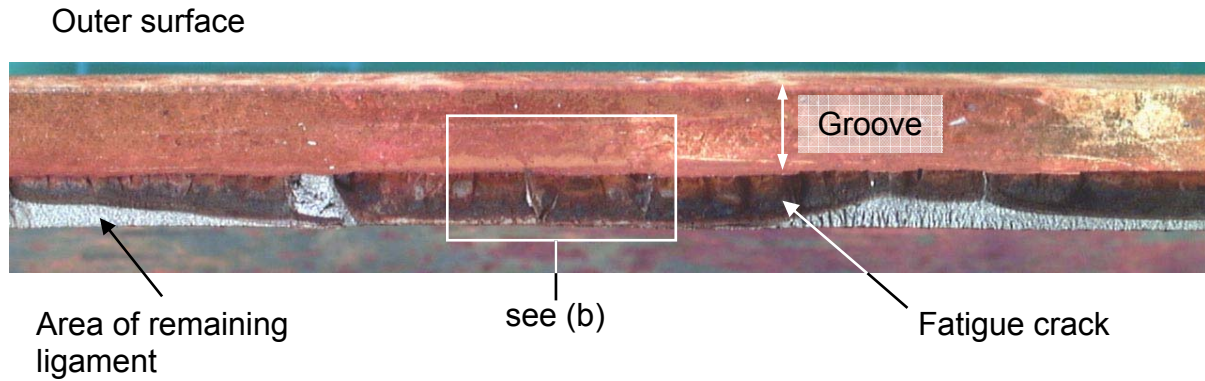
(b) removal of defect D2 via flame cutting (cutting process cuts a weld prep onto the ends of the pup pieces containing defects D1, D3 and D4)



(c) defect D2 is extracted and the two vessel ends are butt welded together. Pressure cycling is then resumed.

Figure 25. Illustration of repair methodology (not to scale).





(a) Multiple crack initiation sites along outer surface of defect, which eventually coalesce to form one large fatigue crack



(b) Cleaned up image of typical crack initiation site at location of through wall breach, as enveloped in (a) above.

Figure 26. Defect D3: Stereo optical microscope images of crack face features.



(a) Crack initiation site along outer surface of defect



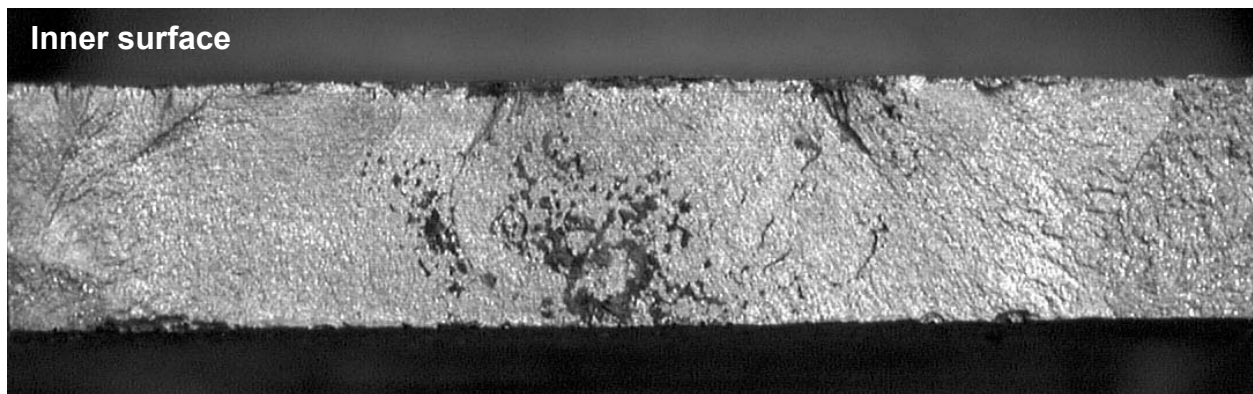
(b) Cleaned up image of crack initiation site and location of through wall breach. Beach markings clearly visible, showing crack propagation from the outer to the inner surface (top to bottom in image).

Figure 27. Defect D2: Stereo optical microscope images of crack face features.



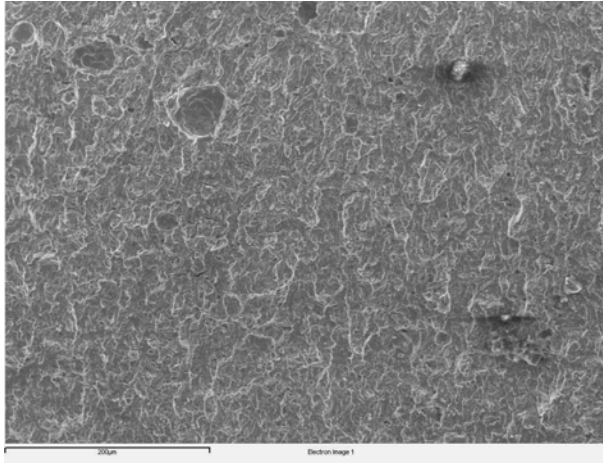


(a) Crack initiation site along inner surface of defect

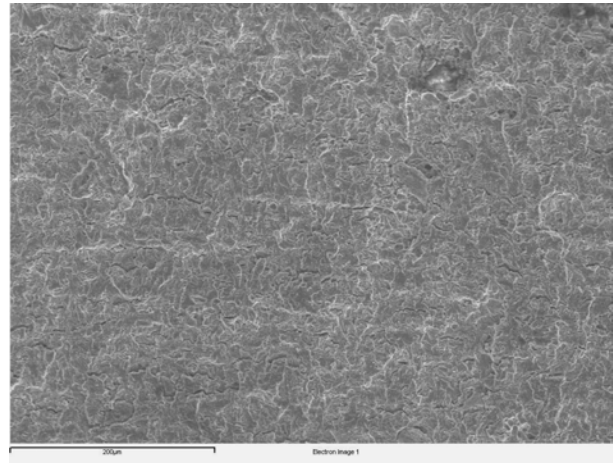


(b) Cleaned up image of multiple crack initiation sites and location of through wall breach. Crack propagation from the inner to the outer surface (top to bottom in image).

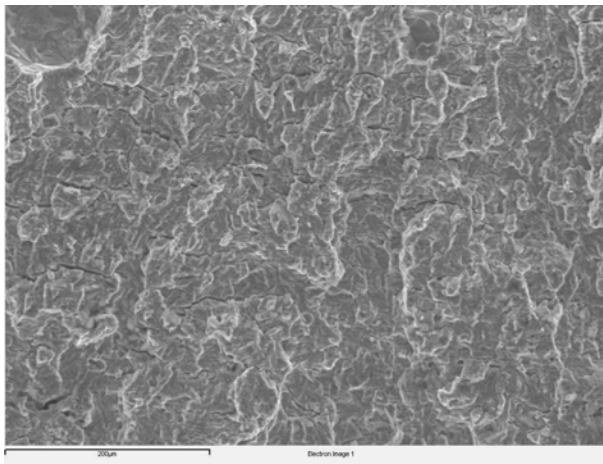
Figure 28. Defect D4: Stereo optical microscope images of crack face features.



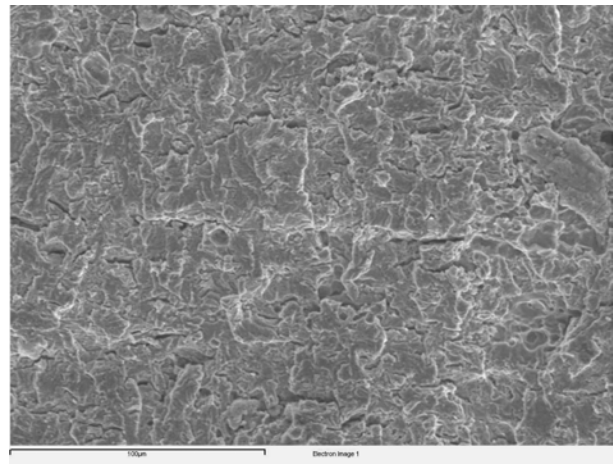
Fatigue crack surface features – **outer**, 200µm scale



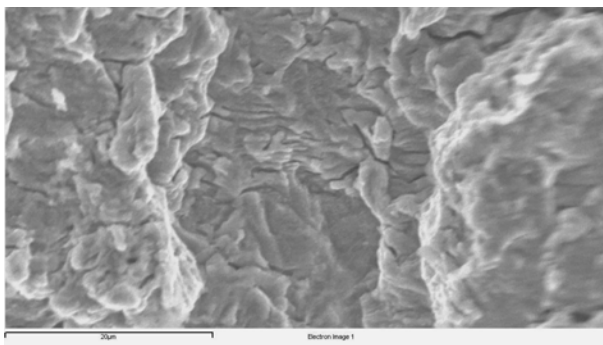
Fatigue crack surface features – **inner**, 200µm scale



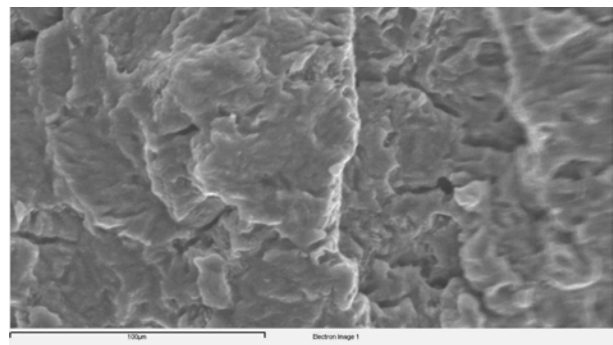
Fatigue crack surface features – **outer**, 100µm scale



Fatigue crack surface features – **inner**, 100µm scale



Striations – **outer**, 20µm scale

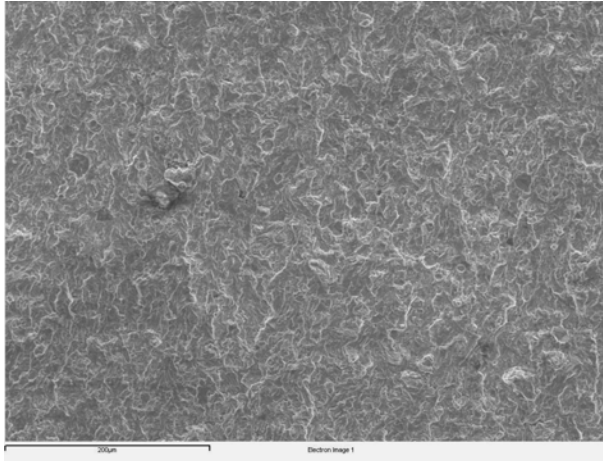


Striations – **inner**, 20µm scale

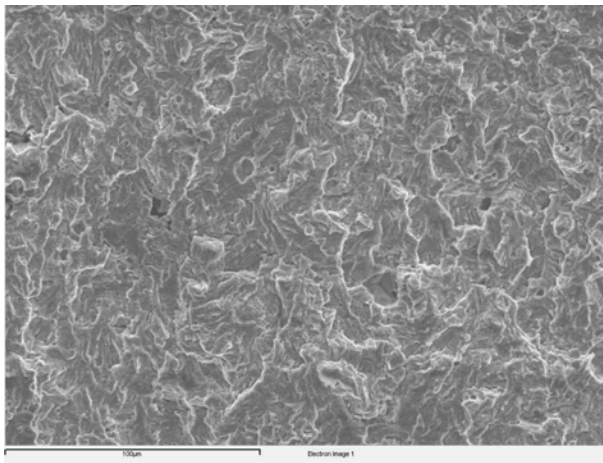
**Notes:** **outer** and **inner** refer to crack face areas in relation to the outer and inner pipe surfaces

Figure 29. Defect D3: Scanning electron microscope images (crack growth direction is top to bottom in all images).

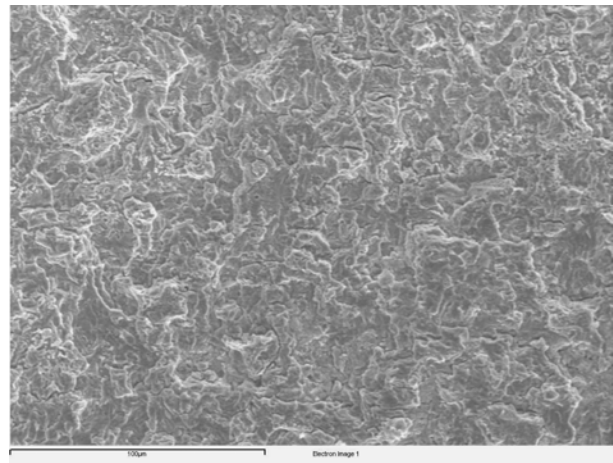




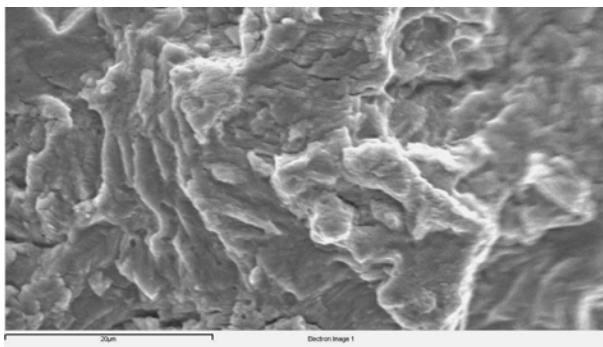
Fatigue crack surface features – **outer**, 200 $\mu$ m scale



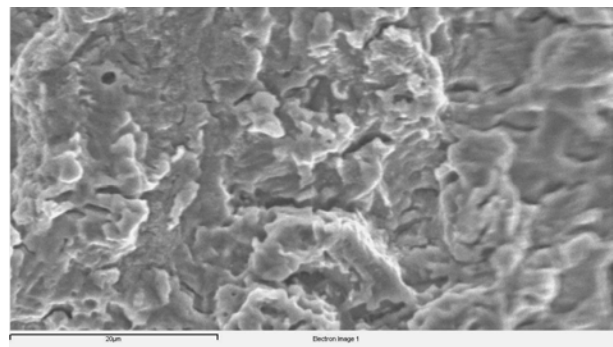
Fatigue crack surface features – **outer**, 100 $\mu$ m scale



Fatigue crack surface features – **inner**, 100 $\mu$ m scale



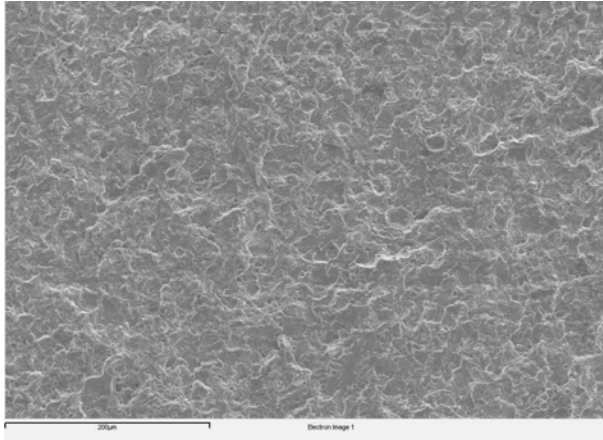
Striations – **outer**, 20 $\mu$ m scale



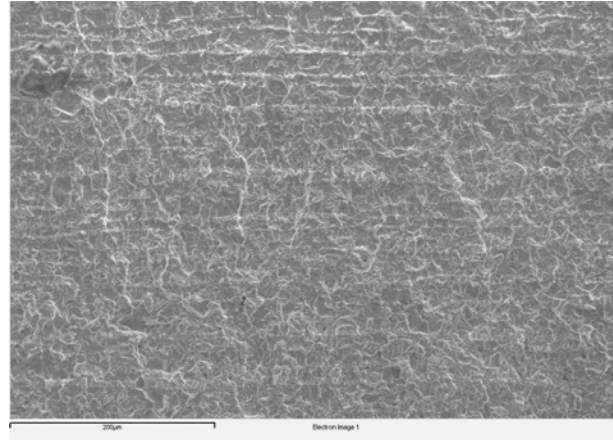
Striations – **inner**, 20 $\mu$ m scale

**Notes:** **outer** and **inner** refer to crack face areas in relation to the outer and inner pipe surfaces

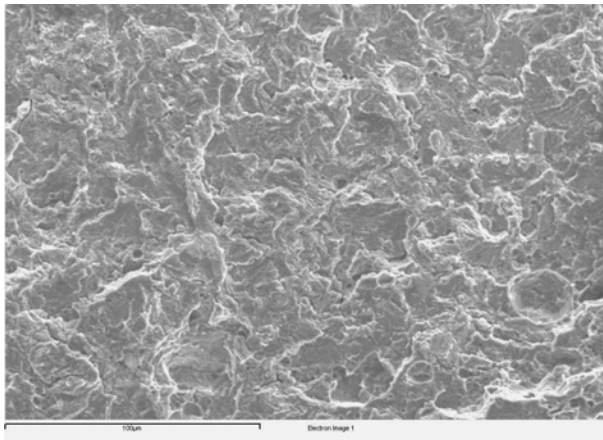
Figure 30. Defect D2: Scanning electron microscope images (crack growth direction is top to bottom in all images).



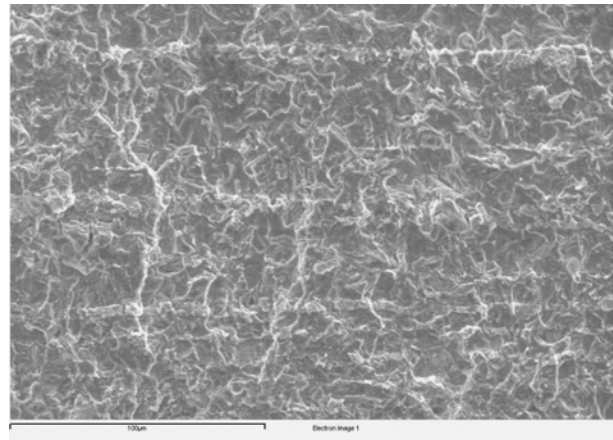
Fatigue crack surface features – **outer**, 200µm scale



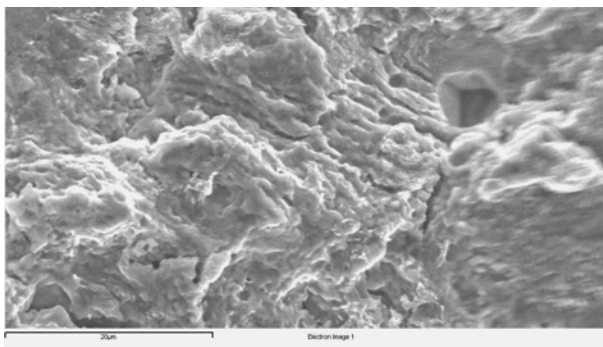
Fatigue crack surface features – **inner**, 200µm scale



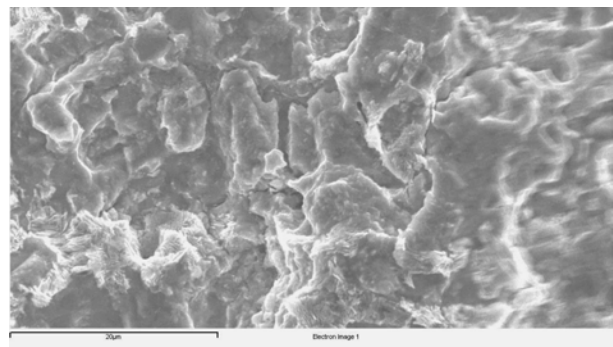
Fatigue crack surface features – **outer**, 100µm scale



Fatigue crack surface features – **inner**, 100µm scale



Striations – **outer**, 20µm scale



Striations – **inner**, 20µm scale (not as clear as on **outer** surface)

**Notes:** **outer** and **inner** refer to crack face areas in relation to the outer and inner pipe surfaces

Figure 31. Defect D4: Scanning electron microscope images (crack growth direction is top to bottom in all images).

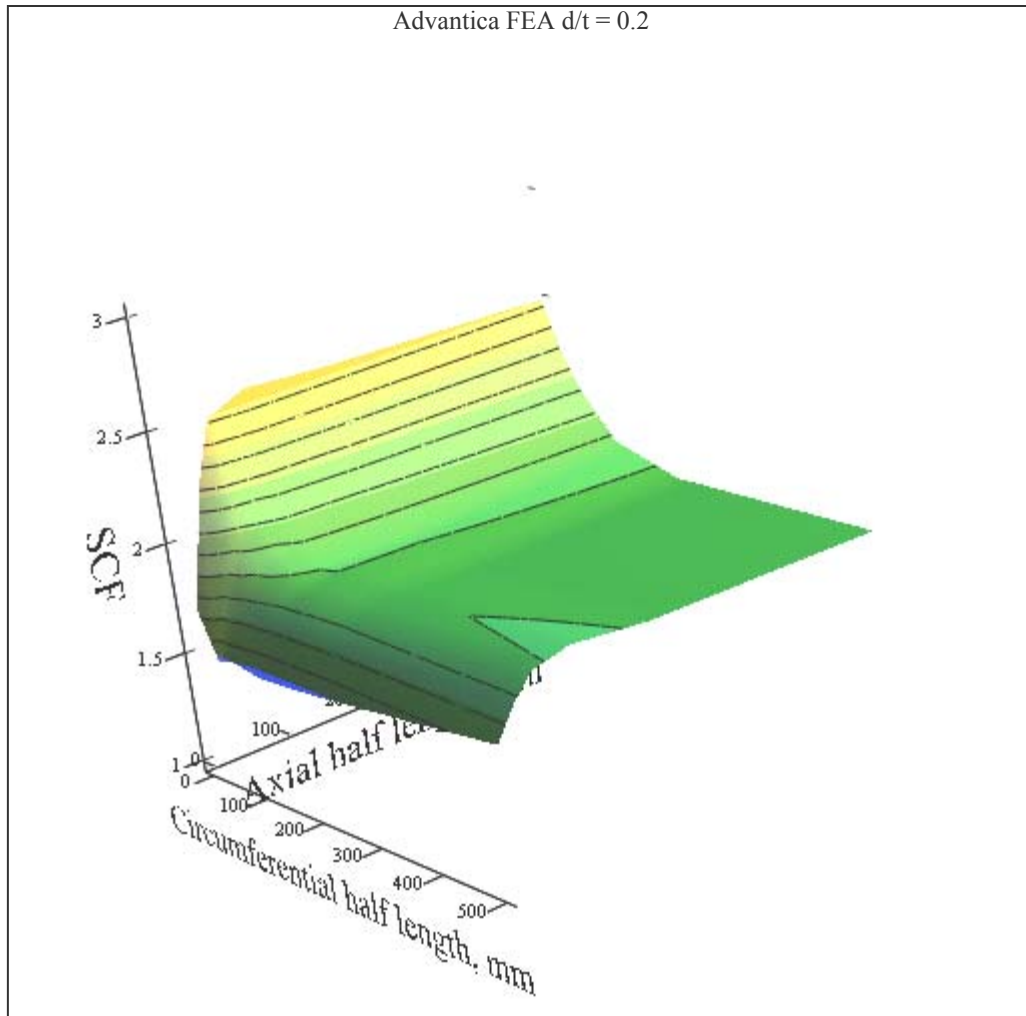


Figure 32. Surface plot of SCF results for a defect depth  $d/t=0.2$

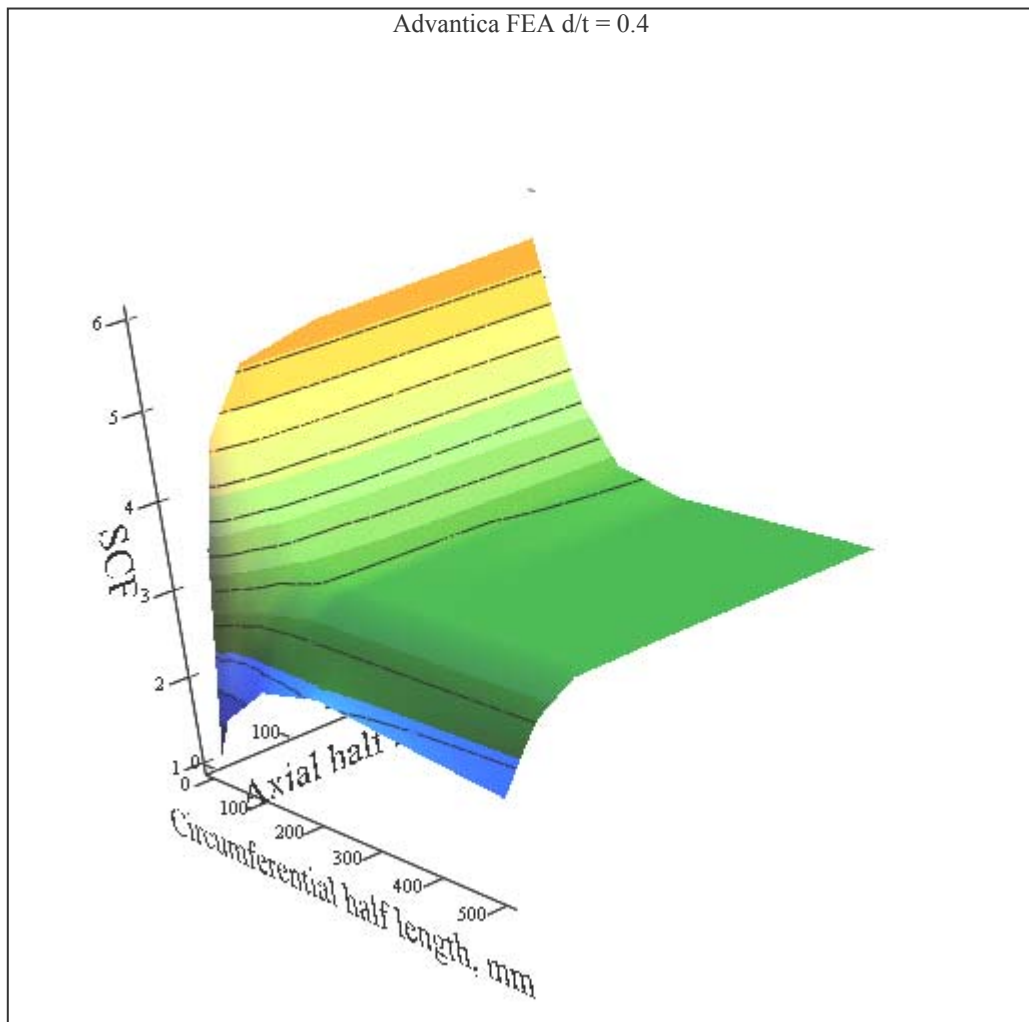


Figure 33. Surface plot of SCF results for a defect depth  $d/t=0.4$



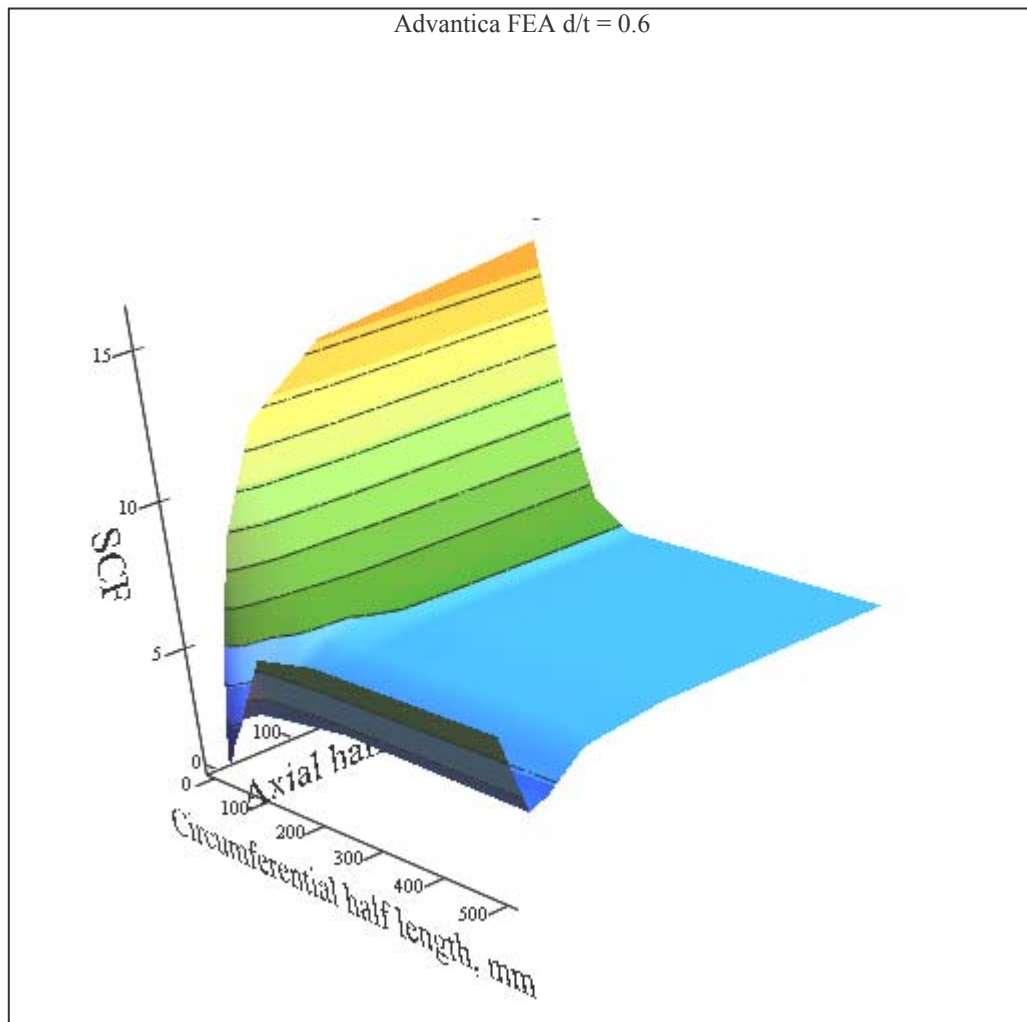


Figure 34. Surface plot of SCF results for a defect depth  $d/t=0.6$

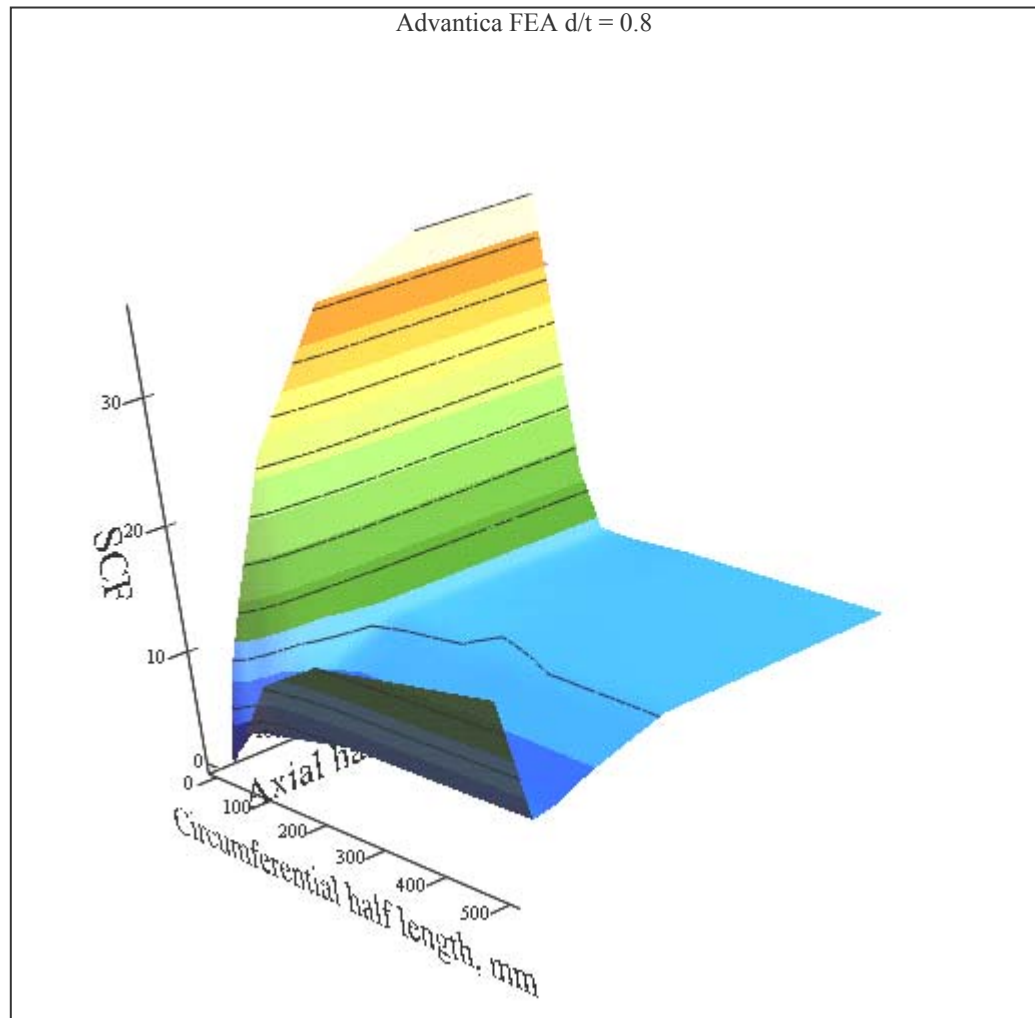


Figure 35 Surface plot of SCF results for a defect depth  $d/t=0.8$

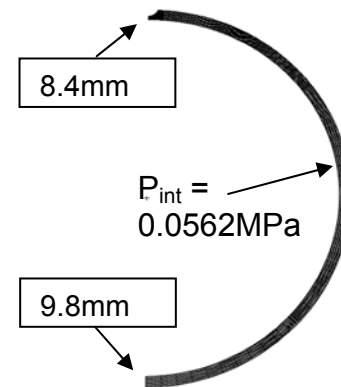
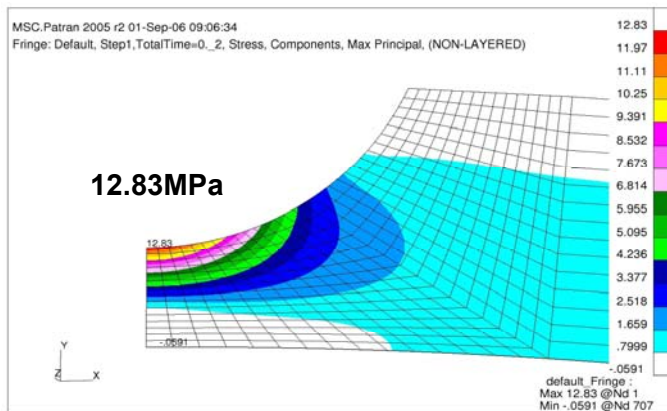
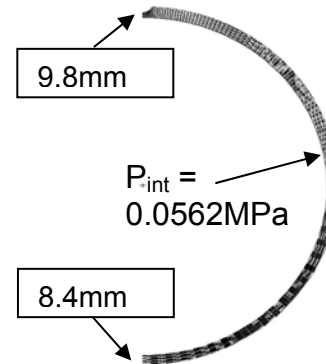
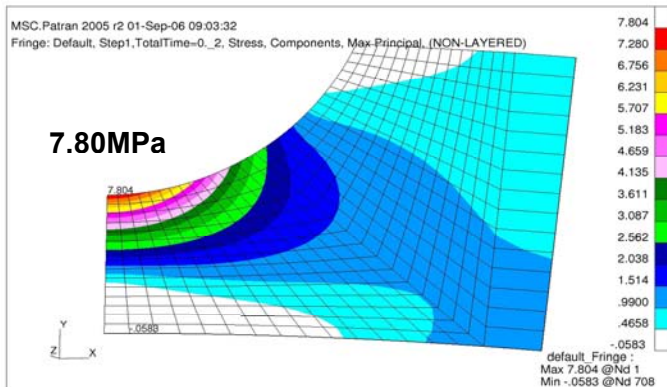
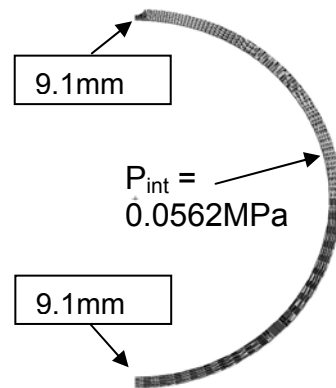
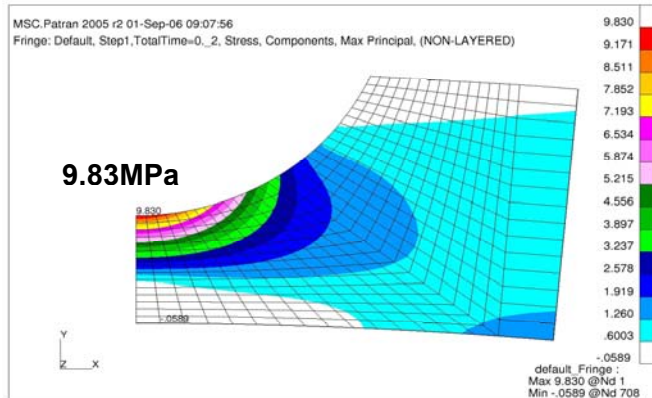


Figure 36. Plane strain finite element models showing the effect of an eccentric bore on the SCF

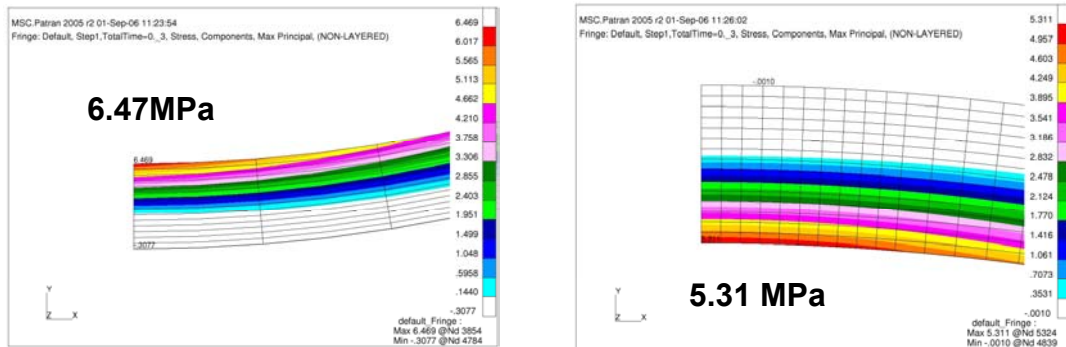


Figure 37. Local maximum principal stress contours for defect free pipe with an eccentric bore. Left, thinnest area; right, thickest area

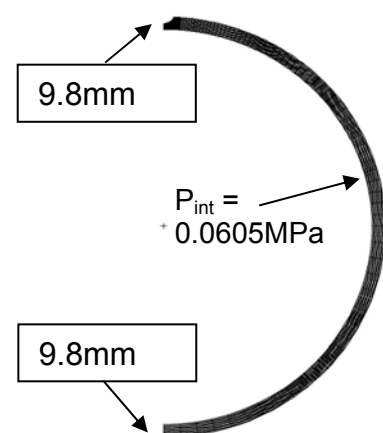
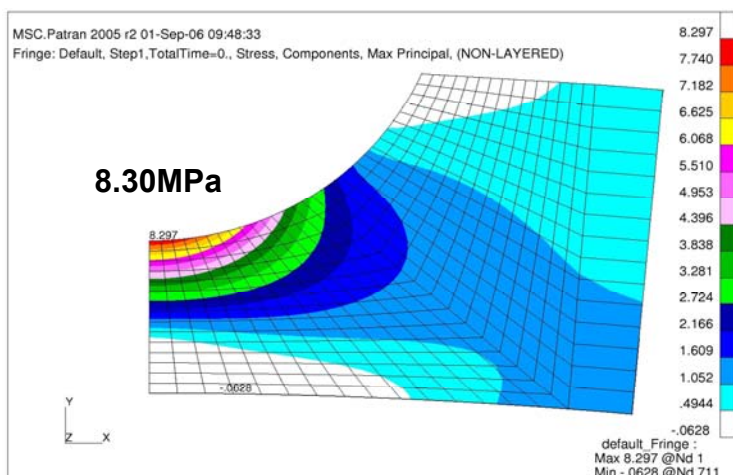
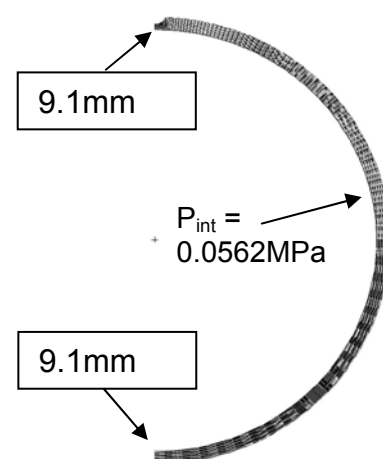
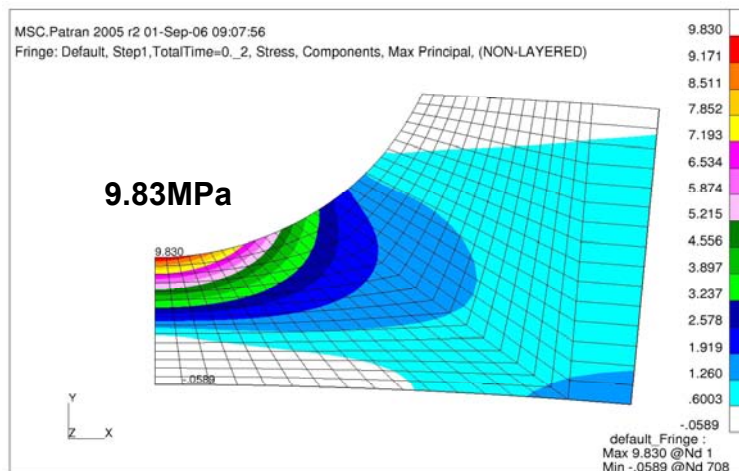
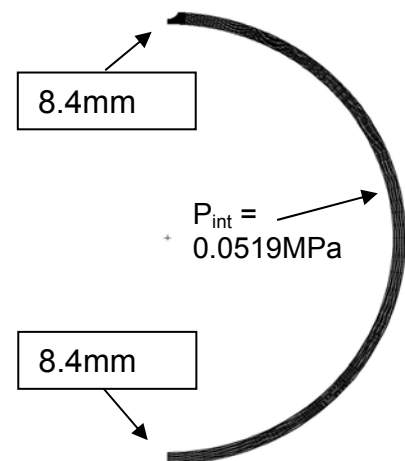
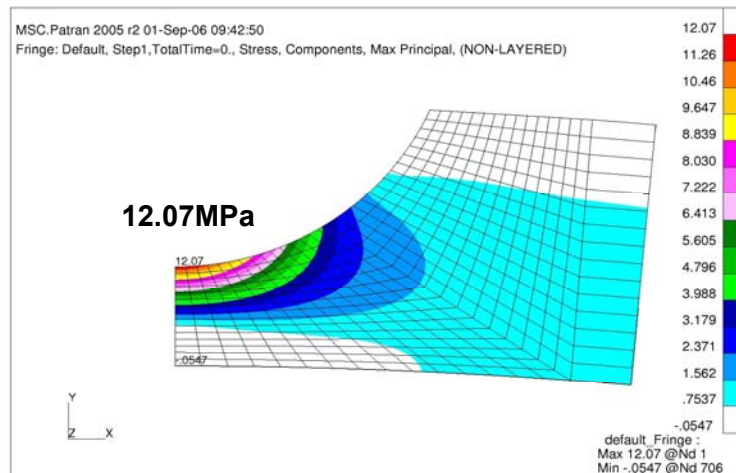


Figure 38. Effect of varying pipe wall thickness for a constant groove depth; Hoop stress  $1.0 \text{ N/mm}^2$  in each case

## APPENDIX A MATERIAL TEST CERTIFICATE





**Dalmine**PLANT:  
DALMINE

## INSPECTION CERTIFICATE

(UNI EN 10204 3.1.B) **1023884**

N. 99/02010

Page 2

**9900043347**

(%): requir.min 25,0 **100000** result 36,8  
 1^IMPACT TEST - 50,0°C REMARKS OR SPEC. : KCV LONG - 050 C JOULE  
 TEST SPECIMEN : LONGIT. 10 X 7,50 MM requ.JOULE min 28,0 avg 40,0  
 : result 220,0 218,0 213,0  
 2^IMPACT TEST - 50,0°C REMARKS OR SPEC. : KCV TRASV - 050 C JOULE  
 TEST SPECIMEN : TRANSV. 10 X 5,00 MM requ.JOULE min 17,5 avg 24,5  
 : result 106,0 92,0 86,0  
 HARDNESS HRC requ. max 22,0 result 0,0  
 HARDNESS HRB requ. max 100,0 result 86,2

TEST N. R7133/10 HEAT N. 990178

## TENSION TEST + 20,0°C

TEST SPEC. : LONGITUDINAL WIDTH 16,10 THICK. 8,40 SECTION 135,2 mm2  
 YIELD POINT 0,5% (N/MM2 ): requir min 358 result 439,0  
 TENSILE STRENGTH (N/MM2 ): requir min 460 max 620 result 551,0  
 ELONGATION : CALIBRATED ON 5D 65,0 mm  
 (%): requir.min 20,0 result 26,1  
 HARDNESS HRC requ. max 22,0 result 0,0  
 HARDNESS HRB requ. max 100,0 result 85,7

HEAT N. 990178

## HEAT ANALYSIS %

C 0,12 Mn 1,28 Si 0,29 P 0,011 S 0,002 Cu 0,17  
 Sn 0,014 Ni 0,12 Cr 0,10 Mo 0,04 Al 0,035 Ti 0,004  
 Nb 0,024 V 0,06 N 0,0078 B 0,0002 Ca 0,0018 As 0,0108  
 Sb 0,0032 Pb 0,0014 Bi 0,0018

SOLUBLE ELEMENTS : Al 0,033  
 (Cr+Mo+Ni+Cu) = 0,43  
 (Nb+V) = 0,079  
 (Nb+Ti+V) = 0,083  
 (Al-A@) = 0,002  
 (A@/N) = 4,231

CARBON EQUIVALENT : L.F. (C+Mn/6+(Cr+Mo+V)/5+(Ni+Cu)/15) 0,39

---&gt; A@ = soluble Al

## PRODUCT ANALYSIS %

C 0,12 Mn 1,28 Si 0,28 P 0,010 S 0,002 Cu 0,17  
 Sn 0,013 Ni 0,12 Cr 0,10 Mo 0,04 Al 0,036 Ti 0,004  
 Nb 0,023 V 0,06 N 0,0077 B 0,0002 Ca 0,0018 As 0,0098  
 Sb 0,0024 Pb 0,0013 Bi 0,0017

SOLUBLE ELEMENTS : Al 0,036  
 (Cr+Mo+Ni+Cu) = 0,43  
 (Nb+V) = 0,078  
 (Nb+Ti+V) = 0,082  
 (Al-A@) = 0,00  
 (A@/N) = 4,675

CARBON EQUIVALENT : L.F. (C+Mn/6+(Cr+Mo+V)/5+(Ni+Cu)/15) 0,39

---&gt; A@ = soluble Al

Questo certificato è emesso da un sistema computerizzato ed è valido senza firma. Il certificato originale riporta il marchio C in colore verde lungo una diagonale. Il possessore dell'originale, qualora rilasci copia, deve attestare a suo nome la conformità, assumendosi ogni responsabilità per usi illeciti o semplicemente non consentiti dalla Dalmine.

Alterazioni e/o falsificazioni saranno perseguite a termini di legge.

This certificate is issued by a computerized system and it is valid without signature. On the original certificate the trade-mark C green coloured along the diagonal is stamped. In case the owner of the original certificate would release a copy of it, he must attest its conformity to the original one taking upon himself the responsibility for any unlawful or not allowed use.

Any alteration and/or falsification will be subject to the law.

Le certificat est rédigé par un système d'ordinateur et il est valable sans signature. Le certificat original mentionne la marque C de couleur verte en diagonale. Dans le cas où le possesseur de l'original délivrerait une copie, il devra attester la conformité en son nom, en s'engageant toute la responsabilité pour des usages illicites ou, tout simplement, pas permis par Dalmine. Toute altération ou contrefaçon seront susceptibles d'entraîner des poursuites légales.



DATE

03/02/1999

QUALITY  
 CERTIFICATION DPT  
 Flaviana CERRI

CHIEF OF QUALITY  
 CERTIFICATION DPT  
 Marco BELLOLI





**Dalmine**

PLANT:  
DALMINE

INSPECTION CERTIFICATE

(UNI EN 10204 3.1.B)

N. 99/02010

Page 3

PRODUCT ANALYSIS %

C 0,12	Mn 1,29	Si 0,28	P 0,010	S 0,002	Cu 0,18
Sn 0,014	Ni 0,12	Cr 0,11	Mo 0,04	Al 0,035	Ti 0,004
Nb 0,023	V 0,05	N 0,0075	B 0,0002	Ca 0,0017	As 0,0101
Sb 0,0027	Pb 0,0010	Bi 0,0016			

SOLUBLE ELEMENTS : Al 0,034

(Cr+Mo+Ni+Cu) = 0,45  
(Nb+V) = 0,077  
(Nb+Ti+V) = 0,081  
(Al-A@) = 0,001  
(A@/N) = 4,533

CARBON EQUIVALENT : L.F. (C+Mn/6+(Cr+Mo+V)/5+(Ni+Cu)/15) 0,40

---> A@ = soluble Al

LEAK-TIGHTNESS TEST PERFORMED WITH SATISFACTORY RESULTS BY:

HYDRAULIC TEST PRESSURE

15,9 MPA

FOR 5 Sec

VISUAL AND DIMENSIONAL CONTROL OF THE TUBES HAS BEEN CARRIED OUT WITH SATISFACTORY RESULT

STEEL IS FULLY KILLED AND PRODUCED BY ELECTRIC FURNACE

REMARKS:

ALL TUBES HAVE BEEN NORMALIZED AT 920°C FOR 20 MINS.

HEAT TREATMENT BY CONTINUOUS METHOD - FINE GRAIN PRACTICE.

HARDNESS HRC 22 MAX., ACC. TO NACE MR-01-75 L.E.


ALL TUBES HAVE BEEN TESTED BY ULTRASONIC INSPECTION FOR LONGITUDINAL INSIDE/OUTSIDE DEFECTS (NOTCH 5%), ACCORDING TO API 5L-SR4 AND PT COQU 10.05 R.0, WITH SATISFACTORY RESULT.

THE WALL THICKNESS CONTROLLED ON FULL LENGTH BY U.T. OF EACH PIPE IS WITHIN THE TOLERANCE REQUESTED (GQ 13.022/Da L.R.).

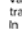
ALL PIPES HAVE BEEN TESTED BY U.T. ON FULL LENGTH FOR LAMINATION DETECTION, ACCORDING TO GQ 13.020/Da L.R. - BS 5996 L4, WITH SATISFACTORY RESULT.

THE BEVELLED ENDS (for 300 mm.) HAVE BEEN TESTED WITH WET FLUORESCENT MAGNETIC PARTICLES (P.T. COQU 10.76 R.0), WITH SATISFACTORY RESULT.

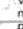
\*-----\*  
\* CERTIFIED FACTORY UNI EN ISO 9001: I.G.Q. N. 8603 \*  
\*-----\*

Questo certificato è emesso da un sistema computerizzato ed è valido senza firma. Il certificato originale riporta il marchio  in colore verde lungo una diagonale. Il possessore dell'originale, qualora rilasci copia, deve attestare a suo nome la conformità, assumendosi ogni responsabilità per usi illeciti o semplicemente non consentiti dalla Dalmine.

Alterazioni e/o falsificazioni saranno perseguite a termini di legge.

This certificate is issued by a computerized system and it is valid without signature. On the original certificate the trade-mark  green coloured along the diagonal is stamped. In case the owner of the original certificate would release a copy of it, he must attest its conformity to the original one taking upon himself the responsibility for any unlawful or not allowed use.

Any alteration and /or falsification will be subject to the law.

Le certificat est rédigé par un système d'ordinateur et il est valable sans signature. Le certificat original mentionne la marque  de couleur verte en diagonale. Dans le cas où le possesseur de l'original délivrerait une copie, il devra attester la conformité en son nom, en s'engageant toute la responsabilité pour des usages illicites ou, tout simplement, pas permis par Dalmine. Toute altération ou contrefaçon seront susceptibles d'entraîner des poursuites légales.

DATE

03/02/1999

QUALITY  
CERTIFICATION DPT  
Flaviana CERRI

CHIEF OF QUALITY  
CERTIFICATION DPT  
Marco BELLOLI

## APPENDIX B    INSPECTION CERTIFICATE (DEFECTS)

<b>PMC AMBERGATE</b>		<b>PMC NO. 4011733</b> <b>GENERAL INSPECTION REPORT</b> <small>PAGE 1 OF 2</small>		
PROJECT CLIENT <u>ADVANTICA</u>		DATE <u>28-2-03</u>		
LOCATION: <u>PMC AMBERGATE</u>		INSPECTOR (CAPITALS): <u>R. ELLIOTT</u>		
INSPECTION TECHNIQUE				
<u>ADVANTICA 1/076202MOS</u>		<small>ALL MEASUREMENTS IN MILLIMETRES</small>		
<div style="display: flex; justify-content: space-between; margin: 0 10px;"> <span>8.9</span> <span>8.9</span> <span>8.9</span> </div>				
8.9	<div style="border: 1px solid black; border-radius: 15px; padding: 5px; display: inline-block;"> 1.94 * </div>	1.73	<div style="border: 1px solid black; border-radius: 15px; padding: 5px; display: inline-block;"> 1.65 * </div>	8.9
9.1	<small>LENGTH 398.95 WIDTH 11.21</small>	9.1	DEFECT 1	9.1
<div style="display: flex; justify-content: space-between; margin: 0 10px;"> <span>8.7</span> <span>8.7</span> <span>8.7</span> </div>				
8.7	<div style="border: 1px solid black; border-radius: 15px; padding: 5px; display: inline-block;"> 3.23 * </div>	3.43	<div style="border: 1px solid black; border-radius: 15px; padding: 5px; display: inline-block;"> 3.44 * </div>	8.7
8.7	<small>LENGTH 404.49 WIDTH 13.26</small>	8.6	DEFECT 2	8.6
<div style="display: flex; justify-content: space-between; margin: 0 10px;"> <span>9.6</span> <span>9.6</span> <span>9.7</span> <span>9.5</span> </div>				
9.8	<div style="border: 1px solid black; border-radius: 15px; padding: 5px; display: inline-block;"> 5.17 * </div>	4.90	<div style="border: 1px solid black; border-radius: 15px; padding: 5px; display: inline-block;"> 5.21 * </div>	9.7
9.2	<small>LENGTH 405.75 WIDTH 16.20</small>	9.3	DEFECT 3	9.1
<div style="display: flex; justify-content: space-between; margin: 0 10px;"> <span>9.2</span> <span>9.2</span> <span>9.2</span> </div>				
9.1	<div style="border: 1px solid black; border-radius: 15px; padding: 5px; display: inline-block;"> 3.7 * </div>	3.6	<div style="border: 1px solid black; border-radius: 15px; padding: 5px; display: inline-block;"> 4.5 * </div>	9.2
9.1	3.2	3.1	4.2	9.3
8.9	<div style="border: 1px solid black; border-radius: 15px; padding: 5px; display: inline-block;"> 2.9 * </div>	2.9	<div style="border: 1px solid black; border-radius: 15px; padding: 5px; display: inline-block;"> 3.6 * </div>	9.0
9.0	<small>LENGTH 398.27 WIDTH 13.76</small>	9.1	DEFECT 4	9.0
SIGNATURE <span style="float: right;"><i>R Elliott</i></span>				
APPROVAL & No. BGAS <u>SJ1 2513</u>				
DATE <u>1-3-06</u>				
CIRCULATION				
Document No: NDT-004			Issue 3 Dated 3.4.00	

<b>PMC AMBERGATE</b>		<b>PMC NO. 4411733 GENERAL INSPECTION REPORT</b> <i>Page 2 of 2</i>	
PROJECT CLIENT <i>ADVANTICA</i>		DATE <i>28-2-03</i>	
LOCATION <i>PMC AMBERGATE</i>		INSPECTOR (CAPITALS): <i>R. ELLIOTT</i>	
INSPECTION TECHNIQUE			
<i>ADVANTICA 1/076202M05</i>			
<u>DEFECT 1</u>			
MAXIMUM DEPTH OF DEFECT $\frac{1.94 \text{ mm}}{8.9 \text{ mm}} = 21.79\%$ WALL LOSS MINIMUM WALL THICKNESS			
<u>DEFECT 2</u>			
MAXIMUM DEPTH OF DEFECT $\frac{3.44 \text{ mm}}{8.6 \text{ mm}} = 40\%$ WALL LOSS MINIMUM WALL THICKNESS			
<u>DEFECT 3</u>			
MAXIMUM DEPTH OF DEFECT $\frac{5.21 \text{ mm}}{9.1 \text{ mm}} = 57.25\%$ WALL LOSS MINIMUM WALL THICKNESS			
<u>DEFECT 4</u>			
MAXIMUM DEPTH OF DEFECT $\frac{6.0 \text{ mm}}{8.9 \text{ mm}} = 67.41\%$ WALL LOSS MINIMUM WALL THICKNESS			
SIGNATURE <i>R. Elliott</i> APPROVAL & No. BGAS 501 2513 DATE <i>1-3-06</i>			
CIRCULATION			
Document No: NDT-004		Issue 3 Dated 3.4.00	